

# COMPUTATIONAL INVESTIGATIONS: ABIOTIC ORIGIN OF ADENINE, DINITROGEN ACTIVATION, MOLECULES WITH NOVEL BONDING

by

DEBJANI ROY

(Under the Direction of Paul von Ragué Schleyer)

## ABSTRACT

This dissertation applies quantum chemical methods to study the structure, properties, and the mechanisms, for the formation of adenine in interstellar space and under pre-biotic conditions. The mechanism for the remarkable activation of inert dinitrogen at room temperature, using lithium clusters, has been reported. Further, computational methods are applied to design molecules with novel bonding patterns.

Two major unsolved mechanistic puzzles are addressed. The first one is: how did biomolecules originate under prebiotic condition starting from abiotic precursors? The theoretical explorations (using Density functional and ab-initio calculations) of detailed, plausible, step by step mechanisms, for the chemical evolution of adenine (a bio-molecule, which is one of the four fundamental nucleobases of DNA) under pre-biotic Earth (or interstellar medium) starting from abiotic starting materials, is reported in this dissertation. The pathway was unknown, but possible intermediates have been isolated. Experimental investigations are precluded by low yields and many side reactions. The thermodynamically feasible mechanism to

explain how adenine might be built up from the combination of five hydrogen cyanide molecules has been reported.

The second unsolved mechanistic puzzle addressed is: what is the mechanism for activation of inert molecular nitrogen, by using lithium clusters? Activation and reduction of dinitrogen remains a fundamental challenge to synthetic as well as to theoretical chemistry. Lithium is exceptional among the main group elements in that it slowly reacts with  $N_2$  at room temperature, leading finally to  $(NLi_3)_x$ . This dissertation is aimed at understanding the molecular dinitrogen activation mechanism using model lithium clusters, and how this model study can be used to design multimetallic catalysts, which will be able to activate as well as cleave  $N_2$ .

This dissertation further reports the theoretical design of molecules with novel bonding patterns, such as planar tetra-coordinated carbon (ptC) in transition metal clusters. The molecular orbitals, electronic structures, energies, and magnetic properties of  $CM_4^{n+}$  species (where M represents isoelectronic combinations of Cu, Ni, Ag, and Pd, and n is the charge) have been studied to determine the plausible candidate for experimental detection of ptC in transition metal cluster.

The extension of the concept of aromaticity, from 2 electron singlet species, to open-shell doublet systems with one delocalized electron, is discussed. The degree of one electron delocalization using energetic, geometric and magnetic criteria for a multitude of theoretically designed two and three dimensional cationic, anionic and neutral monoradical systems is reported in the dissertation.

INDEX WORDS: Adenine, Prebiotic chemistry, Reaction mechanism, Density functional theory, Lithium-nitrogen clusters, Dinitrogen activation, Computational

chemistry, Planar tetracordinate carbon, Transition metal clusters,  
Aromaticity, One electron aromatics.

COMPUTATIONAL INVESTIGATIONS: ABIOTIC ORIGIN OF ADENINE, DINITROGEN  
ACTIVATION, MOLECULES WITH NOVEL BONDING

by

DEBJANI ROY

B.S., Lady Brabourne College, University of Calcutta, India, 2001

M.S., Indian Institute of Technology- Kanpur (IITK), India, 2003

A Dissertation Submitted to the Graduate Faculty of The University of Georgia in Partial  
Fulfillment of the Requirements for the Degree

DOCTOR OF PHILOSOPHY

ATHENS, GEORGIA

2009

© 2009

Debjani Roy

All Rights Reserved

COMPUTATIONAL INVESTIGATIONS: ABIOTIC ORIGIN OF ADENINE, DINITROGEN  
ACTIVATION, MOLECULES WITH NOVEL BONDING

by

DEBJANI ROY

Major Professor: Paul von R Schleyer

Committee: Henry F Schaefer  
Robert J Woods

Electronic Version Approved:

Maureen Grasso  
Dean of the Graduate School  
The University of Georgia  
May 2009

## DEDICATION

*I dedicate this dissertation to my parents, my sister and Siddhartha.*

## ACKNOWLEDGEMENTS

First and foremost, I would like to thank my graduate advisor Prof. Schleyer for giving me challenging problems to solve throughout my graduate career, which has instilled in me the confidence to approach chemical problems with clarity and vision. He had given me great freedom to choose problems of my liking, which had made research endeavors exciting and enjoyable. He taught me the art, as well as the science, of writing scientific articles. His eye for minute details has taught me to be a perfectionist, and his enthusiasm towards chemistry has inspired me to overcome scientifically difficult hurdles, and continue fundamental research in computational quantum chemistry, under his guidance.

I am very pleased to have learned the fundamentals of molecular modeling from Prof. Woods, through a course and several technical discussions. I thank him for introducing this new subject to me and for being a patient teacher, encouraging mentor and very helpful co-advisor. I sincerely appreciate Prof. Schaefer's very kind and helpful nature. I am thankful to be able to attend the group meetings, and the Mulliken and Coulson lectures organized by CCC. Each and every seminar has enhanced my breadth of knowledge. I also thank him for providing me the facilities and resource at CCC. I want to thank my fellow graduate students, and current lab mates, Judy, Keigo and Chad, and erstwhile members, Dr. Chen, Matt, Clemence and Chait, for making the atmosphere in the lab congenial for scientific research, as well as a fun place to work.

I want to thank my teachers, Dr. Dinabandhu Kundu and Dr. Chandan Kumar Pal, who were my mentors in Chemistry during my undergraduate days, and taught me the fundamentals



of chemistry in extraordinary clarity, which enabled me to get a chance to study at the Indian Institute of Technology at Kanpur in India. Dr. Purabi Dutta of Lady Brabourne college in India, encouraged me, and taught me fundamentals of inorganic chemistry, the knowledge of which is useful to me to this day. My teachers at school, especially Purnima mam, Basanti mam, Alam mam, and many others, encouraged me to pursue a career in science, and also instilled in me the love for music and arts in general, which have been my intellectual companion throughout my life.

I would like to thank my parents, for instilling in me the confidence to excel in academia, and for their constant love and affection. My mother's simplistic and uncomplicated view of life has shaped my outlook for ever, and has taught me the importance, and the necessity, to harbor pleasantness and humility in my demeanor. My father, a mathematician and a statistician, has been instrumental in shaping my concepts in mathematics and logic – key tools required for any successful scientist. I am gratified that my sister, pursuing a career in computer science, has been imbibed with the same tutelage, as that of me, from my father. I am lucky to have a sweet sister like her, who looks up to me, argues with me, and is a protagonist for my academic and musical achievements. My maternal grandmother has always supported me - it gives her great satisfaction when she learns about her grand daughter's academic achievements. My cousins cannot be left either - being the eldest in the herd of cousins - both from paternal and maternal sides - they had looked upon me for academic guidance, loved me and cherished my achievements.

My father-in-law, an Anthropologist by profession and passion, was especially interested in my work on the origin of biomolecules in primitive Earth. I thank him for talking about my work with his colleagues, and encouraging me to continue doing work on this area. I

am grateful to my mother-in-law, who supported and encouraged me, and has put special emphasis on the fact that I need to be an example for women scientists.

Finally, I want to thank Siddhartha for instilling in me a sense of the ‘art’ in sciences. His extraordinary aesthetic sense has enabled me to consider aesthetic embellishments in my presentations and figures for manuscripts. He taught me how to use the Internet for enhancing productivity, extract knowledge, and inform myself on activities around the world. Despite being from a computer science background, he could follow the innumerable research ideas that I narrated to him, and provided informed criticism from time to time.

## TABLE OF CONTENTS

	Page
ACKNOWLEDGEMENTS .....	v
LIST OF TABLES .....	xi
LIST OF FIGURES .....	xii
CHAPTER	
1 INTRODUCTION AND LITERATURE REVIEW .....	1
1.1 PREAMBLE .....	1
1.2 METHODOLOGICAL CONSIDERATIONS .....	2
1.3 ABIOTIC ORIGIN OF ADENINE .....	4
1.4 ACTIVATION OF MOLECULAR DINITROGEN .....	5
1.5 ONE ELECTRON AROMATICS .....	6
1.6 PLANAR TETRACOORDINATE CARBON .....	7
1.7 REFERENCES .....	9
2 CHEMICAL EVOLUTION: THE MECHANISM OF THE FORMATION OF ADENINE UNDER PREBIOTIC CONDITIONS .....	14
2.1 ABSTRACT .....	15
2.2 INTRODUCTION .....	15
2.3 PREBIOTIC EXPERIMENTS AND PROPOSED PATHWAYS FOR THE FORMATION OF ADENINE .....	19
2.4 COMPUTATIONAL INVESTIGATION .....	22

2.5 THERMOCHEMISTRY OF PENTAMERIZATION .....	24
2.6 THERMODYNAMICALLY VIABLE STEP BY STEP MECHANISM .....	24
2.7 CONCLUSION .....	39
2.8 ACKNOWLEDGEMENT .....	42
2.9 REFERENCES AND NOTES .....	42
3 MODELING DINITROGEN ACTIVATION BY LITHIUM: A MECHANISTIC INVESTIGATION OF THE CLEAVAGE N <sub>2</sub> BY STEPWISE INSERTION INTO SMALL LITHIUM CLUSTERS.....	46
3.1 ABSTRACT .....	47
3.2 INTRODUCTION .....	47
3.3 COMPUTATIONAL METHODS .....	49
3.4 RESULT AND DISCUSSION .....	50
3.5 CONCLUSION .....	65
3.6 ACKNOWLEDGEMENT .....	66
3.7 REFERENCES .....	66
4 AROMATICS WITH ONE DELOCALIZED ELECTRON.....	70
4.1 ABSTRACT .....	71
4.2 INTRODUCTION .....	72
4.3 COMPUTATIONAL METHODS .....	73
4.4 RESULTS AND DISCUSSION .....	74
4.5 CONCLUDING REMARKS .....	85
4.6 REFERENCES .....	86

5	PLANAR TETRACOORDINATE CARBON ATOMS CENTERED IN BARE	
	FOUR-MEMBERED RINGS OF LATE TRANSITION METALS .....	90
	5.1 ABSTRACT .....	91
	5.2 INTRODUCTION .....	91
	5.3 COMPUTATIONAL DETAILS .....	92
	5.4 STRUCTURE AND ENERGETICS.....	93
	5.5 MOLECULAR ORBITAL AND NBO ANALYSIS .....	97
	5.6 MAGNETIC PROPERTIES .....	99
	5.7 EXPLORATION OF POTENTIAL ENERGY SURFACE.....	100
	5.8 CONCLUSION .....	105
	5.9 ACKNOWLEDGEMENT.....	105
	5.10 REFERENCES .....	105
6	CONCLUSION.....	109

## LIST OF TABLES

	Page
Table 3-1: Variation of N-N bond length and charge for the important stationary points on N <sub>2</sub> : Li <sub>n</sub> (n=6,8) reaction profile with step by step reduction of dinitrogen with six and eight Lithium atoms respectively .....	60
Table 3-2: The atomization energy/alkali metal (for BM <sub>3</sub> , CM <sub>4</sub> , NM <sub>3</sub> , OM <sub>2</sub> , PM <sub>3</sub> and SiM <sub>4</sub> ).The Li compounds have highest AE/atom, ~1.5 times of Na and K, in accord with lithium's unusual reactivity pattern among the alkali metals .....	62
Table 3-3: Bond length and Natural Charges for compounds of alkali metal- first row and second row elements (Charges computed with NBO 5.0 program@ B3LYP/6-311+G* level)63	63
Table 4-1: GIAO-NICS index for both the 2 $\pi$ and 1 $\pi$ electron aromatics in ppm at PW91/6- 311+G**. Negative NICS value at the ring center indicates the circulation of induced diatropic ring current. The totally delocalized SOMO <sup>a</sup> for the open shell compounds are depicted in column 1 .....	78
Table 4-2: GIAO-NICS index in ppm for 4c-2e and 4c-1e aromatics (two dimensional double aromatics) at PW91/6-311+G** .....	83
Table 4-3: GIAO-NICS index in ppm 4c-2e and 4c-1e three dimensional aromatics at PW91/6- 311+G** .....	84

## LIST OF FIGURES

	Page
Figure 1-1: Example of theoretically designed molecules containing planar tetracoordinate carbon .....	7
Figure 2-1: The progress in prebiotic chemistry for last two centuries .....	16
Figure 2-2: Products isolated from HCN in water-ammonia solution .....	17
Figure 2-3: Proposed outline of steps for the formation of adenine in aqueous ammonium cyanide solution [11, 13, 39-43]. Experimentally detected putative intermediates in the abiotic formation of adenine are enclosed in boxes. Two tautomers of AICN can exist; AICN(b) is the more stable. Note that a photoisomerisation step is proposed for the formation of AICN from DAMN. DAMN has not been demonstrated to be an adenine intermediate in a non-photolytic reaction .....	21
Figure 2-4: Thermochemistry of pentamerization of HCN. The relative energies in gas phase are in kcal/mol computed at B3LYP/6-311+G**+ZPVE. Entropy is unfavorable, but is not considered. Note that the last crucial step for formation of pentamer (adenine) from tetramer [AICN (b)] is highly exothermic. Overall energy for pentamerization of adenine ( $5 \text{ HCN} \rightarrow \text{C}_5\text{H}_5\text{N}_5$ ) is 93.8 kcal/mol [ $\Delta G^{298} = 53.7 \text{ kcal/mol}$ ] .....	24
Figure 2-5: DAMN and AICN are both $\text{C}_4\text{H}_4\text{N}_4$ isomers. Like adenine, both AICN (a) and (b) has a C-C-C-N sequence, whereas DAMN has a C-C-C-C backbone not present in adenine .....	25

Figure 2-6: Anionic mechanisms are unfeasible in isolation. Upon optimization both ii and iii revert back to i (reactants). Free radical as well as neutral *uncatalyzed* mechanisms are also not viable due to the very large reaction barriers for the two steps shown.....27

Figure 2-7: Reaction profile for adenine formation from the less stable AICN(a) isomer with one H<sub>2</sub>O acting as a catalyst ( gas phase). This pathway is precluded by the second high barrier, which requires over 44 kcal/mol activation from the preceding lowest energy minimum. ....29

Figure 2-8: Gas phase reaction barrier for the key first addition step (B3LYP/6-311+G\*\* level of theory) Optimized geometries in Å for reactant complexes (RC), transition states (TS) and product complexes (PC) for systems with 0, 1 and 2 water molecules are given. The reaction barrier (ZPVE corrected) for the neutral uncatalyzed pathway is ~60.4 kcal/mol. Water (solvent) is an active participant in the transition step. Incorporation of one and two water molecules reduces the reaction barrier to 38.0 and 37.6 kcal/mol, respectively.....30

Figure 2-9: Reaction profiles for the formation of adenine starting from AICN(b) and HCN in gas phase and in the solvent phase via explicit water catalyzed mechanism (two water molecules). The barrier height are reported with both 6-31G\* and at 6-311+G\*\* basis set (in parentheses). All the stable minima are shown. The comparison of reaction profiles in a vacuum and in aqueous solution clearly shows that the transition states are stabilized through electrostatic effect of the solvent. The two H<sub>2</sub>O or NH<sub>3</sub> molecules participate in proton relay. They form the H-bonded “wire” for the proton transfer via 6 membered transition state. The reaction seems easier in aqueous solution than in the gas phase: the first step is rate-determining in both cases.....32



Figure 2-10: Reaction profiles for the formation of adenine starting from AICN(b) and HCN in the gas phase and with simulated bulk water solvation via explicit solvent catalyzed mechanisms (two explicit NH <sub>3</sub> molecules) .....	33
Figure 2-11: Stationary points for the ammonia (two explicit molecules) catalyzed pathway. The transition state structures are depicted by a ‡ sign .....	35
Figure 2-12: Geometries of reactant, product and transition state for HCN+NH <sub>3</sub> +H <sub>2</sub> O system (simulated the first HCN + RNH <sub>2</sub> addition step with the highest barrier) at the B3LYP level of theory with various basis sets are shown. Comparison of density functional theory (DFT) and CCSD (T) reaction barriers are given. ....	36
Figure 2-13: Summary of the step by step mechanism for the formation of adenine. The last crucial pentamer formation step is catalyzed by specific solvent molecule (water/ammonia). The CN building blocks are circled in red in the diagram.....	38
Figure 3-1: The computed geometries, N-N stretching frequencies and intensities for [LiN <sub>2</sub> ] and [Li <sub>2</sub> N <sub>4</sub> ] species.....	50
Figure 3-2: Pathway for the insertion of N <sub>2</sub> into the D <sub>∞h</sub> Li <sub>2</sub> cluster showing intermediates and transition structures. Energies relative to the initial complex are in kcal/mol (B3LYP/6-311+G*). The overall reaction is endothermic and the final D <sub>2h</sub> N <sub>2</sub> Li <sub>2</sub> complex is even 1.2 kcal/mol higher in energy than the separates Li <sub>2</sub> and N <sub>2</sub> species .	53
Figure 3-3: Pathway for the insertion of N <sub>2</sub> into the D <sub>2h</sub> Li <sub>4</sub> cluster showing intermediates and transition structures. Energies relative to the initial complex are in kcal/mol (B3LYP/6-311+G*).....	54
Figure 3-4: N <sub>2</sub> Li <sub>6</sub> [minima] with various NN distances (in Å) located by stochastic searches. B3LYP/6-311+G* energies in kcal/mol) relative to <b>1</b> are given in parentheses.....	56

Figure 3-5: Pathway for the N <sub>2</sub> insertion into a Li <sub>6</sub> cluster. Structures of transition states, intermediates, and products are shown (B3LYP/6-311+G*). The zero point vibrational energy corrected energies (ZPVE) are reported in parenthesis .....	57
Figure 3-6: N <sub>2</sub> Li <sub>8</sub> [minima] with various NN distances (in Å) located by stochastic searches. B3LYP/6-311+G* energies in kcal/mol relative to 1' are given in parentheses. ....	58
Figure 3-7: Reaction profile for the insertion of N <sub>2</sub> into Li <sub>8</sub> cluster. Only the structures and the N-N bond length of the minima are depicted. Note the low barrier of the initial stages of the reaction and the agreement between the B3LYP and X3LYP mechanistic details. The zero point vibrational energy (ZPVE) corrected energies are reported in parenthesis .....	59
Figure 3-8: The bond elongation of dinitrogen is linearly related to the energy gap between the 2π <sub>g</sub> and 3σ <sub>g</sub> type orbitals of the N <sub>2</sub> moieties of the N <sub>2</sub> Li <sub>n</sub> (n=6,8) clusters. Representative molecular orbitals (MOs) are shown for one complex in each case.....	61
Figure 3-9: Plot of atomization energy vs e <sup>2</sup> /R for alkali metal containing B, C and N molecules (e= natural charge on M) .....	64
Figure 4-1: The frontier molecular orbital occupancy of C <sub>3</sub> H <sub>3</sub> <sup>+</sup> and C <sub>3</sub> H <sub>3</sub> <sup>2+</sup> (B3LYP and PW91/6-311+G**). .....	75
Figure 4-2: The two and three dimensional one π electron species .....	77
Figure 4-3: Isomers (minima on potential energy surface) of closed shell Al <sub>3</sub> H <sub>3</sub> <sup>2-</sup> and open shell Al <sub>3</sub> H <sub>3</sub> <sup>-</sup> . Two potential one electron aromatic candidates are highlighted. However, other open shell species (devoid of totally symmetric HOMO) are lower in energy ....	81

Figure 5-1: B3LYP/TZPP structures of the transition metal cages (for Ag, Pd B3LYP/LANL2DZ ECP and valence basis sets) containing planar tetracoordinate carbons. The selected bond lengths are in Å. The smallest vibrational frequency (mode corresponding to pyramidalization) and the HOMO-LUMO separations (in eV) are given for all the species. ....	94
Figure 5-2: Alternative geometries for $\text{CCu}_2\text{Ni}_2$ and $\text{CAg}_2\text{Pd}_2$ . $\text{C}_{2v}$ $\text{CCu}_2\text{Ni}_2$ is 6.0 kcal mol <sup>-1</sup> less stable than the $\text{D}_{2h}$ analog and $\text{C}_1$ $\text{CAg}_2\text{Pd}_2$ is 7.0 kcal mol <sup>-1</sup> more stable than the $\text{D}_{2h}$ analog (reported in Figure 5-1) .....	95
Figure 5-3: Dimerization of neutral $\text{CCu}_4$ or $\text{CCu}_2\text{Ni}_2$ subunits into their respective $\text{C}_{2h}$ dimers is favored by more than 120 and 75 kcal mol <sup>-1</sup> .....	96
Figure 5-4: The full set of molecular orbitals of $\text{CCu}_4^{2+}$ ( $\text{D}_{4h}$ ) (B3LYP/TZVPP). Illustrative molecular orbitals are enclosed in a square. The isosurface value is 0.05 au .....	98
Figure 5-5: Two-dimensional grids (0.6 X 5.0 Å) of $\text{NICS}_{zz}$ points and $^{13}\text{C}$ chemical shifts ( $\delta^{13}\text{C}$ ) for <b>2-5</b> (PW91/TZVPP) $\text{CAI}_4\text{Na}^+$ (PW91/IGLOIII) and for the previously studied $\text{C}_5\text{Li}_2$ .....	99
Figure 5-6: Three of the four stationary points of $\text{CCu}_4^{2+}$ obtained at the B3LYP/TZVPP level are displayed on the right side. NIMAG is the number of imaginary harmonic frequencies. $\Delta E$ is the energy relative to <b>2</b> . All distances are in Å. Illustrative preliminary structures, generated by the “kick” method at HF/STO- 3G (see text) are shown on the left side. These all led to the ptC global minimum ( <b>2</b> ) upon further refinement at the higher theoretical level .....	101
Figure 5-7: Stationary points on the potential energy surface of $\text{CCu}_3\text{Ni}^+$ .....	102
Figure 5-8: Stationary points on the potential energy surface of $\text{CCu}_2\text{Ni}_2$ .....	103

Figure 5-9: Isomers for $\text{CCuNi}_3^-$ obtained by employing “kick” method .....	104
--	-----

# CHAPTER 1

## INTRODUCTION AND LITERATURE REVIEW

### 1.1 Preamble

Computational quantum chemistry uses physical laws in mathematical terms to make predictions on different chemical phenomena and molecular structural facets. There are two different aspects to computational quantum chemistry. Firstly, computational studies can be carried out in order to find a starting point for a laboratory synthesis, or to assist in understanding experimental data, such as the position and source of spectroscopic peaks. Secondly, computational studies can be used to predict the possibility of so far entirely unknown molecules, or to explore reaction mechanisms that are not, or cannot be, readily studied by experimental means. Thus, computational chemistry can assist the experimental chemist to find entirely new chemical objects.

This dissertation deals with both the aspects of computational quantum chemistry described above - i.e. finding hitherto unobserved novel molecules, as well as assisting chemists to understand experiments and investigate reaction mechanisms which are otherwise difficult to study experimentally.

The major focus of chapter 2 is to use computational chemistry to solve mechanistic riddles for the formation of adenine (a key component of DNA) under abiotic conditions. Many experiments have shown how adenine might have been generated abiotically. Although several speculative reaction pathways have been suggested to account for the formation of adenine (a

pentamer of HCN), the mechanistic details have not been explored. Experimental investigations would be very difficult since adenine is not formed cleanly, yields are small, and many steps are involved. In contrast, our extensive computations of the sequential reaction steps along possible pathways predict a plausible mechanism.

Next, this dissertation reports the step by step migratory insertion reaction mechanism of inert molecular nitrogen into lithium cluster in chapter 3.

An extension of the concept of aromaticity, from even electron singlet species, to open-shell systems with odd numbers of electrons, has been reported in this dissertation. An evaluation of the degree of electron delocalization using energetic, geometric and magnetic criteria for a multitude of theoretically designed two and three dimensional cationic, anionic and neutral monoradical systems has been reported in chapter 4. It will be interesting challenge for chemist to detect this theoretically designed ptC and one electron systems experimentally.

This dissertation further reports the use of Computational quantum chemistry to design molecules with novel bonding pattern. The theoretical design principle, bonding patterns and properties of compounds with planar tetra coordinate carbon (ptC) encapsulated in transition metal rings is reported in chapter 5.

## **1.2 Methodological considerations**

In recent times, density functional theory (DFT) has emerged as an important device in computational chemistry in making reliable estimates and predictions of molecular structures and properties. Originally developed as a tool to study condensed matter problems in physics, DFT has become very popular in theoretical explorations of chemical phenomena [1]. Throughout this dissertation, the DFT – Hartree Fock hybrid B3LYP functional - is the primary theoretical model

employed. DFT currently accounts for approximately 90% of all quantum chemical calculations being performed [2-4]. The cheap scaling, efficient implementation of analytic derivatives of DFT based techniques and proven chemical accuracy have made them a cost effective tool in carrying out theoretical investigations in intermediately large molecular systems [2-4]. However DFT is unable to give a reliable reaction barrier, and in the case of Chapter X: adenine reaction mechanism study, where a reliable reaction barrier is required, we employ correlated coupled cluster theory (CCSD(T)) [5-7] to validate the accuracy of the DFT relative energies.

In addition to selecting an appropriate theoretical method, the selection of a basis set for quantum chemical calculations is also very important. It is sometimes possible to use small basis sets to obtain good chemical accuracy, but calculations can often be significantly improved by the addition of diffuse [8-10] and polarization functions [11]. Basis functions can be considered as representing the atomic orbitals of atoms in a molecule, and in principle, one would employ the largest basis set available in order to model molecular orbitals as accurately as possible. In practice, however, computational cost grows rapidly with the size of the basis set, so a compromise must be sought between accuracy and cost. The popular Pople type basis sets are contracted sets (i.e. linear combinations) of atom-centered Gaussian functions which are computationally efficient and able to yield chemical accuracy.[12,13]. Pople type 6-31G(d) and 6-311+G(d, p) basis sets have been used throughout this dissertation. Both basis sets include *d* polarization functions on heavy atoms, while the later also includes *p* functions on hydrogen. The “+” symbol in 6-311+G(d,p) indicates the presence of so called diffuse functions, which are especially important when modeling anion properties. Moreover, we have used Karlsruhe valence triple- $\xi$  valence basis sets augmented with double polarization functions (TZVPP) for C,

Ni and Cu,[14] or with the LANL2DZ combination of valence and ECP basis sets (Ag, Pd) in Chapter 2 [15].

### **1.3 Abiotic origin of adenine**

Deducing the mechanism of the abiotic origin of biomolecules on earth (1, 2) has always remained a fascinating but unsolved puzzle. Some have considered it too difficult for scientific study, because the direct evidence is long gone and we can only work by plausible inference. Although this a difficult problem to approach experimentally, a number of striking observations over the years have allowed the formulation of plausible scenarios for the prebiotic synthesis of various biomolecules. The starting materials for synthesis of these bio-molecules are considered to be simple organic compounds like hydrogen cyanide (HCN), cyanogen, cyanoacetylene etc., whose existence under natural and (potentially) prebiotic conditions has been demonstrated by numerous observations(48). A startling example is the abiotic synthesis of adenine (one of the four purine nucleobases present in DNA and RNA) in an abiogenic experiment from aqueous solution containing ammonia and hydrogen cyanide in 1960 [49,50]. Since 1961, several reaction pathways have been reported in literature to account for the formation of adenine in prebiotic earth condition [50, 51-57]. In this chapter we report for the first time the thermodynamically feasible step-by- step pathway for the formation adenine under prebiotic condition. The predictions are based on extensive computations of sequences of reaction steps along several possible mechanistic routes. H<sub>2</sub>O- or NH<sub>3</sub>-catalyzed pathways are more favorable than uncatalyzed neutral or anionic alternatives, and they may well have been the major source of adenine on primitive earth. This dissertation chapter is aimed to provide a more detailed understanding of some of the chemical processes involved in chemical evolution.



## 1.4 Activation of Molecular Dinitrogen

Because of the inertness of molecular nitrogen, its reduction and practicable activation of under mild condition remains a fundamental challenge to synthetic as well as to theoretical chemistry. Unlike the Haber-Bosch hydrogenation of  $N_2$  to give ammonia [58], which requires high pressure and high temperatures, nitrogenase enzymes activate dinitrogen under ambient conditions at transition metal (Fe/Mo, V)-sulfide cluster sites [59-62]. Metal complexes capable of cleaving the extremely robust dinitrogen triple bond are formed typically from low-valent early transition-metal precursors. Since the first discovery of a dinitrogen complex in 1965, inorganic and organo-metallic chemists have been key players in this area and have contributed much fundamental knowledge on structures, binding modes, and reactivity patterns Nature can do it easily; chemists should be able to achieve comparable success [63-80]. Lithium metal is exceptional, but it exemplifies the possibilities. Remarkably, lithium is the only metal that reacts slowly with  $N_2$  at room temperature and it even burns in a pure nitrogen atmosphere, leading finally to  $(NLi_3)_x$ . This dissertation chapter reports the study this remarkable reaction for the first time.

An extensive computational study which elucidates the mechanism of the ready reactions of  $N_2$  with various model clusters,  $Li_2$ ,  $Li_4$ ,  $Li_6$ , and  $Li_8$ , leading to stepwise NN cleavage and dinitrogen reduction,  $N_2^0$  to  $2 N_3^-$  is reported in the chapter. Eight lithium atoms are needed to cleave the triple bonded nitrogen completely. Moreover, we provide an explanation for the exceptional reactivity of  $N_2$  with Li, compared to the other alkali metals, e.g., Na and K. Li is a very strong reducing agent as its nitrides have the highest atomization energy, the shortest M-N bond distance, and the largest M-N charge separation as well as interaction energy. The detailed mechanism of the insertion of  $N_2$  into model lithium clusters, reported in here delineates the

general manner in which molecular nitrogen can be activated sequentially by electron transfer and bond elongation, to give a series of increasingly reduced complexes.

### 1. 5 One electron aromatics

The criteria for aromaticity, in case of neutral even-electron singlet species, are cyclic conjugation of  $(4n+2)$   $\pi$ -electron, stabilization by enhanced delocalization, bond lengths equalization, diatropic  $^1\text{H}$  NMR shift, large negative NICS [34-36]. However the concept was extended in Post-Huckel period and the concept of  $\sigma$ -aromaticity [37-39], double aromaticity [40], three dimensional aromaticity [41-44] were introduced. The extension of the concept of aromaticity to the odd-electron  $\pi$  systems may be considered questionable, as the first criterion for aromaticity is the presence of  $(4n + 2)$   $\pi$ -electron cyclic conjugation, thus not including odd electron systems. However, the second criterion refers to whether cyclic conjugation stabilizes or destabilizes a system, and this criterion is independent of whether there are an odd number of electrons. Similarly, geometric criteria and others may be applied to odd-electron systems. In practice, the question of aromatic or antiaromatic character of odd-electron  $\pi$  systems has been asked by some authors but not by others. Aromaticity in neutral free radical (cycloheptatrienyl radical) was considered explicitly by Vincow in 1971 [45]. A related question involving aromaticity in triplet state of even  $(4n\pi)$ -electron annulenes was pointed out by Baird in 1972 [46] and elaborated by Schleyer et al.[47]. Is it possible to have aromatic systems from delocalization of only *one* electron ( $3C-1e$ ,  $4C-1e$ )? Are one electron aromatics half as aromatic compared to the two electron singlet?

In this chapter, we evaluated the degree of electron delocalization by energetic, geometric and magnetic criteria for a multitude of theoretically designed two and three dimensional cationic, anionic and free radical “one electron aromatic” systems.\

### 1.6 Planar tetracoordinate carbon

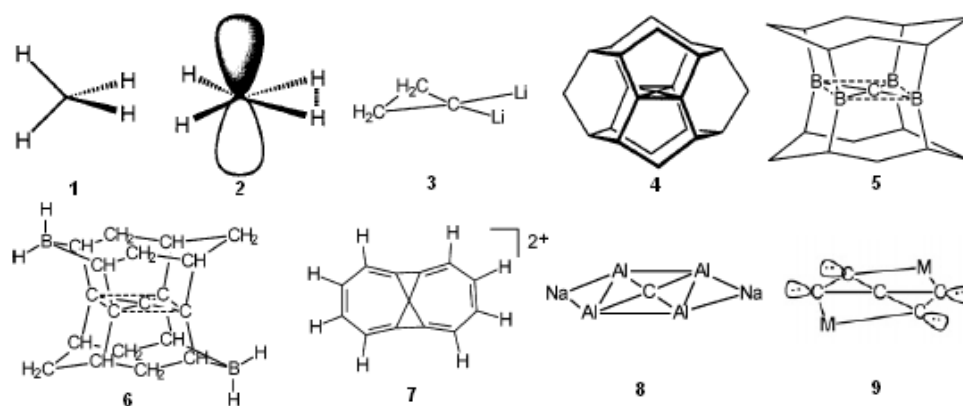


Figure 1-1. Example of theoretically designed molecules containing planar tetracoordinate carbon

In 1874, van't Hoff and LeBel postulated one of the most important paradigms of organic chemistry: the tetrahedral carbon atom, (**1**, Figure 1-1) [16, 17] Planar tetracoordinate carbon (ptC) alternatives were long thought to be too high in energy to be viable [18] until, in 1970, Hoffmann, Alder, and Wilcox formulated “electronic” strategies for reducing the relative energies of ptC structures [19]. The lone pair (**2**, Figure 1-1) can be stabilized by replacing one or more hydrogen atoms with good  $\sigma$ -donor/ $\pi$ -acceptor ligands or by incorporating the lone pair

into a  $(4n + 2) \pi$  delocalized system. In 1976, Schleyer and co-workers computed the energies of planar versus tetrahedral geometries of a remarkably extensive set of simple molecules [20]. Their systematic and extensive computational investigation led to the first example of a ptC molecule, 1,1-dilithiocyclopropane (**3**, Figure 1-1), by employing an additional “mechanical” strategy. Another approach for stabilizing a ptC is to impose geometrical constraints that force the central carbon atom and its nearest neighbors to be in a plane. This mechanical approach can be achieved by building a cage around the ptC (**4**, Figure 1-1), as it has been done in the alkapanes [21-23]. Although approaching a planar  $C(C)_4$ -type ptC more closely than ever before, such “mechanical” designs without “electronic” assistance must struggle hard to overcome the enormous strain of a ptC with a  $p-\pi$  lone pair HOMO. However, Wang and Schleyer found unique structures in the alkaplane family, with a set of boron bisubstituted spiroalkanes (**5**, Figure 1-1) with a  $ptC(C)_4$ , which is stabilized by both strategies, mechanical and electronic [24]. Using a novel charge-compensation strategy Wang and Schleyer designed for the first time structures (**6**, Figure 1-1) containing planar  $C(C)_4$  substructures [25]. Schleyer’s charge-compensation concept which favors anti-van’t Hoff geometry [26] stimulated further computational explorations (**7**, Figure 1-1)[27-29]. An interesting approach for designing new ptC molecules is to focus on small five-atom species, the smallest possible (pentaatomic) tetracoordinate planar carbon-containing molecules, with ligands different from carbon (**8**, Figure 1-1), were proposed by Boldyrev and Schleyer(SB) in 1991 [30]. In 2003 Vela et al. described the hypothetical dianion  $C_5^{2-}$  (the smallest carbon skeleton) as the leading structural entity for formation of neutral (and charged) molecules (**9**, Figure 1-1) with a planar tetracoordinate carbon [31]. The 1991 SB computational predictions were verified

experimentally by the detection of the isoelectronic anions,  $\text{CAI}_3\text{Si}^-$  [32] and the closely related  $\text{NaCAI}_4^-$  [33].

In this dissertation, we report another design strategy where planar tetracoordinate carbons (ptC's) can be stabilized by four-membered ring perimeters composed of four bare transition metal atoms. The molecular orbitals, electronic structures, energies, and magnetic properties of these  $\text{CM}_4$  species (where M represents isoelectronic combinations of Cu, Ni, Ag, and Pd) reveal striking similarities with main group metal ptC analogues (e.g.,  $\text{CAI}_2\text{Si}_2$ ,  $\text{CAI}_4\text{Na}^-$ , and  $\text{C}_5\text{Li}_2$ ). While the  $\text{CCu}_4^{2+}$ ,  $\text{CAg}_4^{2+}$ , and  $\text{CNiCu}_3^+$  ions have the largest HOMO-LUMO separations,  $\text{CCu}_4^{2+}$  is the best candidate for detection by gas-phase photoelectron spectroscopy.

## 1. 7 Reference

- 1) Gill, P. M. W. In *The Encyclopedia of Computational Chemistry*; Schleyer, P. v. R., Allinger, N. L., Clark, T., Gasteiger, J., Kollman, P. A., Schaefer III, H. F., Schreiner, P. R., Eds.; John Wiley & Sons: Chichester, 1998; pp 678-689.
- 2) Foresman, J. B.; Frisch, A. E. *Exploring Chemistry with Electronic Structure Methods*; 2nd. ed.; Gaussian, Inc.: Pittsburgh, 1996.
- 3) Hu, C.-H.; Chong, D. P. In *The Encyclopedia of Computational Chemistry*; Schleyer, P. v. R., Allinger, N. L., Clark, T., Gasteiger, J., Kollman, P. A., Schaefer III, H. F., Schreiner, P. R., Eds.; John Wiley & Sons: Chichester, 1998; pp 664-678.
- 4) Koch, W.; Holthausen, M. C. *A Chemist's Guide to Density Functional Theory*; Wiley-VCH: Weinheim, 2000.
- 5) Bartlett, R. J.; Watts, J. D.; Kucharski, S. A.; Noga, J. *Chem. Phys. Lett.* **1990**, *165*, 513-522.

- 6) Gauss, J. In *The Encyclopedia of Computational Chemistry*; Schleyer, P. v. R., Allinger, N. L., Clark, T., Gasteiger, J., Kollman, P. A., Schaefer III, H. F., Schreiner, P. R., Eds.; John Wiley & Sons: Chichester, 1998; pp 688-701. 22
- 7) Raghavachari, K.; Trucks, G. W.; Pople, J. A.; Head-Gordon, M. *Chem. Phys. Lett.* **1989**, *157*, 479-483.
- 8) Clark, T.; Chandrasekhar, J.; Spitznagel, G. W.; Schleyer, P. v. R. *J. Comput. Chem.* **1983**, *4*, 294.
- 9) Spitznagel, G. W.; Clark, T.; Chandrasekhar, J.; Schleyer, P. v. R. *J. Comput. Chem.* **1982**, *3*, 363.
- 10) Spitznagel, G. W.; Clark, T.; Schleyer, P. v. R.; Hehre, W. J. *J. Comput. Chem.* **1987**, 1109.
- 11) Dunning Jr., T. H. In *The Encyclopedia of Computational Chemistry*; Schleyer, P. v. R., Allinger, N. L., Clark, T., Gasteiger, J., Kollman, P. A., Schaefer III, H. F., Schreiner, P. R., Eds.; John Wiley & Sons: Chichester, 1998; Vol. 1, pp 88-114.
- 12) Szabo, A.; Ostlund, N. S. *Modern Quantum Chemistry*; Macmillan: New York, 1982.
- 13) Schleyer, P. v. R.; Allinger, N. L.; Clark, T.; Gasteiger, J.; Kollman, P. A.; Schaefer III, H. F.; Schreiner, P. R. *The Encyclopedia of Computational Chemistry*; John Wiley & Sons. Ltd.: Chichester, 1998.
- 14) Weigend, F.; Ahlrichs, R. *Phys. Chem. Chem. Phys.* **2005**, *18*, 3297.
- 15) Hay, P. J.; Wadt, W. R. *J. Chem. Phys.* **1985**, *82*, 299.
- 16) van't Hoff, J. H. *Arch. Neerl. Sci. Exactes Nat.* 1874, 445.
- 17) LeBel, J. A. *Bull. Soc. Chim. Fr.* 1874, 22.
- 18) Monkhorst, H. J. *J. Chem. Soc., Chem. Commun.* **1968**, 1111.

- 19) Hoffmann, R.; Alder, R. W.; Wilcox, C. F. *J. Am. Chem. Soc.* **1970**, 92, 4992.
- 20) Collins, J. B.; Dill, J. D.; Jemmis, E. D.; Apeloig, Y.; Schleyer, P. v. R.; Seeger, R.; Pople, J. A. *J. Am. Chem. Soc.* **1976**, 98, 5419.
- 21) McGrath, M. P.; Radom, L. *J. Am. Chem. Soc.* **1993**, 115, 332.
- 22) Rasmussen, D. R.; Radom, L. *Angew. Chem., Int. Ed.* **1999**, 38, 2876.
- 23) Rasmussen, D. R.; Radom, L. *Chem. Eur. J.* **2000**, 6, 2470.
- 24) Wang, Z.X.; Schleyer, P. v. R. *J. Am. Chem. Soc.* **2001**, 123, 994.
- 25) Wang, Z. X.; Schleyer, P. v. R. *J. Am. Chem. Soc.* **2002**, 124, 11979.
- 26) Lammertsma, K.; Schleyer, P. v. R. *J. Phys. Chem.* **1988**, 92, 881.
- 27) Priyakumar, U. D.; Reddy, A. S.; Sastry, G. N. *Tetrahedron Lett.* **2004**, 45, 2495.
- 28) Priyakumar, U.; Sastry G. N. *Tetrahedron Lett.* **2004**, 45, 1515.
- 29) Esteves, P. M.; Ferreira, N. B. P.; Correa, R. J. *J. Am. Chem. Soc.* **2005**, 127, 8680.
- 30) Schleyer, P. v. R.; Boldyrev, A. I. *J. Chem. Soc., Chem. Commun.* **1991**, 1536.
- 31) Merino, G.; Mendez-Rojas, M. A.; Vela, A. *J. Am. Chem. Soc.* **2003**, 125, 6026.
- 32) Boldyrev, A. I.; Simons, J. *J. Am. Chem. Soc.* **1998**, 120, 7967.
- 33) Li, X.; Zhang, H.F.; Wang, L.S.; Geske, G. D.; Boldyrev, A. I. *Angew. Chem., Int. Ed.* **2000**, 39, 3630.
- 34) A. D. Allen, T. T. Tidwell, *Chem. Rev.* **2001**, 101, 1333.
- 35) Z. Chen, C. S. Wannere, C. Corminboeuf, R. Puchta, P. von R. Schleyer, *Chem. Rev.* **2005**, 105, 3842;
- 36) P. von R. Schleyer, *Chem. Rev.* **2005**, 105, 3433.
- 37) M. J. S. Dewar, *Bul. Soc. Chim. Belg.* **1979**, 88, 957.
- 38) M. J. S. Dewar; M. L. McKee, *Pure Appl. Chem.* **1980**, 52, 1431.

- 39) M. J. S. Dewar, *J. Am. Chem. Soc.* **1984**, *106*, 669.
- 40) J. Chandrasekhar, E. D. Jemmis, P. von R. Schleyer, *Tetrahedron Lett.* **1979**, 3707. This paper coined the terms “double aromaticity” and “in-plane aromaticity”.
- 41) J. Aihara, *J. Am. Chem. Soc.* **1976**, *98*, 2750. This paper coined the term three-dimensional aromaticity.
- 42) J. Aihara, *Inorg. Chem.* **2001**, *40*, 5042.
- 43) E. D. Jemmis,; P. von R. Schleyer, *J. Am. Chem. Soc.* **1982**, *104*, 4781.
- 44) R. B. King, *Chem. Rev.* **2001**, *101*, 1119 and references therein.
- 45) G. Vincow, In *Aromaticity, Pseudo-aromaticity, and Anti-aromaticity*; Bergmann, E. D., Pullman, B., Eds.; Academic Press: New York, 1971; pp 336-347.
- 46) N. C. Baird, *J. Am. Chem. Soc.* **1972**, *94*, 4941-4948.
- 47) V. Gogonea, P. von R. Schleyer, P. R. Schreiner, *Angew Chem., Int. Ed. Engl.* **1998**, *37*, 1945-1948.
- 48) A. Eschenmoser, E. Loewenthal, *Chem. Soc. Rev.*, 1992, 1-16.
- 49) J. Oró. *Biochem. Biophys. Res. Commun.* **2**, 407-412 (1960).
- 50) J. Oró. 1961. *Nature* **191**, 1193.
- 51) J.P. Ferris, R.A. Sanchez, L.E. Orgel, *J. Mol. Biol.* **33**, 693 (1968).
- 52) M. Levy, S.L. Miller, J. Oró, *J. Mol. Evol.* **49**, 165-168 (1999).
- 53) J. P. Ferris, P. C Joshi, E. H. Edelson, J. G. Lawless, *J. Mol. Evol.* **11**, 293–311 (1978).
- 54) R. F. Shuman, W. E. Shearin, R. J. Tull, *J. Org. Chem.* **44**, 4532–4536 (1979).
- 55) A. B. Voet, A. W Schwartz, *Bioorg. Chem.* **12**, 8–17 (1983).
- 56) G. Zubay, T. Mui, *Orig. Life Evol. Biosph.* **31**, 87-102 (2001).
- 57) E.C. Taylor, C.C. Cheng, *Tetrahedron letters*, **12**, 9 (1959).



- 58) V. Smil, *Enriching the Earth* (The MIT Press, Cambridge, MA, 2001).
- 59) M. Hidai, *Coord. Chem. Rev.***1999**, *85*, 99-108.
- 60) G. J. Leigh, *Acc. Chem. Res.* **1992**, *25*, 177-181.
- 61) R. R. Eady, *Chem. Rev.* **1996**, *96*, 3013-3030.
- 62) B. A. MacKey, M. D. Fryzuk, *Chem. Rev.***2004**, *104*, 385–401 and references there in.
- 63) G. V. Chertihin , L. Andrews, C. W. Bauschlicher, *J. Am. Chem. Soc.* **1998**, *120*, 3205-3212.
- 64) G. V. Chertihin, W. D. Bare, L. Andrews, *J. Phys.Chem.A.***1998**, *102*, 3697-3704.
- 65) A. Citra, L. Andrews, *J. Am.Chem. Soc.* **1999**, *121*, 11567-11568.
- 66) H. J. Himmel, O. Hubner, W. Kloppe, L. Manceron, *Angew. Chem. Int. Ed.* **2000**. *45*, 2799- 2802.
- 67) E. E. Tamelen, G. Boche, S. W. El, R. B. Fechter, *J. Am. Chem. Soc.*, **1967**, *89*, 5707.
- 68) N. Kuganathan, J. C. Green, H. J. Himmel, *New J. Chem.* **2006**, *30*, 1253-1261.
- 69) M.F. Zhou, X. Jin, Y. Gong, J. Li, *Angew. Chem. Int. Ed.***2007**. *46*, 2911 –2914.
- 70) H. J. Himmel, M. Reiher, *Angew. Chem. Int. Ed.* **2006**, *45*, 6264-6288.
- 71) V. Bonačić-Koutecký, P. Fantucci, J. Koutecký, *Chem. Rev.* **1991**, *91*, 1035.
- 72) J. Li, and S. Li, *Angew. Chem. Int. Ed.* **2008**, *47*, 8040- 8043.
- 73) J. A. Pool, E. Lobkovsky, P. J. Chirik, *Nature* **2004**, *427*, 527–530.
- 74) L. P. Spencer, B. A. MacKay, B. O. Patrick, M. D. Fryzuk, *Proc. Natl. Acad. Sci. U.S.A.* **2006**, *103*, 17094–17098.
- 75) F. Akagi, T. Matsuo, H. Kawaguchi, *Angew. Chem., Int. Ed.* **2007**, *46*, 8778–8781.
- 76) R. R. Schrock, *Angew. Chem. Int. Ed.*,**2008**, *47*, 5512 – 5522.
- 77) S. Gambarotta, J. Scott, *Angew. Chem. Int. Ed.*, **2004**, *43*, 5298 –5308.

- 78) M. D. Fryzuk, *Acc. Chem. Res.*, **2009**, 42 (1), 127-133.
- 79) S. Schenk, M. Reiher, *Inorg. Chem.*, **2009**, 48 (4), 1638-1648.
- 80) S. Gambarotta, *J. Organomet. Chem.* **1995**, 500, 117–126.

CHAPTER 2

CHEMICAL EVOLUTION: THE MECHANISM OF THE FORMATION OF ADENINE  
UNDER PREBIOTIC CONDITIONS\*

---

\* Roy, D., Najafian, K., Schleyer, P. v. R. (2007). *Proc. Natl. Acad. Sci. U.S. A.* 104, 17272-17277

Reproduced in part by permission of copyright (2007) National Academy of Sciences, U.S.A and Roy,D, Schleyer, P. v. R , Matta C. *Quantum Biochemistry: Electronic Structure and Biological Activity*,2009 (in press).Copyright Wiley-VCH Verlag GmbH & Co. KGaA. Reproduced in part with permission.

## 2.1 Abstract

Fundamental building blocks of life have been detected extra-terrestrially, even in interstellar space, and are known to form non-enzymatically. Thus, the HCN pentamer, adenine (a nucleic acid present in DNA and RNA), was first isolated in abiogenic experiments from an aqueous solution of ammonia and HCN in 1960. Although many variations of the reaction conditions giving adenine have been reported subsequently, the mechanistic details remain unexplored. Our predictions are based on extensive computations of sequences of reaction steps along several possible mechanistic routes.  $\text{H}_2\text{O}$  or  $\text{NH}_3$  catalyzed pathways are more favorable than uncatalyzed neutral or anionic alternatives, and may well have been the major source of adenine on primitive earth. Our report provides a more detailed understanding of the some of chemical processes involved in chemical evolution, and a partial answer to the fundamental question of molecular biogenesis. Our investigation should trigger similar explorations of the detailed mechanisms of the abiotic formation of the remaining nucleic acid bases as well as other biologically relevant molecules.

## 2.2 Introduction

Experiments show that simple molecules combine under prebiotic conditions to give the fundamental building blocks of life – amino acids, nucleotides, carbohydrates and other essential compounds. However, the origin of even the simplest of these biomolecules remains a fascinating but unsolved puzzle[1, 2]. They could have formed from smaller molecules present on primitive earth, either very slowly over millions of years, or rapidly before the earth cooled down. Asteroids may have brought them from outer space. This chapter provides a detailed examination of the chemical processes involved in the genesis of adenine, one of the four

building blocks of DNA, and an abundant biochemical molecule found on earth. First we mention a chronology of research in prebiotic chemistry, followed by the details on the experiments which led to the detection of biomolecules under simulated prebiotic conditions. We then elucidate the quantum chemical investigation for a thermodynamically viable, step by step pathway, for the formation of adenine under prebiotic conditions.

### 2.2.1 Prebiotic chemistry: Experimental endeavor to synthesize the building blocks of biopolymers

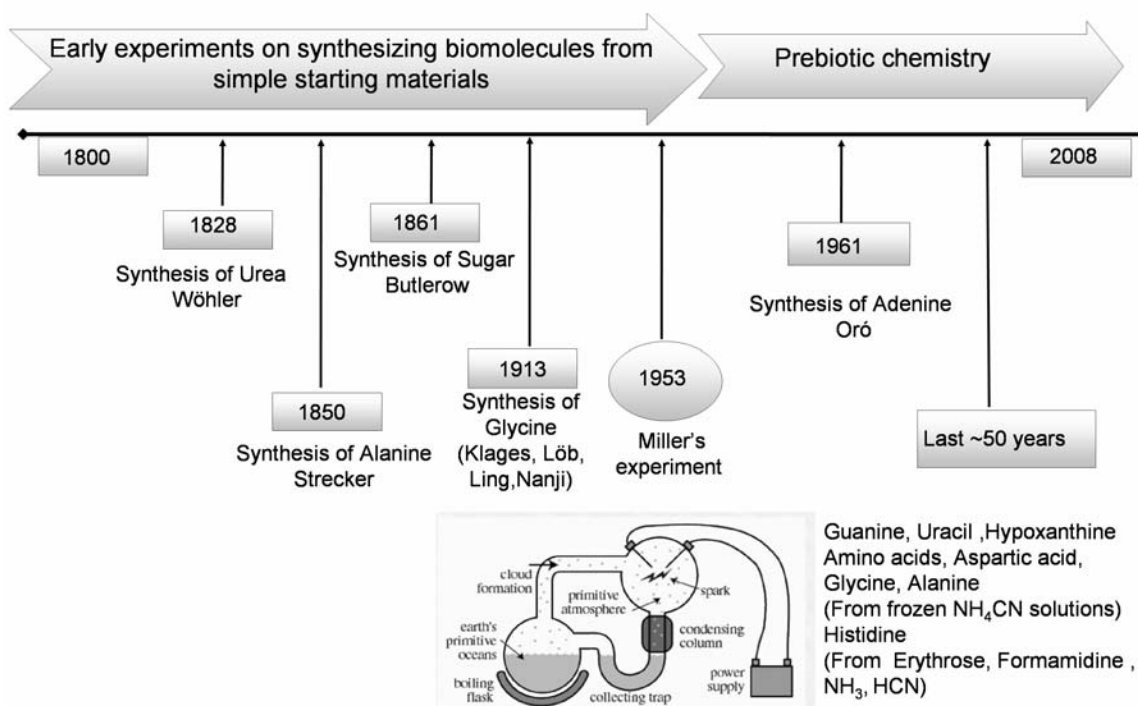


Figure 2-1. The progress in prebiotic chemistry for last two centuries.

In 1828, F. Wöhler reported the first chemical synthesis of a simple organic molecule (urea) from inorganic starting materials (silver cyanate and ammonium chloride)[3]. Wöhler's work led to a new era in prebiotic chemistry. Figure 2-1 demonstrates the occurrences of these research milestones in a somewhat chronological order. The first observations relating to the prebiotic

syntheses of ribose date back to 1861 when Butlerow showed that sugars could be made by mild heating of formaldehyde in the presence of  $\text{Ca}(\text{OH})_2$  catalyst ; this became known as the formose reaction [4].

By the end of the nineteenth century, a large amount of research on organic synthesis had been performed which lead to the abiotic formation of fatty acids and sugars using electric discharges with various gas mixtures [5]. This work was continued into the twentieth century by Löb, Baudish, and others on the synthesis of amino acids by exposing wet formamide ( $\text{HCONH}_2$ ) to a silent electrical discharge [6] and to UV light [7]. This efforts heralded the dawn of prebiotic chemistry (Figure 2-1).

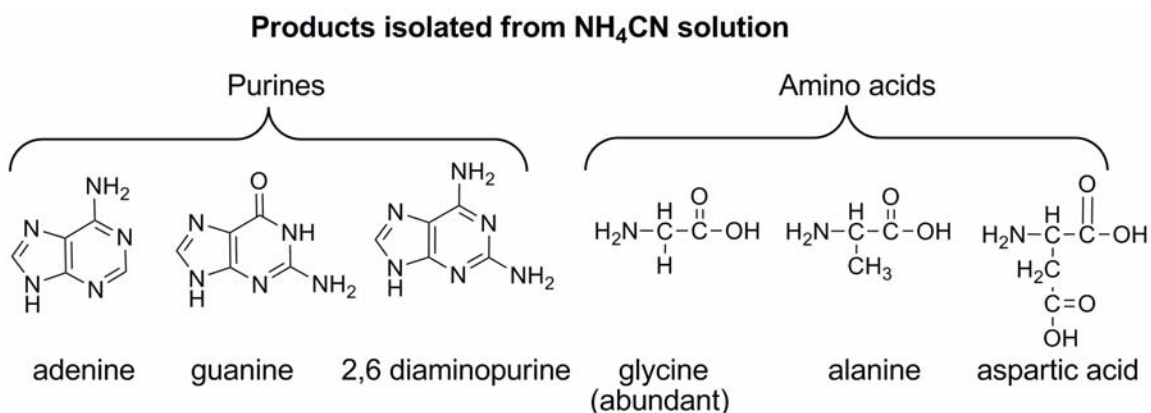


Figure 2-2. Products isolated from HCN in water-ammonia solution.

It was not until 1953, that the first successful synthesis of organic compounds under plausible *primordial conditions* was accomplished, by electric discharges acting for a week on a mixture of  $\text{CH}_4$ ,  $\text{NH}_3$ ,  $\text{H}_2$  and  $\text{H}_2\text{O}$ ; racemic mixtures of several protein amino acids were produced, as well as hydroxy acids, urea and other organic molecules [8,9]. Miller's first paper on the formation of amino acid under possible primitive earth condition was published only a few weeks after Watson and Crick reported their DNA double-helix model in *Nature*. The link

between the two nascent fields began to develop a few years later, when Juan Oró demonstrated the remarkable ease by which adenine, one of the nucleobases in DNA and RNA, could be produced through the oligomerization of hydrogen cyanide under basic conditions[10,11,12]. In 1968, Orgel *et al.* showed that cyanoacetylene is a major product of action of electric discharge on a mixture of methane and nitrogen, and that cyanoacetylene is a possible source of the pyrimidine bases, uracil and cytosine [13]. Purines like adenine[14], guanine[15], uracil[16], and hypoxanthine[17] have been detected in concentrated ammonium cyanide ( $\text{NH}_4\text{CN}$ ) solution after acid hydrolysis (Figure 2-2). Some pyrimidine derivatives, such as orotic acid, 5-hydroxyuracil and 4,5 dihydroxypyrimidine, along with adenine, were detected in a solution of 0.1 M  $\text{NH}_4\text{CN}$  kept for 4-12 months after neutral or acid hydrolysis [18].

Amino acids alanine, glycine and aspartic acid were identified among the products formed by the condensation of hydrogen cyanide in aqueous ammonia [18, 19, 20, 21, 22, 23]. Histidine, a basic amino acid containing an imidazole group, was synthesized from erythrose and formamidine through condensation reaction and a Strecker synthesis without the isolation of any intermediate [24]. The precursor molecules (erythrose , formamidine, hydrogen cyanide , and ammonia ) used for the synthesis of histidine are all considered to be prebiotic compounds. A recent noteworthy achievement should be mentioned which concludes this section on a very exciting note. The 1953 Miller-Urey Synthesis had two sibling studies, neither of which was published. Vials containing the products from those experiments were recently recovered and reanalyzed using modern technology and the results are reported in *Science*![25] Miller identified five amino acids: aspartic acid, glycine, alpha-amino-butyric acid, and two versions of alanine. The 11 vials scientists recovered from the unpublished aspirator experiment, however,

produced 22 amino acids and the same five amines at yields comparable to the original experiment [25].

### **2.2.2 The key role of HCN as a precursor for prebiotic compounds**

Due to its high degree of unsaturation, HCN is an energy rich, reactive molecule, which undergoes addition reactions exothermically. This high energy prebiotic precursor is produced in appreciable amounts, for example, by the action of electric discharge on simulated prebiotic atmosphere [26]. Aqueous solutions of cyanides are frequently used in experiments related to prebiotic chemistry. It is remarkable how some of HCN's reactions appear to aim at "bio-molecular building blocks." Similar processes are expected in present planetary environment, such as Titan [27-29] Europa, [20, 30-32] Ganymede and Callisto [33,34], but in the absence of liquid water, due to abundance of CN group containing molecules the interstellar space [35], in comets [36,37], and in the atmosphere of Titan [27, 38].

### **2.3 Prebiotic experiments and proposed pathways for the formation of adenine**

The HCN pentamer, adenine (a constituent of DNA, RNA and many coenzymes), is one of the most abundant biochemical molecules. The synthesis of adenine from hydrogen cyanide in water-ammonia systems under conditions assumed to have existed on prebiotic earth, first demonstrated by Oró in 1960 [10-12,21], is so remarkable that we believe it to have some relevance to the prebiotic accumulation of purines. In Oró's experiment, adenine was formed in 0.5% yield by heating solutions of ammonium cyanide (>1.0 M) at 70°C for several days. Since then, the abiotic synthesis of adenine from the polymerization of HCN under various conditions has been achieved many times [11, 13, 39- 43]. Adenine also has been obtained in a very high



yield (20% ) by heating HCN with liquid ammonia in a sealed tube [44]. In 1978 Ferris et al. detected 0.04% adenine from 0.1 M  $\text{NH}_4\text{CN}$  kept in dark at room temperature for 4-12 months [45]. In order to simulate prebiotic synthetic processes on Europa and other ice-covered planets and satellites, Levy et al. have investigated the prebiotic synthesis of organic compounds from dilute solutions of  $\text{NH}_4\text{CN}$  frozen for 25 years at  $-20$  and  $-78^\circ\text{C}$  [30]. They found that both adenine and guanine, as well as a simple set of amino acids dominated by glycine, are produced in substantial yields under these conditions[30]. Moreover, Since 1961, several reaction pathways have been reported in literature to account for the formation of adenine in prebiotic earth condition (Figure. 4-3) [11, 13, 39- 43].

However, the puzzle: “how do five HCN molecules combine to form adenine under prebiotic conditions?” remained unsolved. An ab initio mechanistic investigation of the HCN dimerization and an adenine protonation study do shed some light on the problem [46, 47]. We are the first research group to systematically investigate the step-by-step mechanisms for the oligomerization of HCN, by applying quantum-chemical methods and propose a viable route for formation of adenine in prebiotic earth condition [48]. Rainer Glaser et al. published a parallel research, in the journal *Astrobiology*, which also sheds light on the abiotic origins of adenine, although from a different perspective [49].



## 2.4 Computational investigation

Experimental investigation for a thermodynamically feasible pathway for the formation of adenine under prebiotic conditions would be very difficult, since adenine is not formed cleanly, yields are small, and many steps are involved. Some have considered it too difficult for scientific study, because the direct evidence is long gone and we can only work by plausible inference. Quantum chemical methods appear to be a powerful tool to study the structure and behavior of molecules related to prebiotic origin of life. Reaction mechanisms involving several intermediates and transition states (which are difficult to detect and identify experimentally) can be studied effectively computationally. These allow selection among various possibilities. Furthermore, quantum chemical study is more advantageous since interstellar or prebiotic conditions (solvation and high temperature, for instance) are implicitly considered in calculations using the quantum chemical techniques. In case of adenine, although this a difficult problem to approach, a number of striking observations over the years have allowed the formulation of plausible scenarios for its prebiotic synthesis. Clues for finding a viable pathway are provided by four putative intermediates detected in the product mixtures (Figure.4-3): formamidine, diaminomaleonitrile (DAMN), 4-amino-5-cyanoimidazole (AICN) [13, 39, 41-43] and 4-aminoimidazole-5-carboxamidine (AICA)[12,39]. We propose a possible mechanism for prebiotic synthesis of adenine with calculated low energy barriers, where solvent participation is important, especially of the first H<sub>2</sub>O or ammonia molecule. (based on density functional theory (DFT) computations described in the method section)[50].

### 2.4.1 Methods

The computations were performed at the B3LYP level of theory using 6-31G and 6-311+G\*\* basis sets. Also results CCSD (T) (ab initio) theory have been reported where necessary (simulated the first HCN + RNH<sub>2</sub> addition step with the highest barrier). Stable structures and transition states were fully optimized at the mentioned level. All critical points were further characterized by analytic computations of harmonic vibrational frequencies at the same level/basis set. Transition states have been characterized by one imaginary frequency (first order saddle point) on the Potential Energy Surface (PES). Intrinsic Reaction Coordinate (IRC) analysis was performed to determine the Minimum Energy Pathways (MEPs) at the mentioned level of theory. Transition states were found to connect proper reactants and products. Vibrational frequencies were calculated within the harmonic approximation at the same level of theory as for geometries. The reaction barriers are defined as the difference in sum of electronic and zero-point energies ( $\epsilon_0 + \epsilon_{\text{ZPE}}$ ) of the reactant-complex and transition state.  $\Delta G$  is defined as difference between the sum of electronic and thermal free energies ( $\epsilon_0 + G_{\text{corr}}$ ) of reactant and product.

Instead of modelling bulk solvation by an explicit shell involving many solvent molecules surrounding the solute [51] we employed the polarizable continuum model (PCM) implemented in the Gaussian 98 program [52]. The PCM “bulk solvent medium” is simulated as a continuum of dielectric constant  $\epsilon$ . This surrounds a solute cavity, which is defined by the union of a series of interlocking spheres centered on the atoms. Our computed single-point PCM bulk solvent simulations employed the optimized equilibrium geometries. We have added an estimated ~2.5 kcal/mol ZPVE correction to the single-point PCM energy. The derivation of this corrected

energy value is given in notes [53]. More sophisticated solvation treatments are not called for in the absence of experimental data.

## 2.5 Thermochemistry of pentamerization of Adenine

The pentamerization of HCN to give adenine is very exothermic overall ( $\Delta G_{298} = -53.7$  kcal/mol Figure. 4-4). Likewise, each successive step, HCN dimerization as well as the sequential HCN additions to give trimer, tetramer, and pentamer, also is quite exothermic. But a favorable thermochemistry does not insure that reactions actually will proceed, since they may be prevented by insurmountable kinetic impediments.

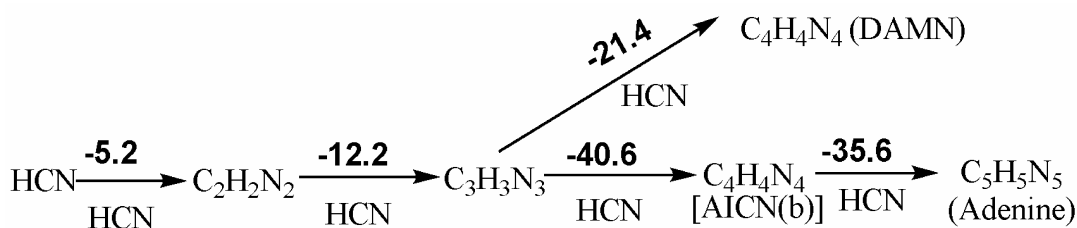


Figure 2-4. Thermochemistry of pentamerization of HCN. The relative energies in gas phase are in kcal/mol computed at B3LYP/6-311+G\*\*+ZPVE. Entropy is unfavorable, but is not considered. Note that the last crucial step for formation of pentamer (adenine) from tetramer [AICN (b)] is highly exothermic. Overall energy for pentamerization of adenine (5 HCN  $\rightarrow$  C<sub>5</sub>H<sub>5</sub>N<sub>5</sub>) is 93.8 kcal/mol [ $\Delta G^{298} = 53.7$  kcal/mol].

## 2.6 Thermodynamically viable step by step mechanism

### 2.6.1. DAMN vs AICN as adenine precursors

We focus here on the last, crucial stage, the reaction of the HCN tetramer, AICN, with a fifth HCN to give adenine. This is the key, rate-limiting step in the general adenine formation pathway starting from HCN (see Figure. 4-4). Although DAMN and AICN are both C<sub>4</sub>H<sub>4</sub>N<sub>4</sub>

isomers, AICN was selected as the adenine precursor because of its much lower energy (19.3 kcal/mol according to our computations) and greater structural similarity to adenine (Figure. 4-5). Like adenine, AICN has a C-C-C-N sequence, whereas DAMN has a C-C-C-C backbone not present in adenine (Figure. 4-5). DAMN may form experimentally as a kinetically-controlled side product. While DAMN cannot be involved directly in the pathway, it may serve as a

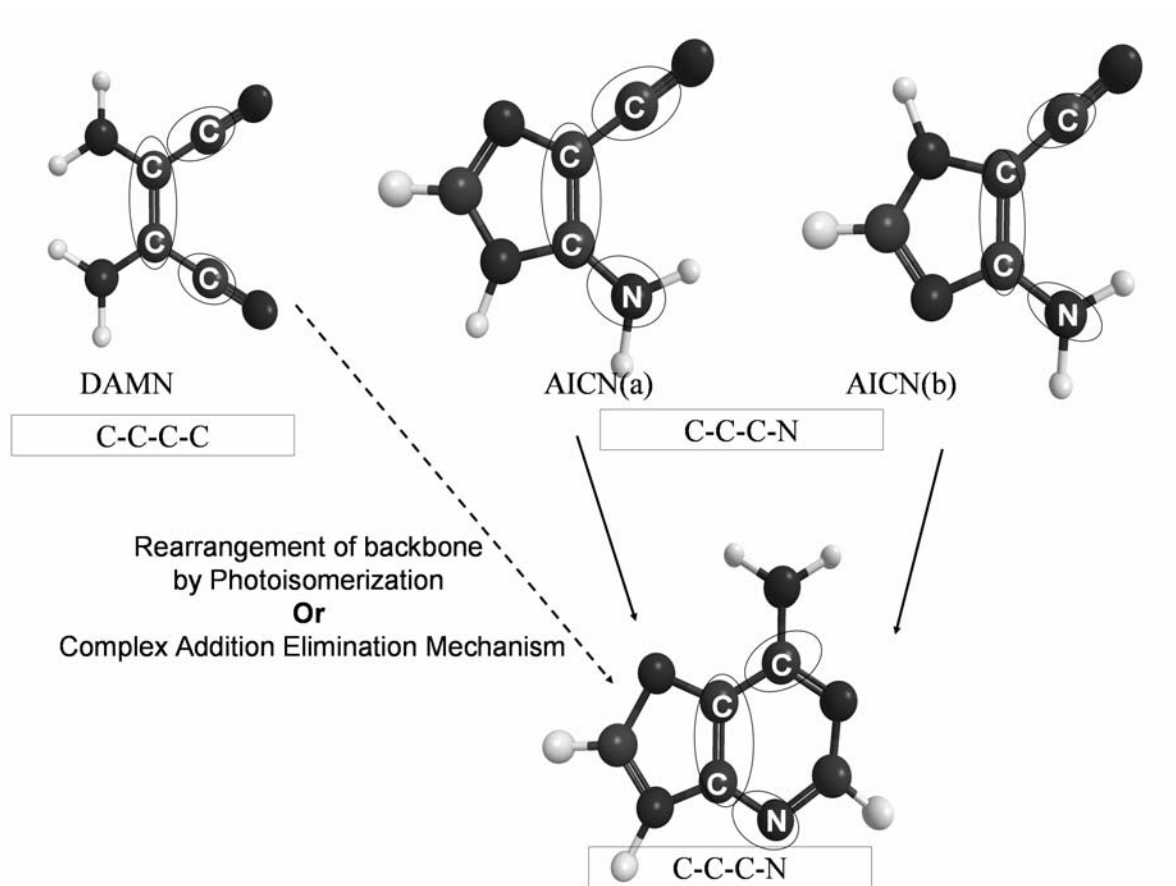


Figure 2-5. DAMN and AICN are both  $C_4H_4N_4$  isomers. Like adenine, both AICN (a) and (b) has a C-C-C-N sequence, whereas DAMN has a C-C-C-C backbone not present in adenine.

“material reservoir.” Indeed, many details of photo-isomerization of DAMN to AICN in water are established [39, 41]. In contrast, the non-photolytic conversion of DAMN to AICN or to adenine has not been observed [42]. We describe our investigation of the mechanism for adenine formation from AICN under non-photochemical conditions (reactions in the dark) here.

### **2.6.2 Is anionic mechanism feasible in isolation?**

An anionic mechanism for the abiotic formation of adenine seems plausible from a physical organic chemist’s point of view. HCN is a weak acid and adenine forms in ammoniacal solution. However, mechanisms involving unsolvated anionic species proved not to be feasible computationally! [54] Ring closure (ii  $\rightarrow$  iii, Figure 2-6) is precluded since the putative anionic intermediates ii and iii are not minima; iii reverts back to the ring-opened isomers on optimization. Mechanisms involving free radical intermediates also were unpromising. In contrast, optimizations of the reactant, product and transition states for the neutral closed-shell mechanism were successful. However, the first step of addition of HCN to the  $\text{NH}_2$  group of AICN proceeds via a four center transition state and has a prohibitively high gas phase activation barrier relative to those of the 1:1 (HCN) (AICN) complex (60.4 kcal/mole) (Figure. 4-6). Moreover, an intermediate step for neutral uncatalyzed mechanism (the concerted six membered ring closure and H transfer step) also has a huge in reaction barrier (53 kcal/mole (Figure. 4-6). Therefore, the neutral uncatalyzed mechanism can also be ruled out as a possibility for the formation of adenine.

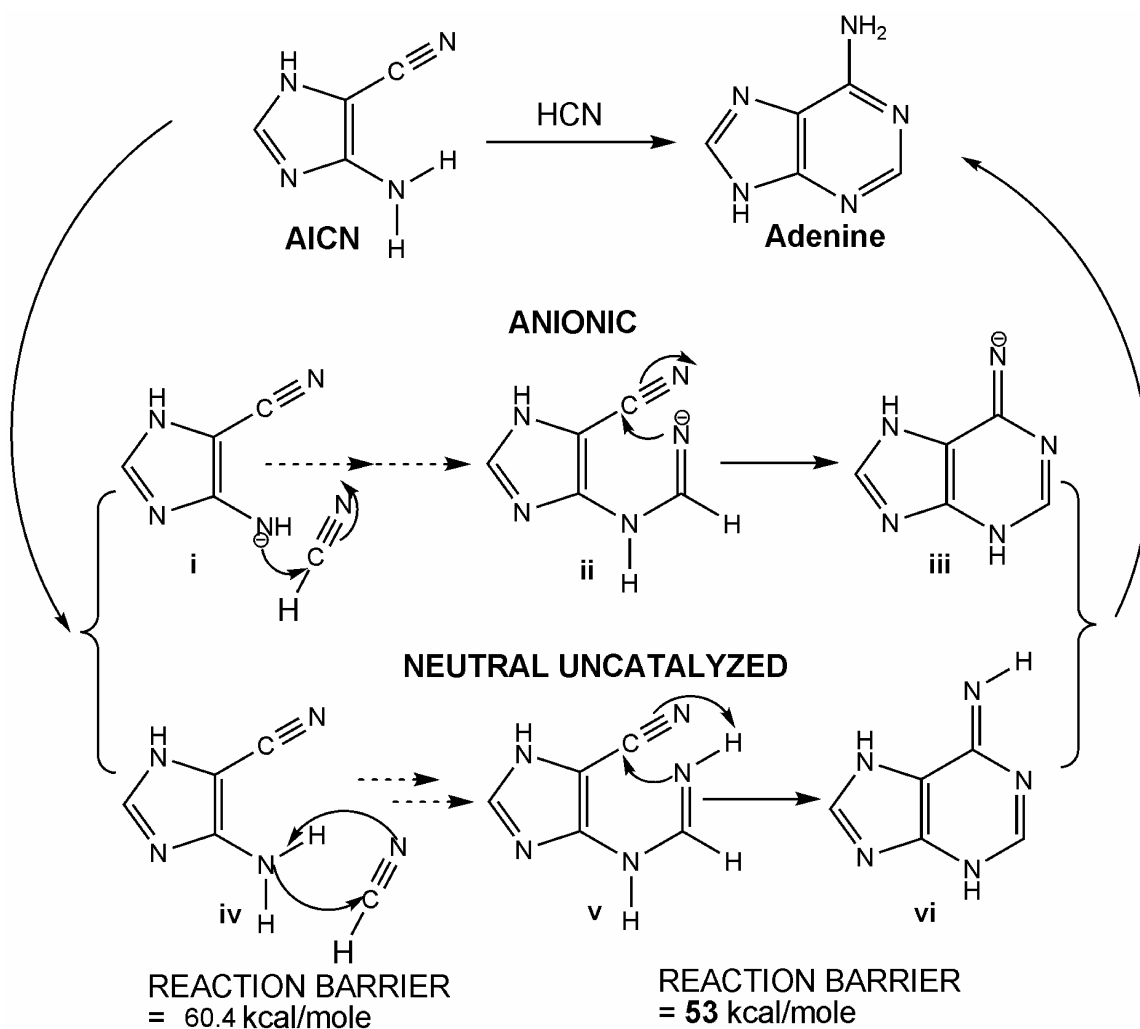


Figure 2-6. Anionic mechanisms are unfeasible in isolation. Upon optimization both ii and iii revert back to i (reactants). Free radical as well as neutral *uncatalyzed* mechanisms are also not viable due to the very large reaction barriers for the two steps shown.



Tautomerization of imidazoles is indeed known, but not the relative energies of the AICN isomers. We first point out explicitly, that two AICN tautomeric forms, AICN(a) and AICN(b) (Figure. 4-3), can exist and that the latter is favored strongly at equilibrium (by  $\Delta G^{298} = 3.73$  kcal/mol in the gas phase and 1.73 kcal/mol with bulk solvation ) [48]. Since the energetically more favorable isomer AICN (b) is not the one assumed in pathways proposed by

experimentalists, we explicitly called attention to the structures and energies of both isomers. The pathway to adenine from the less stable AICN(a) is precluded by the second high reaction barrier (41.6 kcal/mol) associated with the six-membered ring closure step. The reaction profile is depicted in Figure. 4-7. Note that the reaction barriers are reported with a smaller basis set, 6-31G\*. Since we did not consider this pathway to be the viable one, we believe that this is sufficient to explain the qualitative nature of the pathway.

The favorable mechanism of adenine formation starting from the thermodynamically more stable AICN(b) tautomer is reported here. The first step of addition of HCN to the NH<sub>2</sub> group of AICN(b) proceeds via a four centered transition state (TS0) and has a high activation barrier relative to those of the 1:1 (HCN) (AICN) complex (60.4 kcal/mole)(Figure. 4-6 and Figure. 4-8) Moreover, a prohibitive reaction barrier (53 kcal/mol) also precludes a subsequent step in the neutral uncatalyzed pathway (involving the concerted six-membered ring closure and H transfer, Figure. 4-6). The reaction barriers are much too high for this neutral uncatalyzed pathway to be viable for adenine formation at room temperature or below. The involvement of additional molecules serving as catalysts is required to lower the high barriers.

The unfavorable four-center transition structure (TS0) associated with the first step from AICN(b) is shown in Figure. 4-8. The catalytic participation of a water molecule in the six-center alternative (TS1) reduces the barrier considerably (ammonia or similar molecules can function similarly). The importance of water-assisted proton transfer is well known in keto-enol tautomerization [55,56]. The water bridge connects the donor and acceptor sites and stabilizes the transition structure. The classical proton transfer barrier is lowered substantially. The energetically most favorable six-center cyclic transition structure leading to the HCN-AICN(b)

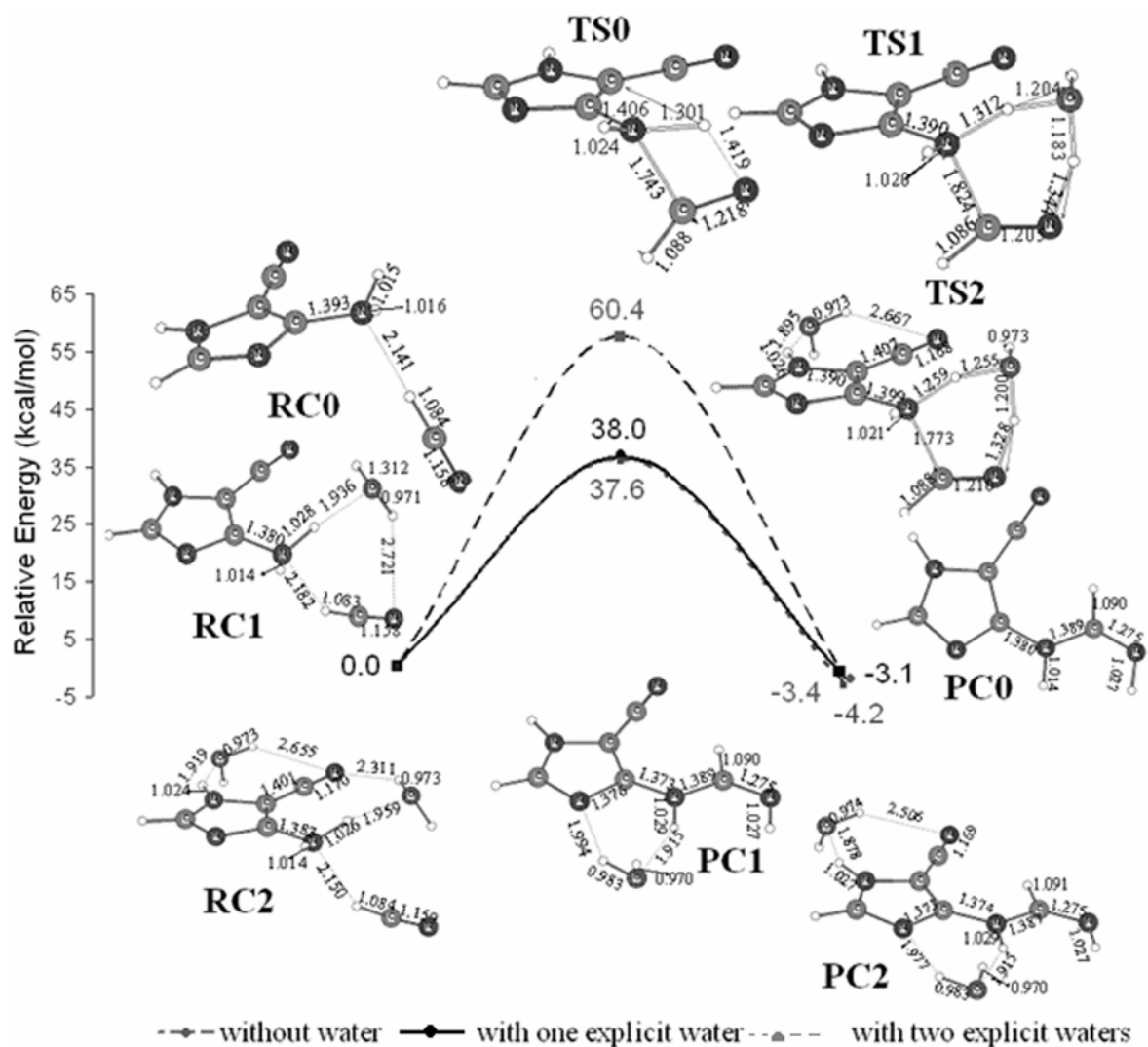


Figure 2-8. Gas phase reaction barrier for the key first addition step (B3LYP/6-311+G\*\* level of theory) Optimized geometries in Å for reactant complexes (RC), transition states (TS) and product complexes (PC) for systems with 0, 1 and 2 water molecules are given. The reaction barrier (ZPVE corrected) for the neutral uncatalyzed pathway is ~60.4 kcal/mol. Water (solvent) is an active participant in the transition step. Incorporation of one and two water molecules reduces the reaction barrier to 38.0 and 37.6 kcal/mol, respectively.

addition product (TS1) (Figure. 4-8) is very different from TS0 for the neutral uncatalyzed mechanism. The water molecule in TS1 transfers its hydrogen-bonded proton to the HCN nitrogen concertedly with the formation of the new bond between the AICN amine nitrogen and the electron deficient HCN carbon.

The inclusion of one specific water molecule decreases the reaction barrier drastically, from 60.4 kcal/mol (without water) to 38.0 kcal/mol (with a single H<sub>2</sub>O) (Fig. 4-8). Consequently, we also explored the effect of more than one solvent molecule in the mechanism. A second H<sub>2</sub>O does not participate in the proton relay effectively, but can form relatively strong hydrogen bonds stabilizing the reactant, product and the transition state complexes. The energetically most favorable transition structure with two water molecules (TS2) also is depicted in Fig. 4-8. However, inclusion of two explicit H<sub>2</sub>O molecules only decreases the reaction barrier by an additional 0.4 kcal/mol (to 37.6 kcal/mol). It does not seem likely that additional explicit H<sub>2</sub>O molecules would have much of a further effect. However, a complete solvation shell does have a significant influence (see below). Almost all the reported abiotic syntheses of adenine were carried out with HCN dissolved in water-ammonia solutions. Besides maintaining the pH of the medium, ammonia also might also participate mechanistically. Indeed, an explicit NH<sub>3</sub> molecule is as good a catalyst as an explicit H<sub>2</sub>O molecule. The reaction barrier for the first step, the NH<sub>3</sub>-catalyzed addition of HCN to AICN(b) (with one explicit NH<sub>3</sub>), is 37.1 kcal/mol, as compared to 38.0 kcal/mol with an explicit H<sub>2</sub>O. While computations based on species in isolation (gas phase) may simulate extraterrestrial conditions, they do not suffice to predict prebiotic processes on the primitive earth, where reactions might have taken place in solution. In addition to the explicit solvent modelling (see above), we simulated the bulk solvation effect by employing the polarizable continuum model (PCM) [50], which considers the solvent as a macroscopic

continuum of dielectric constant . Bulk solvation stabilizes structures involving greater charge separation (e.g., transition states) preferentially. Indeed, bulk solvation reduces the reaction barriers for the rate determining step to 33.8 kcal/mol (from 37.6) and to 34.7 kcal/mol (from 37.6) for specific H<sub>2</sub>O/NH<sub>3</sub> catalyzed mechanisms, respectively. These barriers are low enough to be consistent with the experimental observations as well as conjectures regarding the abiotic genesis of adenine.

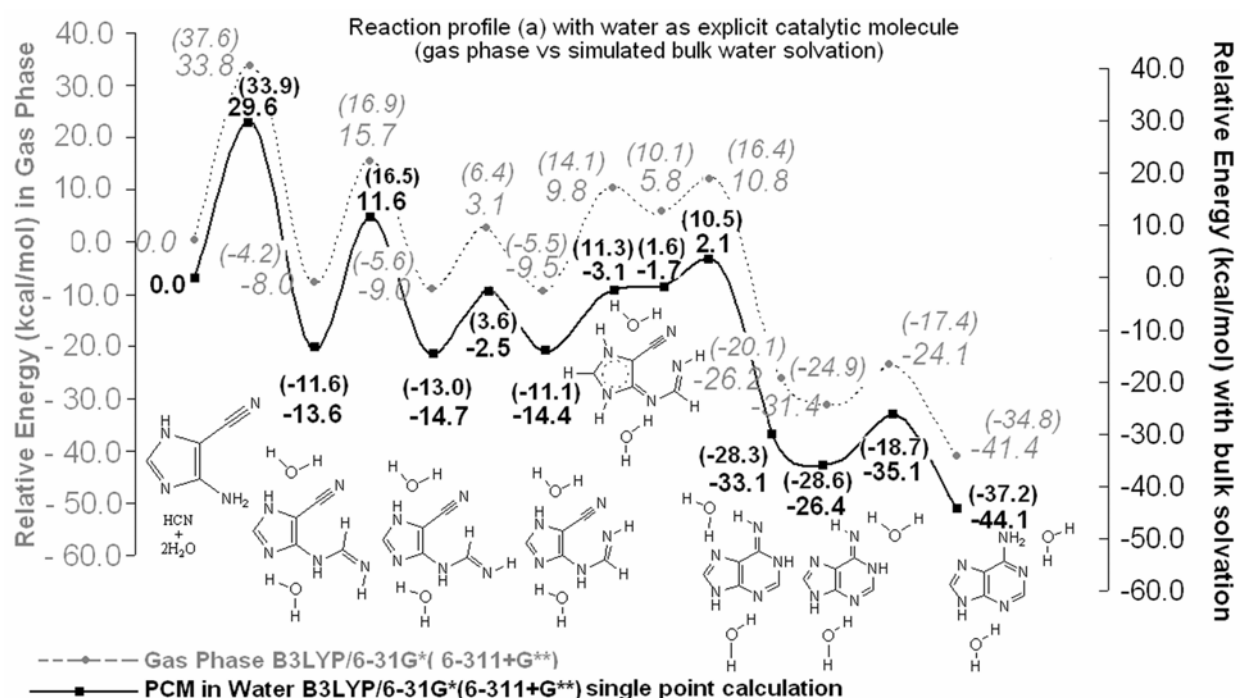


Figure 2-9. Reaction profiles for the formation of adenine starting from AICN(b) and HCN in gas phase and in the solvent phase via explicit water catalyzed mechanism (two water molecules). The barrier height are reported with both 6-31G\* and at 6-311+G\*\* basis set(in parentheses). All the stable minima are shown. The comparison of reaction profiles in a vacuum and in aqueous solution clearly shows that the transition states are stabilized through electrostatic effect of the solvent. The two H<sub>2</sub>O or NH<sub>3</sub> molecules participate in proton relay. They form the H-bonded “wire” for the proton transfer via 6

membered transition state. The reaction seems easier in aqueous solution than in the gas phase: the first step is rate-determining in both cases.

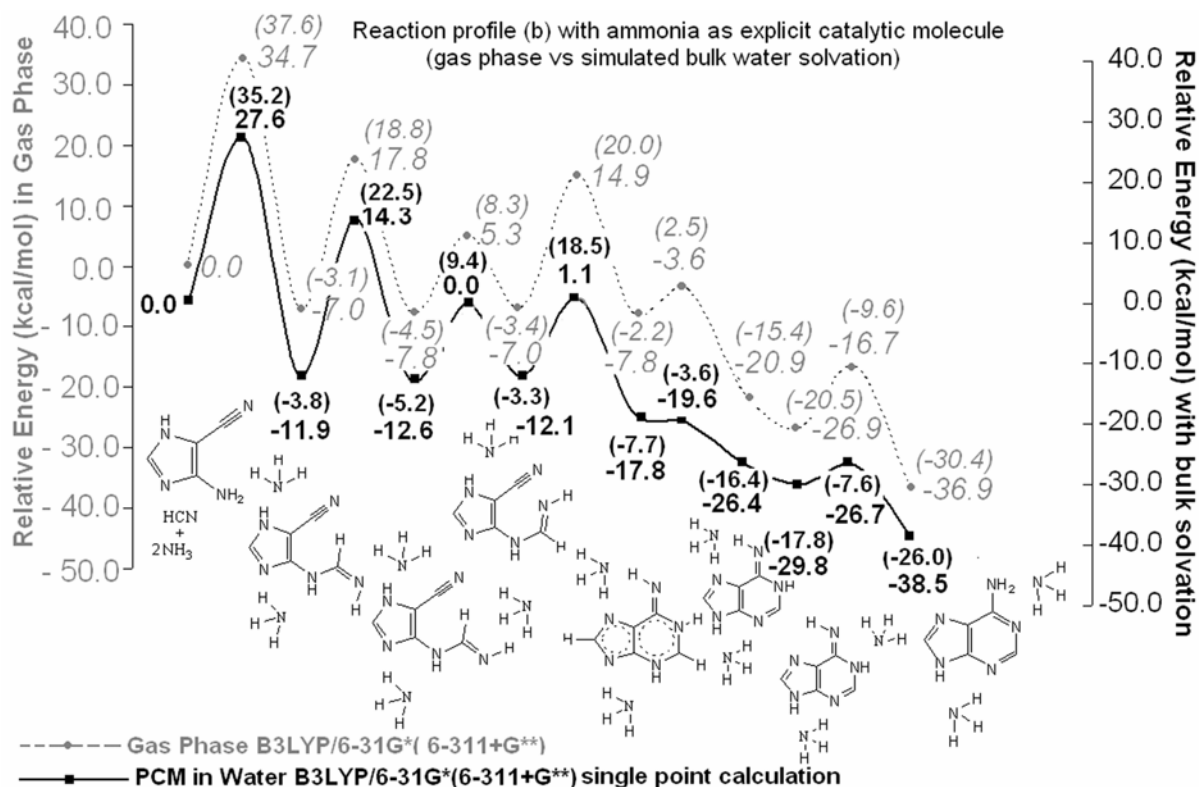


Figure 2-10. Reaction profiles for the formation of adenine starting from AICN(b) and HCN in the gas phase and with simulated bulk water solvation via explicit solvent catalyzed mechanisms (two explicit NH<sub>3</sub> molecules).

The subsequent steps from the HCN–AICN adduct are depicted in Figure 2-9 (for catalysis by two H<sub>2</sub>O's) and Figure 2-10 (for catalysis by two NH<sub>3</sub>'s). The effects of bulk solvation are included in both plots. Except for the syn-anti hydrogen transfer and the C-N bond rotation in the second and third steps, all the stages require the catalytic participation of at least one H<sub>2</sub>O or NH<sub>3</sub>.

molecule. The proton relays across six and five membered rings are interesting mechanistic features, since two H<sub>2</sub>O or NH<sub>3</sub> molecules are needed to complete the H-bonded “circuit.” One molecule participates in the proton transfer directly as a catalyst, while the second H<sub>2</sub>O or NH<sub>3</sub> assists by hydrogen bonding. The detailed step-by-step mechanism for the formation of [adenine.(H<sub>2</sub>O)<sub>2</sub>] starting from AICN(b) + HCN + 2 H<sub>2</sub>O is depicted in Figure 2-9. This reaction profile includes the relative energies of each stationary point (with respect to AICN+HCN+2 H<sub>2</sub>O 1:1:2 reactant complex) without and with bulk solvation. The first step is rate determining (as stated in our earlier discussion). The subsequent steps have lower reaction barriers. The mechanistic features with ammonia catalyzed pathway as shown in Figure 2-10 are different to that of with water catalyzed pathway, since ammonia and water have different Lewis base properties. While the first three steps, i.e., addition of HCN to AICN catalyzed by ammonia, syn-anti hydrogen transfer and rotation around C-N, are similar, concerted six membered ring closure and 1,4 H transfer take place in the NH<sub>3</sub> catalyzed mechanism before 1,3 H transfer. The geometries of the stationary points for the ammonia catalyzed pathway are shown in Figure 2-11.

To summarize, the reaction mechanism for adenine formation is mostly dominated by concerted C-N bond formation and 1-3 H shift (tautomerization). Specific water and ammonia molecule act as a catalyst for stabilizing the transition state and thus lower the barrier to tautomerization. The specific solvent molecule provide bridges that connect the donor and acceptor sites and thus relax the energy required to bring these sites closer together prior to the proton transfer process. For the 1, 3 hydrogen shift, the high classical barrier in the gas phase is due to the four membered transition state and bending of NCN angle. The dihydrated system provides an optimal static condition and lowers the classical barrier for tautomerization.

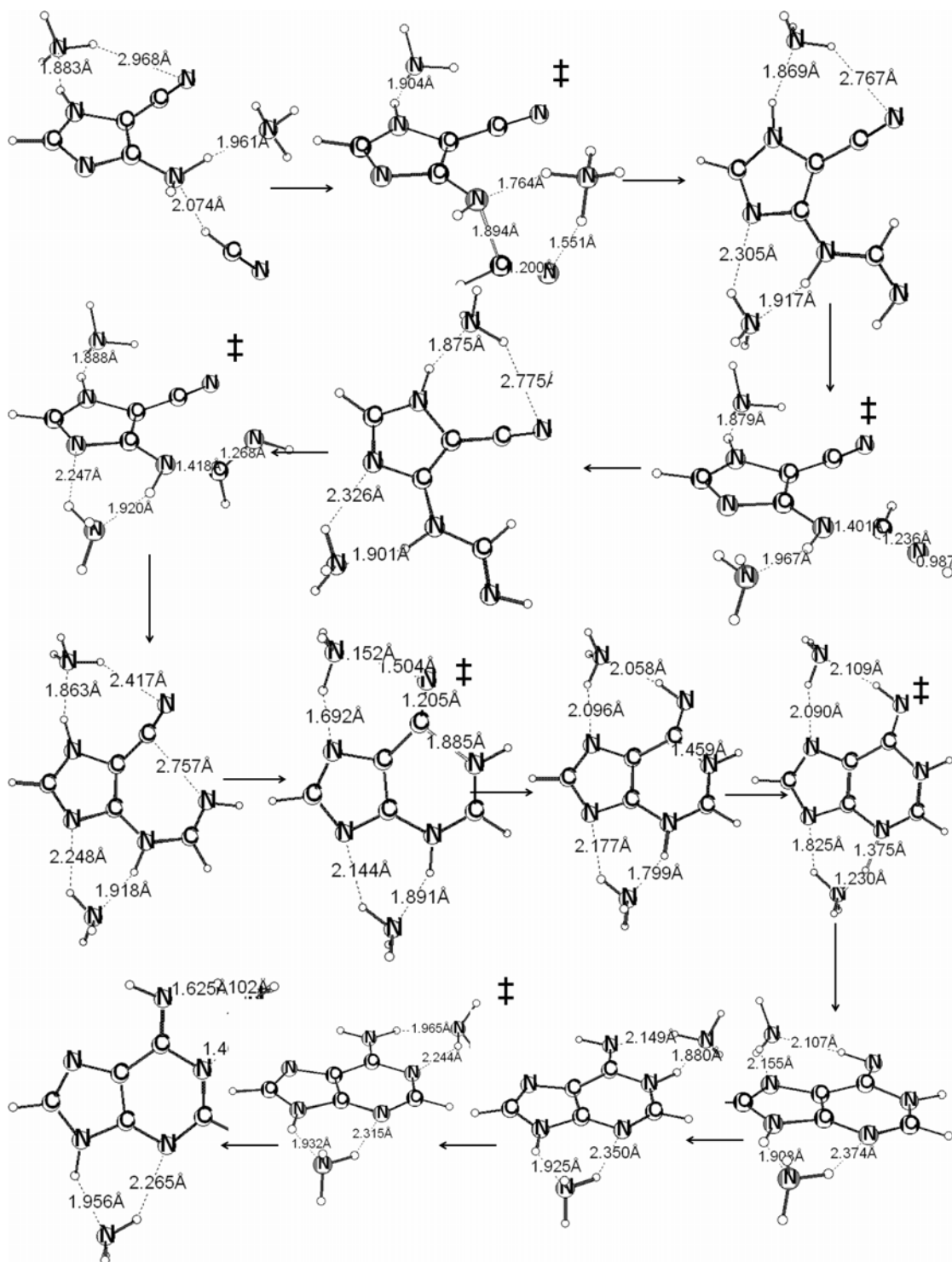
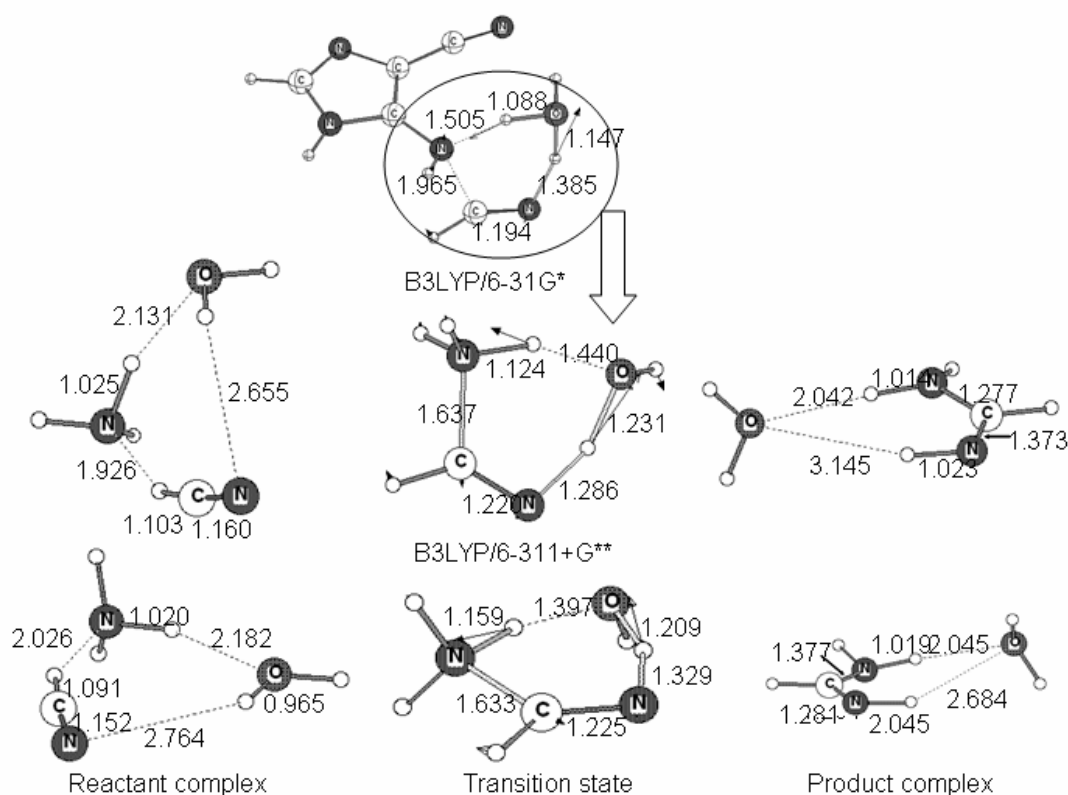


Figure 2-11. Stationary points for the ammonia (two explicit molecules) catalyzed pathway. The transition state structures are depicted by a ‡ sign.



## 2.6.7 Validating the methods used for computing barrier heights



Level of Theory/Basis set	Reaction barrier(+ZPVE) (kcal/mol)
B3LYP/6-31G*	31.3 (30.5)
B3LYP/6-311+G**	34.9 (34.6)
CCSD(T)/aug-ccpVDZ (single point starting from MP2/6-311+G** geometry)	38.4
CCSD(T)/aug-ccpVTZ (single point starting from MP2/6-311+G** geometry)	37.7

Figure 2-12. Geometries of reactant, product and transition state for HCN+NH<sub>3</sub>+H<sub>2</sub>O system (simulated the first HCN + RNH<sub>2</sub> addition step with the highest barrier) at the B3LYP level of theory with various basis sets are shown. Comparison of density functional theory (DFT) and CCSD (T) reaction barriers are given.

Our computed reaction profile with low energy barriers reveals the feasibility of adenine formation from AICN under abiotic condition. But are the computed reaction barriers reliable? The B3LYP DFT method we employed is known to give relatively accurate structures and spectroscopic properties of first row molecules, but activation barriers may be more problematical [58,59]. Our computed reaction barriers at B3LYP/6-31G\* are ~3-4 kcal/mol lower than at B3LYP/6-311+G\*\*. The key rate determining step was recomputed at the MP2/6-311+G\*\* and the gas phase reaction barrier with ZPVE correction is 43.9 kcal/mol, which is higher than that at B3LYP/6-311+G\*\*. It has been reported that although MP2 generally gives accurate geometries for reaction complexes, it also overestimates barrier heights [60, 61]. Thus for calibration, we performed higher level CCSD (T) /cc-pVTZ single-point computations on the simpler HCN + NH<sub>3</sub> + H<sub>2</sub>O system on MP2 geometries optimized at 6-311+G\*\* level. This models the key AICN(b) + HCN + H<sub>2</sub>O rate determining step, since it also involves the addition of an NH bond to HCN. The geometries of the reactants, transition structures, products, and barriers, computed at various levels of theory, are given in Figure 2-12. The CCSD(T)/aug-cc-pVTZ single point reaction barrier is 3 kcal/mol higher than the B3LYP/6-311+G\*\* result.

## 2.7 Conclusion

Our detailed computational investigations of step-by-step formation pathways from AICN(b) show how adenine can arise abiotically. We have deduced a plausible mechanism for formation of abiotic adenine starting from AICN (a tetramer of HCN) (Figure 2-13). While the formation of adenine by the pentamerization of HCN is very exothermic, this process is quite unlikely in isolation (gas phase). Not only must five HCN molecules come together, but also the reaction barriers are very high. The intimate participation of an additional molecule, such as H<sub>2</sub>O or NH<sub>3</sub>

(or perhaps HCN) is needed to lower the barriers considerably to realistic energies. Moreover, an aqueous medium facilitates the reaction, as both specific and bulk solvation lowers the barrier of the rate determining step further. The reaction energetics are mostly governed by the enthalpy change (see caption, Figure 2-4) especially at the low temperatures of some of the experiments.

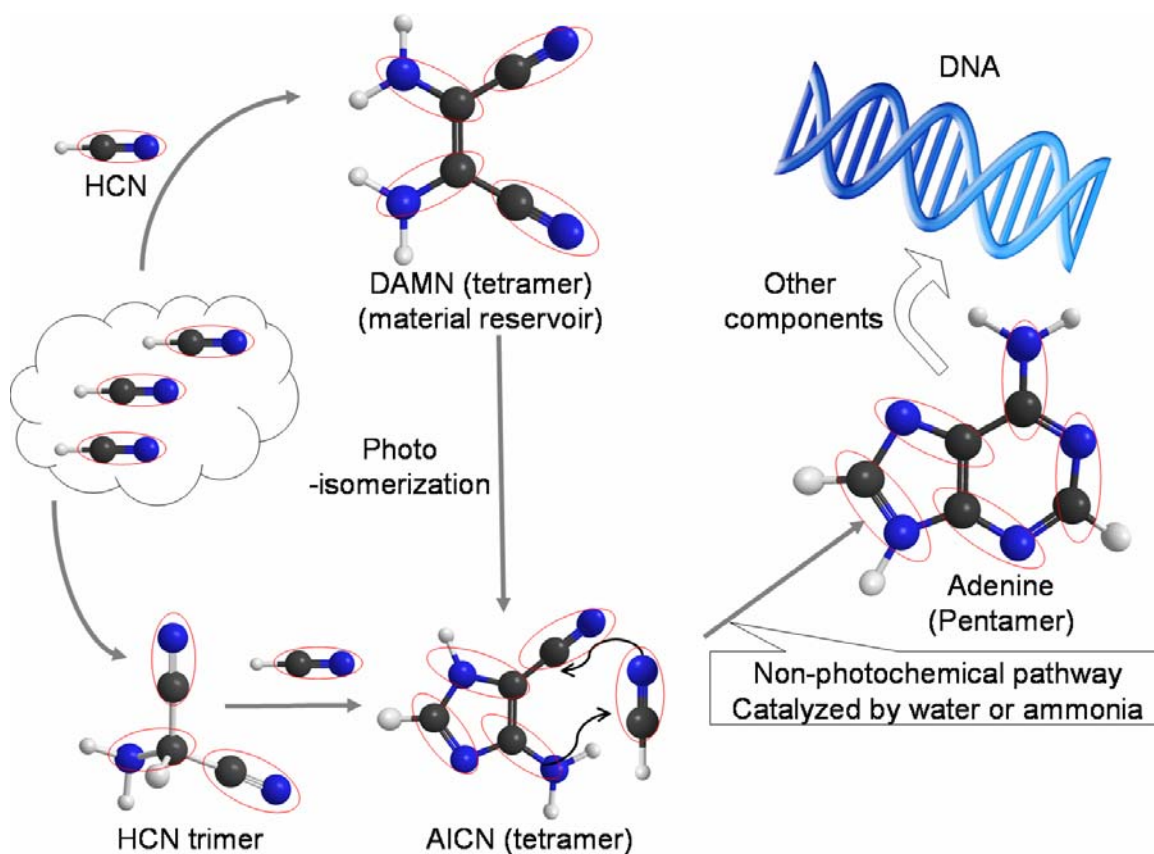


Figure 2-13. Summary of the step by step mechanism for the formation of adenine. The last crucial pentamer formation step is catalyzed by specific solvent molecule (water/ammonia). The CN building blocks are circled in red in the diagram.

Finding a viable, thermodynamically feasible, step-by-step mechanism, which can account for the formation of adenine, did not prove to be easy. Our approach has model character

to it. The "first model" is without water or ammonia; the second model is with explicit participation of ammonia (along with water) in gas phase, the third model adds bulk solvation. As there is no quantitative experimental data to match, a super refined study is not mandatory. However, a more sophisticated treatment can be carried out eventually to model the medium effects. A QM/MM approach can be taken as described by Jorgensen and his co-workers [57]. The energetics of the reacting systems can be described quantum mechanically with *ab initio* or DFT. The environment including solvent molecules can be represented using molecular mechanics and a sampling performed with Monte Carlo statistical mechanics.

An alternate pathway based on the experimental isolation of 2- and 8-cyanoadenine or adenine 8 carboxamide as adenine precursor suggests a further complex mechanism involving hexamer and heptamers of HCN [62]. When we were refining our model over three years, another team published a parallel research that also sheds light on the prebiotic origins of adenine, though from a different perspective [49]. Rainer Glaser and colleagues from the University of Missouri used a theoretical model to predict mechanisms for the production of adenine under photochemical conditions in space. Their study reveals that adenine formation from a HCN pentamer precursor is not viable thermochemically either by proton-catalyzed or by uncatalyzed cyclization, instead photoactivation of one of the cyclization path may lead to imino form of adenine. If, indeed, the production of adenine began in space and came to Earth on asteroids, this could possibly open the idea of life elsewhere to more serious avenues of study. Our study however offers clues to a more *earth-bound* solution to this important compound formed under prebiotic conditions on early earth.

The neutral water or ammonia catalyzed mechanism proposed in our study may well have been a major route for the formation of adenine on primitive earth. However, detailed

calculations on reactions of this kind are needed before a full picture emerges. Mechanisms modeling the formation of other remaining nucleic acid bases and biologically relevant molecules extra-terrestrially, under more restricted conditions, are further challenges.

## 2.8 Acknowledgement

We thank Professor T.T. Tidwell for calling our attention to this problem and for his encouragement. K. Najafian, our collaborator for carrying out extensive computations on intermediates and transition states that might be involved in possible anionic and radical mediated pathways. NSF Grant CHE-0209857 and the University of Georgia supported this work.

## 2.9 References and notes

- 1) S. L. Miller, L. E. Orgel, Eds., *The Origins of Life of Earth* (Prentice-Hall, Englewood Cliffs, N. J., 1974).
- 2) J. W. Schopf, Ed., *Earth's Earliest Biosphere: Its Origin and Evolution* (Princeton Univ. Press, Princeton, N. J., 1983).
- 3) F. Wöhler(1828) *Annalen der Physik und Chemie*, 88, Leipzig.
- 4) A. Butlerow, (1861) *Compt. Redn. Acad.Sci.* 53, 145.
- 5) G. Glocker, and S. Lind. *The Electrochemistry of Gases and Other Dielectrics*. Wiley, New York, 1939.
- 6) W. Löb, (1913) *Chemische Berichte*, 46, 684.
- 7) O. Baudish, (1913) *Zeitschrift Angewandte Chemie*, 26, 612.
- 8) S. L. Miller (1953) *Science*. 117, 528.

- 9) S. L. Miller, H.C. Urey (1959) *Science*. 130, 245.
- 10) J. Oró, (1961) *Nature*. 191, 1193.
- 11) J. Oró, A.P. Kimball (1961) *Arch.Biochem.Biophys.* 94, 217.
- 12) J. Oró, A.P. Kimball (1962) *Arch.Biochem.Biophys.* 96, 293.
- 13) J.P. Ferris, R.A. Sanchez, L.E.Orgel (1968) *J. Mol. Biol.*33, 693.
- 14) J. Oró (1960) *Biochem.Biophys.Res.Comm.* 2, 407.
- 15) M.Levy, S.L. Miller, J. Oró (1999) *J. Mol. Evol.* 49, 165.
- 16) A. B. Voet, A.W.Schwartz (1982) *Origins Life*. 12, 45.
- 17) C. U. Lowe, M. W. Rees, F. R. S. Markham (1963) *Nature*.199, 219.
- 18) J. P. Ferris, P. C. Joshi (1978) *Science*. 201, 361.
- 19) J. Hulshof, C. Ponnampereuma (1976) *Origins of Life*. 197, 224.
- 20) T.B. McCord , G.B. Hansen , F.P. Fanale, R.W. Carlson, D.L. Matson , T.V. Johnson,  
W.D. Smythe, J.K. Crowley, P.D. Martin, A. Ocampo, C.A. Hibbitts, J.C. Granaha  
(1998a.) *Science*. 278, 1242.
- 21) J. Oró, S. S. Kamat (1961) *Nature*. 190, 442.
- 22) C. N. Matthews, R. E. Moser (1967) *Nature*. 215, 1230.
- 23) J.P. Ferris, J.D. Wos, D.W. Nooner, J. Oró (1974) *J. Mol. Evol.* 3, 225.
- 24) C. Shen, L. Yang, S.L. Miller, J. Oró (1990) *J. Mol. Evol.* 31,167.
- 25) P. Johnson, H. J. Cleaves, J. P. Dworkin, D. P. Glavin, A. Lazcano, J. L. Bada (2008)  
*Science*. 322, 404.
- 26) P. H. Abelson (1966) *Proc. Natl. Acad. Sci. U.S. A.* 55, 1365.
- 27) R. Hanel, B. Conrath, F.M. Flasar, V. Kunde, W. Maguire, J. Pearl, J. Pirraglia , R.  
Samuelson, L. Herath, M. Allison, D. Cruikshank, D. Gautier, P. Gierasch, L. Horn, R.  
Koppany, C. Ponnampereuma *Science* 212 (1981), 192.

- 28) F. Raulin, J. C. Frere (1989) *British Interplanetary Society*, 42, 411.
- 29) T. Owen 1982 *J. Mol. Evol.* 18, 150.
- 30) M. Levy, S. Miller, K. Brinton, J. Bada (2000) *Icarus*, 145, 609-613.
- 31) R.T. Reynolds, S.W. Squyres, D.S. Colburn, C.P. McKay (1983) *Icarus*.56, 246.
- 32) C.F. Chyba (1997) *Nature*, 385, 201.
- 33) T.B. McCord , R.W. Carlson, W.D. Smythe, G.B. Hansen, R.N. Clark, C.A. Hibbitts, F.P. Fanale, J.C. Granahan, M. Segura, D.L. Matson, T.V. Johnson, P.D. Martin (1997) *Science*. 278, 271.
- 34) C.N. Matthews (1992) *Orig. Life Evol. Biosph.*21, 421.
- 35) W.M. Irvine(1999) *Space Sci Rev*, 90, 203.
- 36) W.F. Huebner, L.E. Snyder, D. Buhl (1974) *Icarus*, 23, 580.
- 37) K. Magee-Sauer, M.J. Mumma, M.A. DiSanti, N.D. Russo, T.W. Rettig (1999) *Icarus*, 142, 498.
- 38) T. Hidayat,, A. Marten, B. Bezard, D. Gautier, T. Owen, H.E. Matthews, G. Paubert (1998) *Icarus* 126, 170.
- 39) R. F. Shuman, W. E. Shearin, R. J. Tull (1979) *J. Org. Chem.* 44, 4532.
- 40) A. B. Voet, A. W. Schwartz (1983) *Bioorg. Chem.* 12, 8.
- 41) J. P. Ferris, L. E. Orgel (1966). *J. Am. Chem. Soc.* 88, 3829.
- 42) J. P. Ferris, L. E. Orgel (1965). *J. Am. Chem. Soc.* 87, 4976.
- 43) J. P. Ferris, L. E. Orgel (1966) *J. Am. Chem. Soc.* 88, 1074.
- 44) H. Wakamatsu, Y. Yamada, T. Saito, I. Kumashiro, T. Takenishi (1966) *J. Org. Chem.* 31, 2035.
- 45) J. P. Ferris, P. C. Joshi, E. H. Edelson, J. G. Lawless (1978) *J. Mol. Evol.* 11, 293.

- 46) O. Kikuchi, T. Watanabe, Y. Satoh, Y. Inadomi (2000) *J. Mol. Struct.* 507, 53.
- 47) F. Tureček, X. Chen (2005) *J. Am. Soc. Mass Spectrom.* 16, 1713-1726.
- 48) D. Roy, K. Najafian, P. v. R. Schleyer (2007). *Proc. Natl. Acad. Sci. U.S. A.* 104, 17272.
- 49) R. Glaser, B. Hodgen, D. Farrelly, E. McKee (2007) *Astrobiology* 7, 455.
- 50) M. J. Frisch, G. W. Trucks, H. B. Schlegel, G. E. Scuseria, M. A. Robb, J. R. Cheeseman, V. G. Zakrzewski, J. A. Montgomery, Jr., R. E. Stratmann, J. C. Burant, S. Dapprich, J. M. Millam, A. D. Daniels, K. N. Kudin, M. C. Strain, O. Farkas, J. Tomasi, V. Barone, M. Cossi, R. Cammi, B. Mennucci, C. Pomelli, C. Adamo, S. Clifford, J. Ochterski, G. A. Petersson, P. Y. Ayala, Q. Cui, K. Morokuma, P. Salvador, J. J. Dannenberg, D. K. Malick, A. D. Rabuck, K. Raghavachari, J. B. Foresman, J. Cioslowski, J. V. Ortiz, A. G. Baboul, B. B. Stefanov, G. Liu, A. Liashenko, P. Piskorz, I. Komaromi, R. Gomperts, R. L. Martin, D. J. Fox, T. Keith, M. A. Al-Laham, C. Y. Peng, A. Nanayakkara, M. Challacombe, P. M. W. Gill, B. Johnson, W. Chen, M. W. Wong, J. L. Andres, C. Gonzalez, M. Head-Gordon, E. S. Replogle, and J. A. Pople, Gaussian 98 (Revision A.9) (Gaussian, Inc., Pittsburgh, PA, 1998).
- 51) M. Aida, H. Yamataka, M. Dupuis, (1998) *Chem. Phys. Lett.* 292, 474.
- 52) S. Miertus, E. Scrocco, J. Tomasi (1981) *Chem. Phys.* 55, 117.
- 53) The ZPVE corrections to the gas phase energies are nearly the same with different numbers of solvent molecules, zero, one, or two. For example, the relative energy of the transition structure (TS) for the first step without solvent is 62.9 (without) and 60.4 kcal/mol (with ZPVE correction). The relative energy of the TS with one water molecule is 40.5 (without) and 38.0 kcal/mol (with ZPVE). With two water molecules, the TS relative energy is 39.9 (without) and 37.6 kcal/mol (with ZPVE correction).



Consequently, the average ZPVE correction (~2.5 kcal/mol) was added to the PCM single-point energy.

- 54) K. Najafian, our collaborator in the original work, carried out extensive computations on intermediates and transition states that might be involved in possible anionic and radical mediated pathways.
- 55) S. Yamabe, N. Tsuchida, K. Miyajima (2004) *J. Phys. Chem. A*. 108, 2750.
- 56) G. S. M. Kiruba , M. W. Wong (2003) *J. Org. Chem.* 68, 2874.
- 57) W. L. Jorgensen, A. N. Alexandrova (2007) *J. Phys. Chem. B*. 111,720.
- 58) V. Barone (1994) *Chem. Phys. Lett.* 226, 392.
- 59) J. M. Martell, J. D. Goddard, L. A. Eriksson (1997) *J. Phys. Chem. A*. 101, 1927.
- 60) K.B.Wiberg, J.W.Ochterski (1997) *J. Comput. Chem.* 18, 108.
- 61) N. Gonzales-Garcia, À. Gonzales-Lafont, J. M. Lluch (2005) *J. Comput. Chem.* 26, 569.
- 62) E. Borquez, H. J. Cleaves, A. Lazcano, S. L. Miller (2005) *Origins of life*, 35, 79.

CHAPTER 3

MODELING DINITROGEN ACTIVATION BY LITHIUM: A MECHANISTIC  
INVESTIGATION OF THE CLEAVAGE N<sub>2</sub> BY STEPWISE INSERTION INTO SMALL  
LITHIUM CLUSTERS<sup>†</sup>

---

<sup>†</sup> Roy, D.; Navarro-Vázquez, A.; Schleyer, P. v. R. Submitted to *The Journal of American Chemical Society*, 04/06/2009.

### 3.1 Abstract

Practicable activation of molecular nitrogen, under mild conditions, is fundamentally challenging because of its inertness. Nature can do it easily; chemists should be able to achieve comparable success. Lithium is exceptional among the main group elements in that it slowly reacts with  $N_2$  at room temperature, leading finally to  $(NLi_3)_n$ . Although lithium by itself is not a catalyst, but its  $(NLi_3)_n$  lithium nitride product with nitrogen is of interest in its own right, because of its potential as a hydrogen storage medium. We explored this remarkably facile dinitrogen activation reaction by using model lithium clusters. Our extensive computations elucidate mechanisms for the ready reactions of  $N_2$  with various model clusters,  $Li_2$ ,  $Li_4$ ,  $Li_6$ , and  $Li_8$ , leading to stepwise NN cleavage and dinitrogen reduction,  $N_2^0$  to  $2 N_3^-$ . Initial isomeric  $N_2-Li_n$  complexes, retaining NN triple bonds, undergo cluster insertion/reduction processes over generally low barriers. The overall reactions are highly exothermic. Eight lithium atoms are needed to cleave the triple bonded nitrogen completely. Moreover, we provide an explanation for the exceptional reactivity of  $N_2$  with Li, compared to the other alkali metals, e.g., Na and K. Li is a very strong reducing agent as its nitrides have the highest atomization energy, the shortest M-N bond distance, and the largest M-N charge separation as well as interaction energy. Our study delineates the general manner in which molecular nitrogen can be activated sequentially by electron transfer and bond elongation, to give a series of increasingly reduced complexes. We conclude that lithium incorporation into complexes might facilitate the “development of nitrogen fixation catalysts.

### 3.2 Introduction

Nitrogen, beside the noble gases, is the most inert chemical element. Nevertheless, lithium metal burns in a pure nitrogen atmosphere. This behavior is exceptional, since triply bonded  $N_2$

normally is very difficult to reduce due to its very large bond dissociation energy (224.5 kcal mol<sup>-1</sup>), highly negative electron affinity (-1.8 eV), and huge HOMO/LUMO energy gap (22.9 eV) [1-2]. Moreover, N<sub>2</sub> has a high ionization potential (15.0 eV), and does not donate electrons either [1-2]. Although nitrogen exhibits stable oxidation states (0 to -3) in its compounds, N<sub>2</sub> forms complexes reluctantly, and unlike the isoelectronic CO, dinitrogen chemistry is not well established [3].

Reduction of dinitrogen remains a fundamental challenge to synthetic as well as to theoretical chemistry. Unlike the catalytic Haber-Bosch hydrogenation of N<sub>2</sub> to give ammonia, which requires high pressure and high temperatures [4], nitrogenase enzymes activate dinitrogen under ambient conditions at transition metal (Fe/Mo, V)-sulfide cluster sites[5]. Metal complexes capable of cleaving the extremely robust dinitrogen triple bond are formed typically from low-valent early transition-metal precursors. Since the first discovery of a dinitrogen complex in 1965, inorganic and organo-metallic chemists have contributed much fundamental knowledge on structures, binding modes, and reactivity patterns [6]. Moreover, there has been a huge progress in the last years, both practically and computationally, in the field of synthetic nitrogen fixation [7].

Li, in conjunction with transition metals, has been used to activate dinitrogen in several systems. Thus, in the presence of Li, a THF solution of TiCl<sub>4</sub> and TMSCl converts benzoyl chloride to PhCONH<sub>2</sub> in high yields at room temperature [8]. An intermediate complex of the [TiX<sub>m</sub>{N(SiMe<sub>3</sub>)<sub>n</sub>}<sub>p</sub>] form was suggested to bind the amide formed after cleavage of the N<sub>2</sub> bond by the lithium metal. The lithium atom- nitrogen molecule reaction, studied by co-depositing lithium and nitrogen at 15°K, results in two absorptions at 1800 and 1535 cm<sup>-1</sup> for N-N fundamental vibrations. These were assigned to LiN<sub>2</sub> (lithium supernitride) and N<sub>2</sub>Li<sub>2</sub>N<sub>2</sub> (lithium

disupernitride) based on molecular orbital calculations and the use of nitrogen isotopic mixtures. The  $1535\text{ cm}^{-1}$  feature was assigned to a species containing two  $\text{N}_2$  units and  $1800\text{ cm}^{-1}$  feature probably should be due to a single lithium species [9]. The question then arises : i) to what extent is a single Li atom or small Li cluster able to activate  $\text{N}_2$  and ii) how does lithium metal react with  $\text{N}_2$  to form lithium nitride ( $\text{Li}_3\text{N}$ ), a reversible hydrogen storage candidate [10], even at room temperature.

### 3.3 Computational method

The geometries of all the complexes, reactants, intermediates, transition states, and products were optimized using the hybrid density functional B3LYP using ultrafine integration grids[11]. The Gaussian 03 program was employed[12]. Computations with the X3LYP [13] functional confirmed the results. MP2 computations also were performed for critical cases, e.g., the key exothermic step for the reduction of the double to the single  $r_{\text{NN}}$ , the exothermicity of  $\text{N}_2 + \text{Li}_8$  reaction etc. The standard 6-3111+G\* for geometry optimization and aug-cc-pVDZ for natural charge calculation were used. Intrinsic reaction coordinate (IRC) calculations were done for all transition states to confirm their associated reactants and products. The potential energy surfaces were explored using Saunders' stochastic search "kick" method[14], which generates structures randomly, which facilitates thorough exploration of chemically non-intuitive minima with very little human effort[15]. All the atoms are placed at the same point initially and then are "kicked" randomly within a box of chosen dimensions. The kick size was varied from 2.0 to 3.5 Å in the cubic boxes employed here. A total of 2000 kick jobs in independent sets of 100 were performed at the HF/STO-3G level of theory. Redundancies in each set (energies within 0.00001 au) are eliminated. The sets of kick runs were continued until no new structures were generated. The

best structures from the initial level were refined at the B3LYP/6-311+G\* level and the appropriate symmetries were checked by harmonic vibrational frequency computations. Natural population analysis implemented in NBO 5.0 [16] gave Natural atomic charges and the high ionic character of the electron distributions in the  $N_2Li_n$  ( $n=6,8$ ) complexes.

### 3.4 Result and discussion

#### 3.4.1 Revisiting Andrew's 1972 experiment

		N-N stretching B3LYP/6-311+G* (scaled) $cm^{-1}$ (intensity)		Experimental Frequencies
1, $C_{2v}$ , 0.0 kcal/mol	2, $C_{2v}$ , 0.3 kcal/mol	1783 (2397)	1793 (2267)	1800 $cm^{-1}$
3, $C_{2v}$ , 1.2 kcal/mol	4, $C_{2v}$ , 4.2 kcal/mol	1488(in)/2230(out) (435)/(1790)		1535 $cm^{-1}$
5, $C_1$ , 9.1 kcal/mol	6, $C_{2v}$ , 9.6 kcal/mol	1515(in)/2154(out) (442)/(2103)		1535 $cm^{-1}$
7, $C_s$ , 0.0 kcal/mol	8, $C_{2v}$ , 1.2 kcal/mol	2112/2336 1433(in)/2334(out) (1708/1831) (40/317)		$N_2 = 2359 cm^{-1}$
		2024 (6878)	1779 (385)	1800 $cm^{-1}$

Figure 3-1. The computed geometries, N-N stretching frequencies and intensities for  $[LiN_2]$  and  $[Li_2N_4]$  species.

Investigations directly related to the subject of our study, the reaction of  $N_2$  with lithium, are limited to Andrews et.al's 1972 matrix isolation study of the interaction of lithium atom with nitrogen molecules when co-deposited at 15°K. Infrared spectroscopic observation of two

absorptions at 1800 and 1535  $\text{cm}^{-1}$  for NN fundamental vibrations, supported by theoretical computations, suggested the formation of two lithium-nitrogen species,  $\text{LiN}_2$  (“lithium supernitride”) and  $\text{N}_2\text{Li}_2\text{N}_2$  (“lithium disupernitride”), the latter containing two equivalent  $\text{N}_2$  units[9]. Structures were not assigned. The authors proposed that the  $\text{N}_2$  in the observed lithium-nitrogen species is reduced more than in  $\text{N}_2$  transition metal complexes, where the NN modes are higher ( $\sim 2000 \text{ cm}^{-1}$ ) [for example, the NN IR stretch is 1955  $\text{cm}^{-1}$  in  $[(\text{depe})_2\text{Fe}(\text{N}_2)]$   $\text{depe} = \text{Et}_2\text{PCH}_2\text{CH}_2\text{PEt}_2$ ) [5d]. We have reinvestigated possibilities computationally. Based on the match of the experimental and our computed stretching frequencies, we have found alternative structural candidates for the products, two for  $\text{LiN}_2$  and four for  $\text{Li}_2\text{N}_4$  (Figure 3-1).

We searched for stationary points on the  $\text{Li}_2\text{N}_4$  and  $\text{LiN}_2$  potential energy surface (PES) using Saunders’ stochastic “kick” procedure which facilitates thorough exploration of chemically non-intuitive minima with very little human effort (the kick method is described in detail in the method section). We found several interesting stationary points (minima) with  $C_{2v}$  and  $C_1$  symmetry for  $\text{Li}_2\text{N}_4$  species. The NN bond lengths ranged from 1.161 to 1.237 Å (**1-6**, Figure 3-1). The four lowest energy stationary points (**1-4**) have relative energies within  $\sim 4$  kcal/mol. The computed (B3LYP/6-311+G\*) IR stretching frequencies for the  $\text{N}_2$  moieties in the  $\text{Li}_2\text{N}_4$  species **1-4** are 1783, 1793, 1488 and 1515  $\text{cm}^{-1}$ , respectively (a 0.98 scaling factor is applied) [17]. Moreover, we report two other stretching frequencies 2230 and 2154  $\text{cm}^{-1}$  corresponding to N-N stretch for the stationary points **3** and **4** ( $\text{N}_2$  complexed with  $\text{N}_2\text{Li}_2$  moiety in side on and end on fashion). Those stretching frequencies were not observed in the experiment. Evidently, a mixture of  $\text{Li}_2\text{N}_4$  species might have been formed in Andrew’s 1972 experiment. The N-N fundamental stretching corresponding to one of the computed structures (**4**, 1515  $\text{cm}^{-1}$ , *side-on*  $\text{N}_2$  complexed with  $D_{2h}$  planar  $\text{N}_2\text{Li}_2$  moiety) is closest to the experimentally observed N-N fundamental

vibration ( $1535\text{ cm}^{-1}$ ) for  $\text{Li}_2\text{N}_4$  species. However, not only our computed scaled  $1779\text{ cm}^{-1}$  N-N stretching frequency of the  $\text{C}_{2v}$  triangular  $\text{LiN}_2$  species (**8**), but also the  $1783$  and  $1793\text{ cm}^{-1}$  frequencies for **1** and **2**, respectively, correspond with the experimentally observed  $1800\text{ cm}^{-1}$  N-N frequency assigned to a “lithium-nitrogen” species with a single lithium (Figure 3-1). We also have found another bent Li-N-N structure ( $\text{C}_s$ ) which is  $1.2\text{ kcal/mol}$  lower in energy than the  $\text{C}_{2v}$  form. However, the computed scaled stretching frequency for this  $\text{C}_s$  species ( $2024\text{ cm}^{-1}$ ), was not observed in the experiment.

### 3.4.2 Reaction of $\text{N}_2$ with $\text{Li}_2$ and $\text{Li}_4$ cluster

However,  $\text{LiN}_2$  and  $\text{Li}_2\text{N}_4$  are not likely to be key intermediates in the reaction of lithium metal with nitrogen at room or higher temperatures. Such reactions lead to the formation of lithium nitride,  $(\text{Li}_3\text{N})_x$ , evidently by a step-by-step migratory insertion mechanism of  $\text{N}_2$  into lithium surfaces or clusters.

Here in we report computed mechanistic details of step-by-step insertion reactions of  $\text{N}_2$  into lithium cluster models leading to dinitrogen reductions converting  $\text{N}_2^0$  to  $2\text{ N}^{3-}$  (See Computational methods for the theoretical levels employed). The degree of formal reduction of each nitrogen is characterized by its oxidation number, which ranges from zero in  $\text{N}_2$ , to  $-1$  in  $\text{LiN}_2\text{Li}$ , to  $-2$  in the “hydrazido”  $\text{Li}_2\text{NNLi}_2$ , and to  $-3$  in the “nitrido”  $\text{NLi}_3$  (or its oligomers) corresponding to complete N-N cleavage.

For orientation, we first investigated the reaction of  $\text{N}_2$  with  $\text{Li}_2$ . The insertion of  $\text{N}_2$  in  $\text{Li}_2$  is endothermic, hardly any reduction of  $\text{N}_2$  in terms of bond length elongation and even have high barriers associated with this process, suggesting the need for larger Li clusters to model the reduction process. The final product ( $\text{D}_{2h}\text{ N}_2\text{Li}_2$ ) is  $1.2\text{ kcal/mol}$  higher in energy than separated



N<sub>2</sub> and Li<sub>2</sub>. (See Figure 3-2 for the B3LYP/6-311+G\* reaction profile). The doubly bridged D<sub>2h</sub> N<sub>2</sub>Li<sub>2</sub> product resembles the binding mode of N<sub>2</sub> with

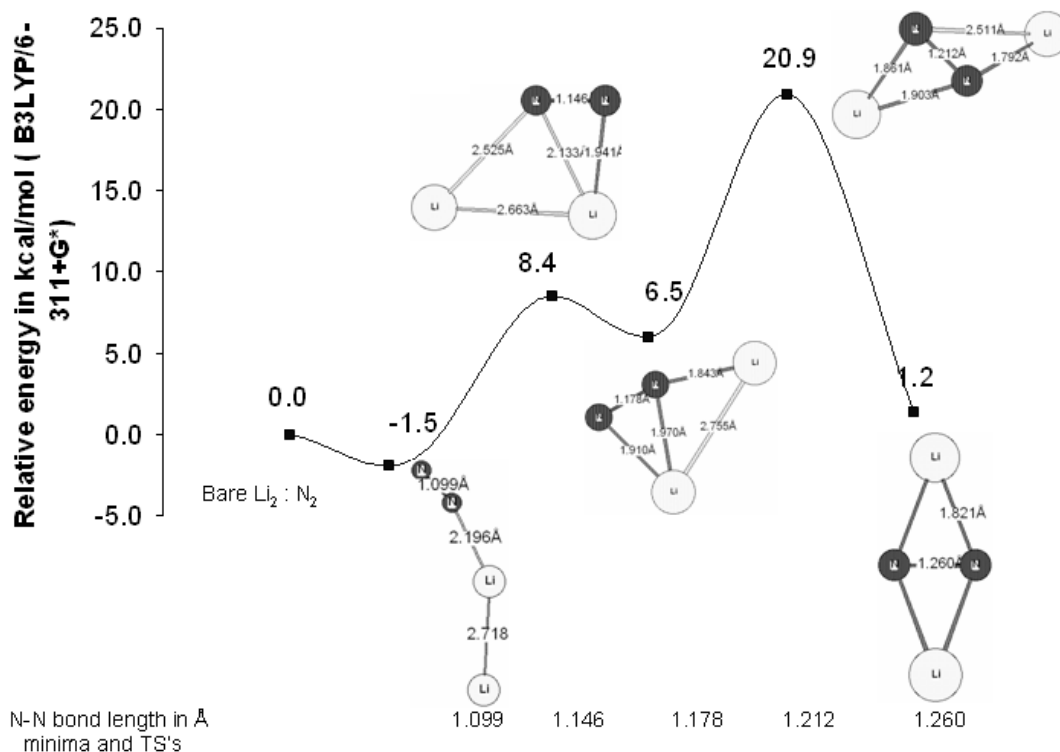


Figure 3-2. Pathway for the insertion of N<sub>2</sub> into the D<sub>∞h</sub> Li<sub>2</sub> cluster showing intermediates and transition structures. Energies relative to the initial complex are in kcal/mol (B3LYP/6-311+G\*). The overall reaction is endothermic and the final D<sub>2h</sub> N<sub>2</sub>Li<sub>2</sub> complex is even 1.2 kcal/mol higher in energy than the separate Li<sub>2</sub> and N<sub>2</sub> species.

Li<sub>2</sub> in [Cp<sub>2</sub>Zr(m-PPh)<sub>2</sub>]{(thf)<sub>3</sub>Li<sub>2</sub>(m-N<sub>2</sub>)}, an experimentally reported very rare example, featuring two lithium's side-on bonded to a N<sub>2</sub> unit [18]. The N<sub>2</sub> bond length in the complex was reported to be very short [1.06(1) Å] hardly distinguishable from that in free N<sub>2</sub>. The bonding interactions between Li and N<sub>2</sub> was attributed to the overlap of the Li(2s) and N(2s)

orbitals based on ab initio molecular orbital calculations on a model dication system  $[(\text{H}_2\text{O})_3\text{Li})_2(\mu\text{-N}_2)]^{2+}$ .

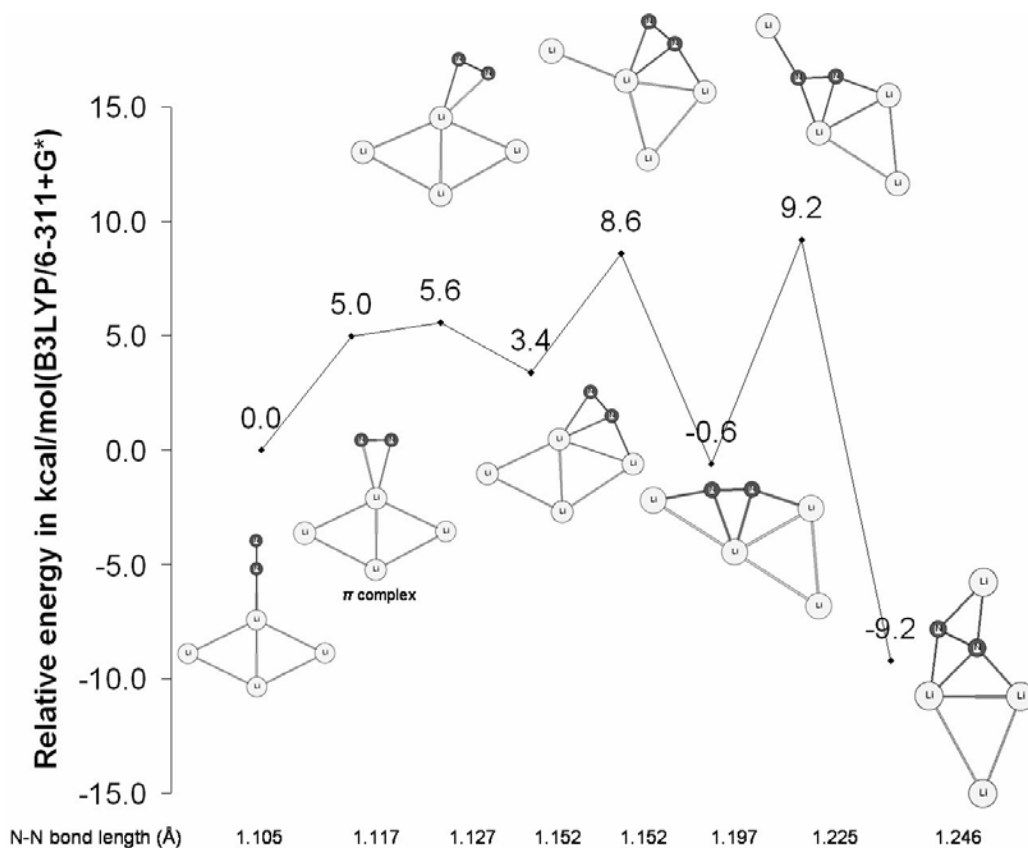


Figure 3-3. Pathway for the insertion of  $\text{N}_2$  into the  $\text{D}_{2h}$   $\text{Li}_4$  cluster showing intermediates and transition structures. Energies relative to the initial complex are in kcal/mol (B3LYP/6-311+ $\text{G}^*$ ).

Since more lithium atoms are needed to achieve full reduction, we next investigated the reaction of  $\text{N}_2$  with the planar  $\text{D}_{2h}$   $\text{Li}_4$  cluster to ascertain the geometrical changes along the reduction pathway. The binding energy of the side-on bound ( $\text{C}_{2v}$ ) complex is  $\sim 5 \text{ kcal mol}^{-1}$ . The reaction profile is depicted in Figure 3-3. Several in- plane Li atom movements eventually lead to a formal dianion unit ( $\text{N}_2^{2-}$ ). The N-N bond length in  $\text{N}_2\text{Li}_4$  ( $\text{C}_s$ ) (1.246 Å) is significantly longer compared to bare  $\text{N}_2$  (1.096 Å). However, dinitrogen is partially activated with four

lithium atoms as the bond length for the final product corresponds to N-N double bond (compared with N-N = 1.235(6) Å, for experimentally isolated {[Me<sub>3</sub>SiNC(Ph)-NSiMe<sub>3</sub>]<sub>2</sub>V}(μ-η<sup>1</sup>:η<sup>1</sup> N<sub>2</sub>)) [19].

### 3.4.3 Migratory insertion of N<sub>2</sub> in Li<sub>6</sub> and Li<sub>8</sub> cluster

Since four lithium atoms are not sufficient to achieve full reduction, we investigated the mechanistic pathway for N<sub>2</sub> insertion into Li<sub>6</sub> clusters. Unlike N<sub>2</sub>Li<sub>4</sub>, finding the starting N<sub>2</sub>Li<sub>6</sub> complex is non-trivial. The N<sub>2</sub>Li<sub>6</sub> potential energy surface (PES) was searched using Saunders' stochastic "kick" procedure (described in Methods)[14], which facilitates thorough exploration of chemically non-intuitive minima with very little human effort[15]. The plethora of interesting N<sub>2</sub>Li<sub>6</sub> geometries we obtained (see Figure 3-4) illustrates the well-precedented complexities of lithium structures [20]. While lithium- nitrogen bonding is largely ionic and bridging is common, the Li cluster moieties have their own preferences[6i]. The structures in Figure 3-4 obtained with "kick" are planar (NN bond lengths ranging from 1.106 to 1.241 Å) or as three dimensional (with 1.106 to 1.574 Å NN lengths). Bare D<sub>2h</sub> Li<sub>6</sub> is 4.8 kcal mol<sup>-1</sup> lower in energy than the planar D<sub>3h</sub> Li<sub>6</sub>. In case of the complexes also, the apex-bound C<sub>4v</sub> N<sub>2</sub>Li<sub>6</sub> complex (3) is 11.6 kcal mol<sup>-1</sup> more stable than its planar C<sub>s</sub> counterpart (1). Similarly, the side-bound nonplanar C<sub>1</sub> N<sub>2</sub> complex (4) is 6.0 kcal mol<sup>-1</sup> lower in energy than the analogous planar C<sub>s</sub> minimum (2) (Figure 3-4). As no planar minimum has NN separations greater than 1.25 Å, we concentrated on the non-planar alternatives.

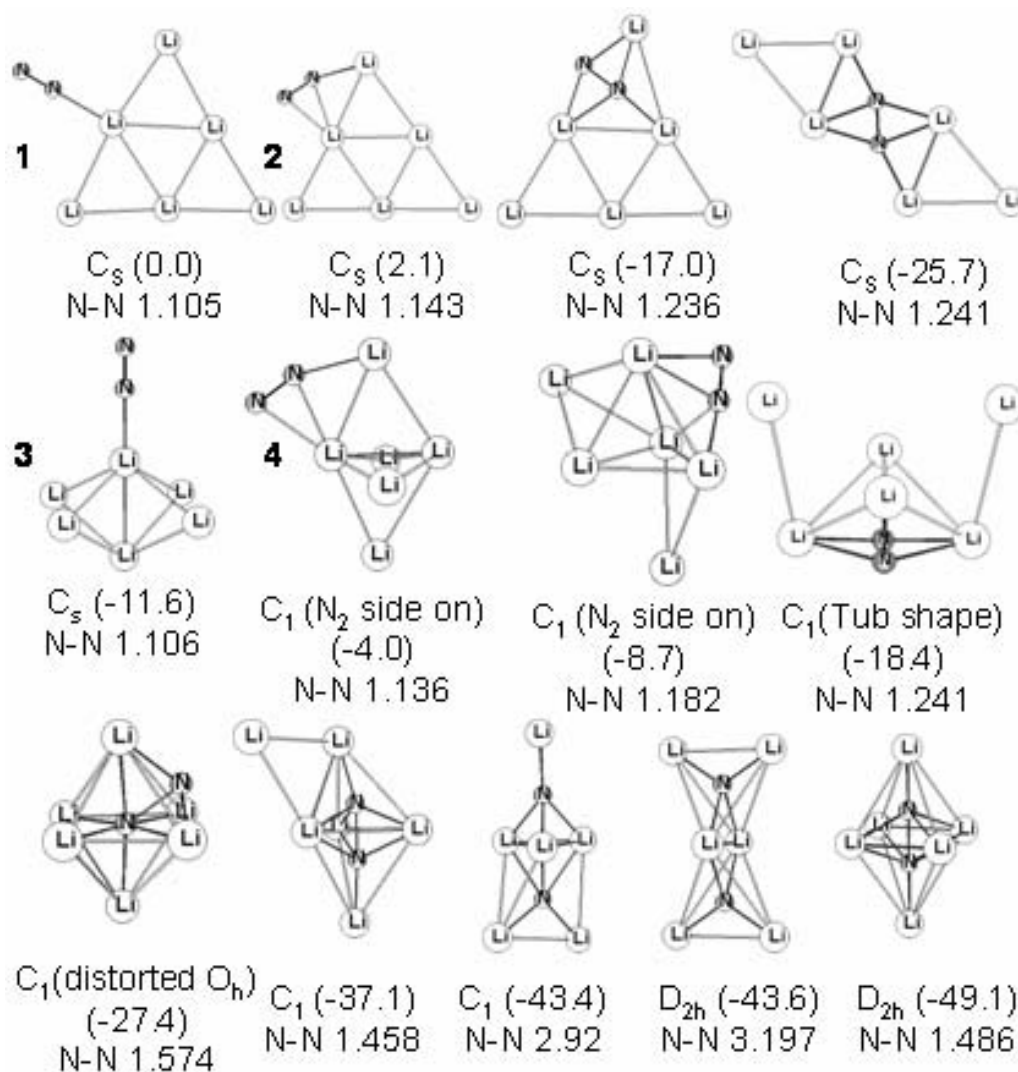


Figure 3-4.  $N_2Li_6$  [minima] with various NN distances (in Å) located by stochastic searches. (B3LYP/6-311+G\* energies in kcal/mol) relative to **1** are given in parentheses.

An energetically viable stepwise mechanism modeling reduction to a nitrido product,  $(NLi_3)_2$ , starting from the  $C_{4v}$   $N_2$ - $Li_6$  complex (**3**), is depicted in Figure 3-5. The 9.4 kcal mol<sup>-1</sup> exothermicity of the initial complex formation surmounts the subsequent reaction barriers for the first stage of NN bond elongation to over 1.2 Å. Several out-of-plane Li atom movements but

very little additional activation needed to give a local minimum with 1.25 Å NN length and the hydrazido ( $D_{2h}$ )  $N_2Li_6$  global minimum  $r_{NN}$  1.487 Å [16].

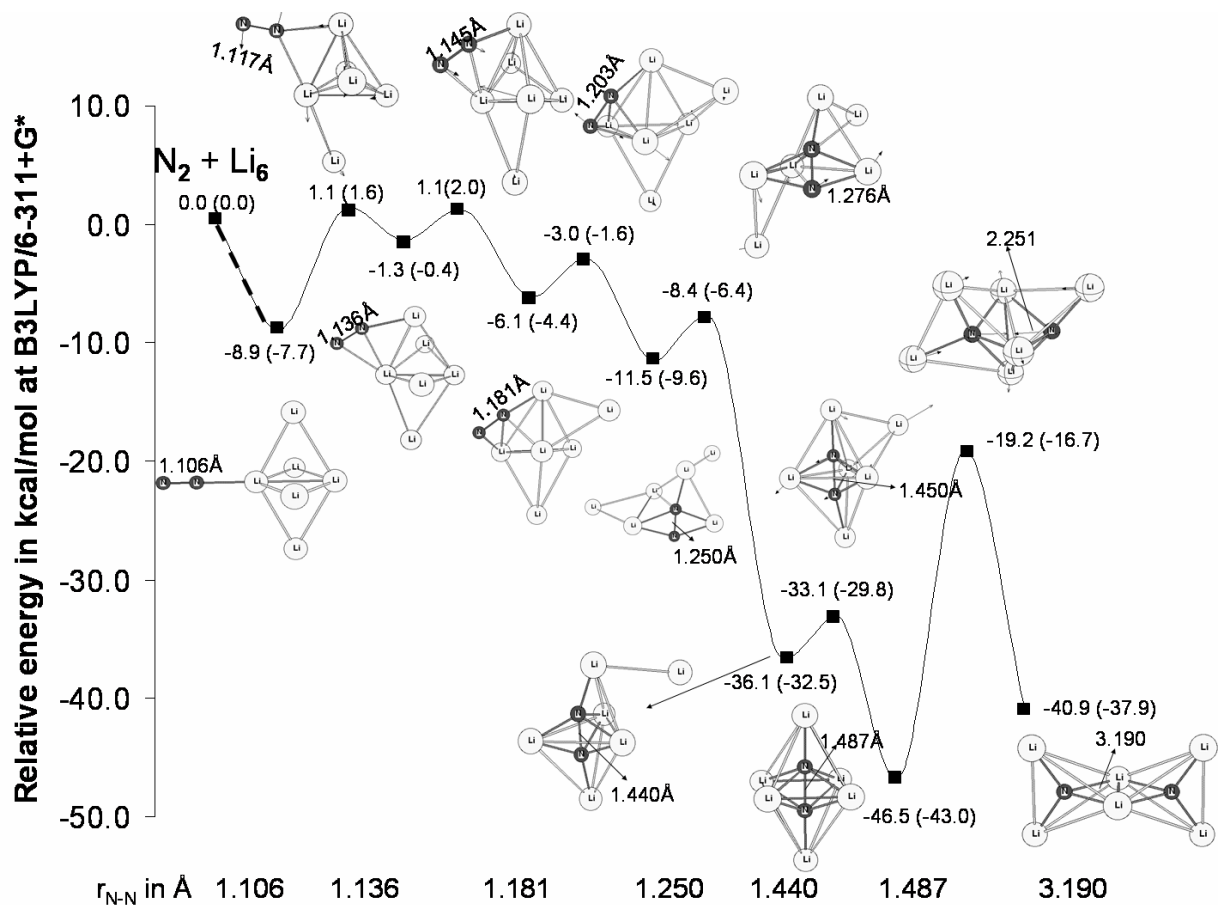


Figure 3-5 Pathway for the  $N_2$  insertion into a  $Li_6$  cluster. Structures of transition states, intermediates, and products are shown (B3LYP/6-311+G\*). The zero point vibrational energy corrected energies (ZPVE) are reported in parenthesis.

Unexpectedly, the fully reduced  $N_2Li_6$  nitrido compound, a  $[(NLi_3)_2]$  complex, with a 3.190 Å separation, is 5.5 kcal. mol<sup>-1</sup> higher in energy. In addition, a large activation barrier (27.6 kcal mol<sup>-1</sup>) hinders the conversion of the hydrazido to the nitrido form.

This problem of incomplete reduction to oxidation number -2 is not encountered when two additional lithiums are included in the process. The  $\text{N}_2\text{Li}_8$  PES, explored using the “kick” stochastic search method [14], has numerous interesting minima with NN bond lengths ranging from 1.1 to over 3 Å (see Figure 3-6). The side-on-bound  $\text{N}_2\text{Li}_8$  complex is higher in energy than the end-on-bound isomers, with  $\text{N}_2$  (1.111Å) extending from one of the  $T_d$   $\text{Li}_8$  edges. Our mechanism for nitrogen insertion into the

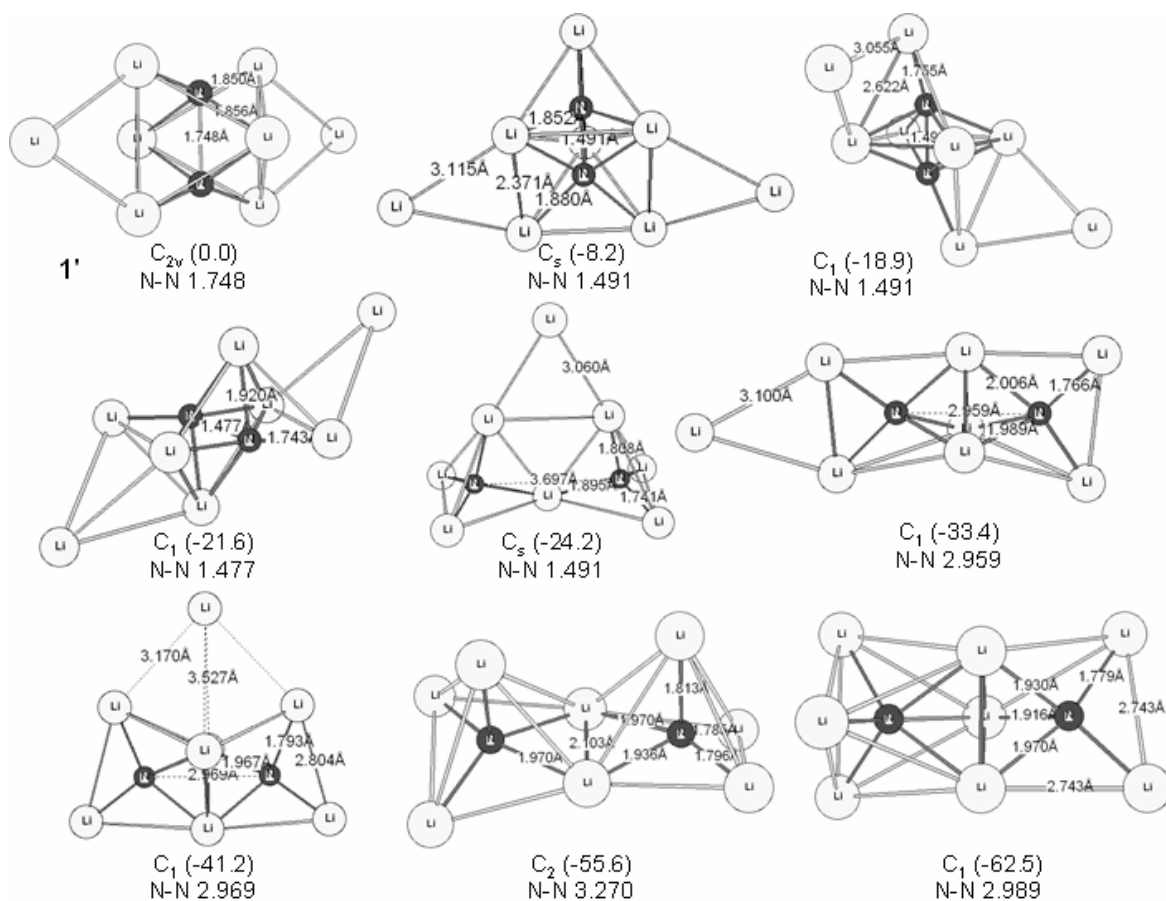


Figure 3-6.  $\text{N}_2\text{Li}_8$  [minima] with various NN distances (in Å) located by stochastic searches. B3LYP/6-311+G\* energies in kcal/mol relative to 1' are given in parentheses.

most stable  $\text{Li}_8$  cluster isomer, known to have  $T_d$  symmetry[22], is shown in Figure. 5-7. However, as depicted in Figure 3-7 side-on complexes are involved in the  $\text{N}_2$  insertion. As with

$\text{N}_2\text{Li}_6$  (see Figure 3-5), the initial reaction profile is rather flat with many minima having similar energies. Precedents for such cluster variants involving lighter metals are well known [6i]. The final fully-reduced  $\text{N}_2\text{Li}_8$  nitrido product with well-separated N's ( $\text{NN} = 3.023\text{\AA}$ ) not only is the global minimum product but also is  $82.4\text{ kcal mol}^{-1}$

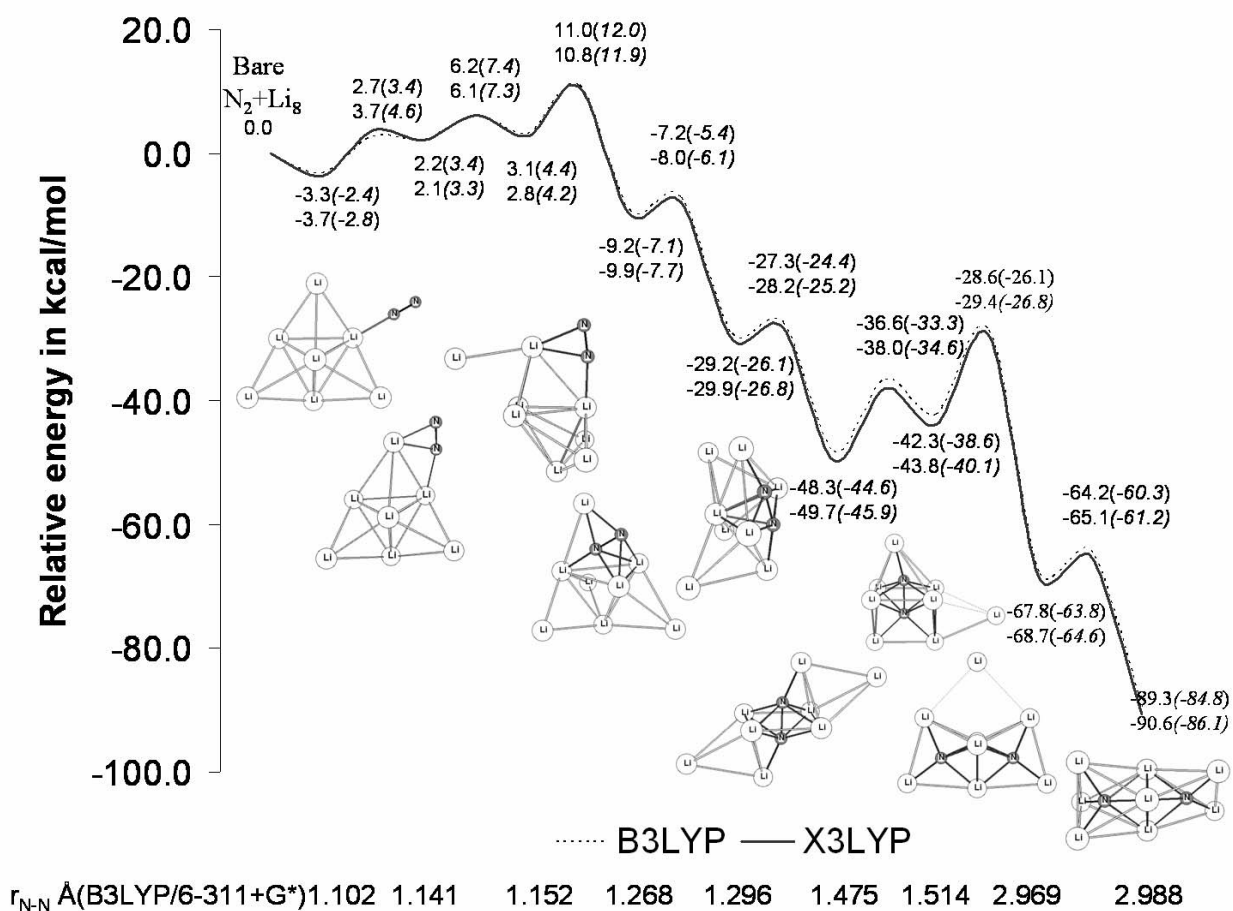







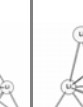




Figure 3-7. Reaction profile for the insertion of  $\text{N}_2$  into  $\text{Li}_8$  cluster. Only the structures and the N-N bond length of the minima are depicted. Note the low barrier of the initial stages of the reaction and the agreement between the B3LYP and X3LYP mechanistic details. The zero point vibrational energy (ZPVE) corrected energies are reported in parenthesis.

more stable than the weakly N<sub>2</sub> bound starting complex! This N<sub>2</sub>Li<sub>8</sub> pathway is much more exothermic than that for N<sub>2</sub> insertion into Li<sub>6</sub> (compare Figure 3-5), where nitrido N<sub>2</sub>Li<sub>6</sub> is 30.2 kcal.mol<sup>-1</sup> lower in energy than the initial complex, and is not the global minimum. Our mechanistic details for nitrogen activation at B3LYP [11] agree well qualitatively (compare the data in Figure 3-7) with those computed using X3LYP[13], an extension of B3LYP by Xu and Goddard to including the Perdew-Wang 1991 gradient exchange correction for treating non-covalent interactions.

### 3.4.4 Analysis of activation of dinitrogen during step by step migratory insertion

Table 3-1. Variation of N-N bond length and charge for the important stationary points on N<sub>2</sub>: Li<sub>n</sub> (n=6,8) reaction profile with step by step reduction of dinitrogen with six and eight lithium atoms respectively.

										
	<b>N<sub>2</sub>Li<sub>6</sub></b>					<b>N<sub>2</sub>Li<sub>8</sub></b>				
N-N Bond Length (Å)	1.106	1.136	1.250	1.487	3.190	1.111	1.148	1.273	1.483	3.023
NBO Charge <sup>a</sup> (N <sub>1</sub> ) (N <sub>2</sub> )	-0.168 0.005	-0.371 -0.116	-1.048 -0.703	-1.802 -1.802	-2.786 -2.787	-0.153 0.019	-0.365 -0.268	-1.081 -0.905	-1.742 -1.742	-2.855 -2.813

<sup>a</sup>Charge from natural population analysis @ B3LYP/aug-ccpVDZ

The extent of activation of dinitrogen during the step-by-step insertion process can be evaluated on the basis of well defined observable properties like the NN bond lengths or the NN stretching vibrational frequencies. Experimental NN bond lengths generally are used for comparison purposes, e.g., N<sub>2</sub> triple bond 1.097 Å (N<sub>2</sub> gas), double bond is 1.236 and 1.255 Å



( $\{[\text{Me}_3\text{SiNC(Ph)-NSiMe}_3]_2\text{V}\}_2(\mu\text{-}\eta^1:\eta^1\text{N}_2)$  and  $\text{PhN=NPh}$ ), and single bond 1.454 Å (hydrazine  $\text{NH}_2\text{-NH}_2$ )[2]. The longest dinitrogen bond distance reported crystallographically to date (1.525 Å) is equivalent to a long single bond and occurs in a hybrid complex of an alkali metal with

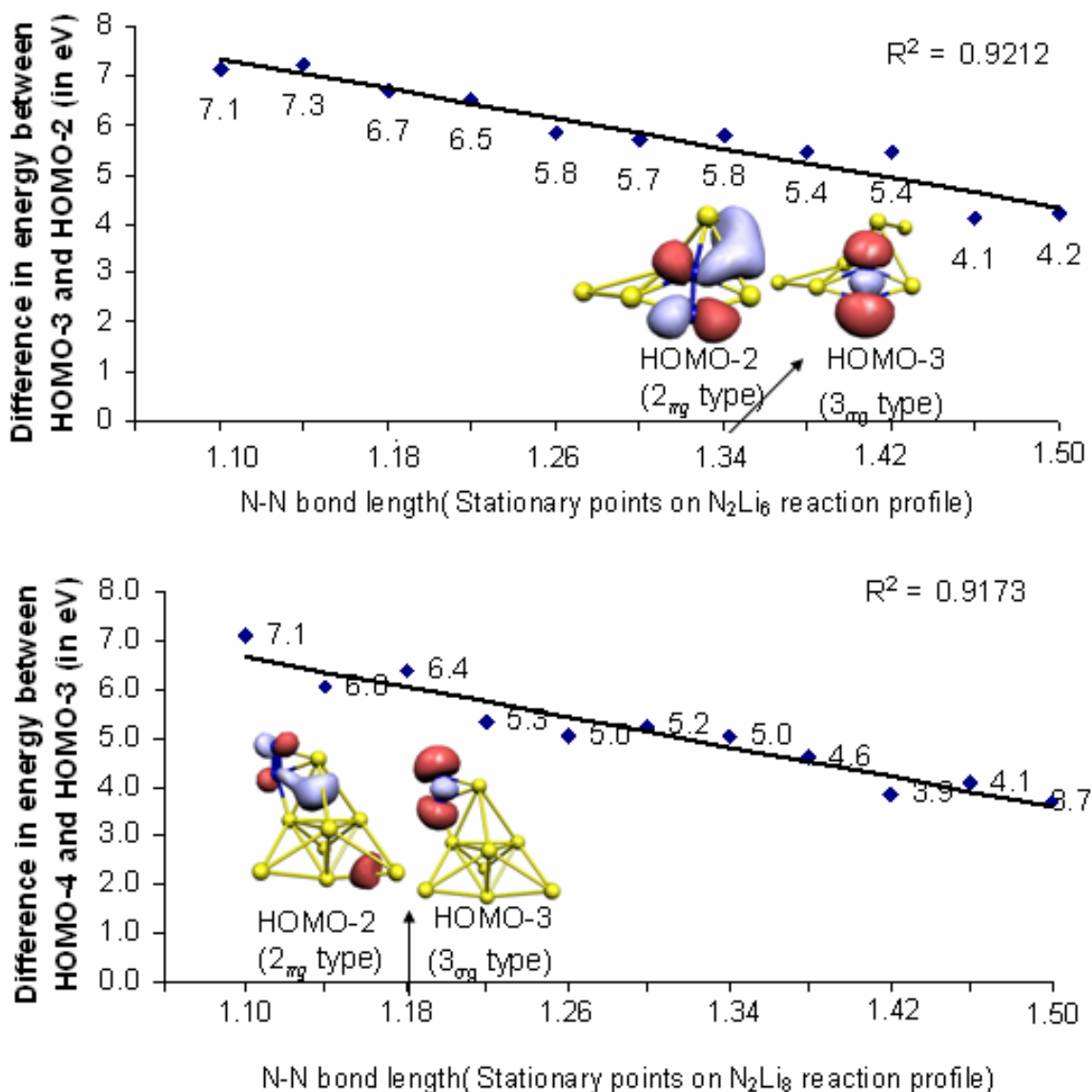


Figure 3-8. The bond elongation of dinitrogen is linearly related to the energy gap between the  $2\pi_g$  and  $3\sigma_g$  type orbitals of the  $\text{N}_2$  moieties of the  $\text{N}_2\text{Li}_n$  ( $n=6,8$ ) clusters. Representative molecular orbitals (MOs) are shown for one complex in each case.

a lanthanide (samarium(II))[23]. Additional criteria, such as partial charges, also can also serve as descriptors. Note the successive increase in the N-N bond length and partial charge (negative) on the N atoms for the selected  $N_2Li_6$  and  $N_2Li_8$  stationary points in Table 3-1 and the correlation between bond length and partial charge. The tendency of lithium atoms to donate valence electrons is also evident from the charge data. Moreover, the very large HOMO ( $3\sigma_g$ )-LUMO( $2\pi_g$ ) gap for molecular dinitrogen (22.9 eV), which contributes to its inertness, is reduced substantially by the donation of electrons from lithium to the  $2\pi_g$  orbitals. The stepwise reduction/bond elongation of dinitrogen is linearly related to the energy gap between  $2\pi_g$  and  $3\sigma_g$  type orbitals for both the  $N_2Li_n$  ( $n=6$  and  $8$ ) complexes (Figure 3-8). The various  $N_2Li_6$  and  $N_2Li_8$  species with various NN bond lengths exhibit different degrees of  $N_2$  reduction.

### 3.4.5 Exceptional reactivity of $N_2$ with Li

Table 3-2. The atomization energy/alkali metal (for  $BM_3$ ,  $CM_4$ ,  $NM_3$ ,  $OM_2$ ,  $PM_3$  and  $SiM_4$ ). The Li compounds have highest AE/atom, ~1.5 times of Na and K, in accord with Lithium's unusual reactivity pattern among the alkali metals.

	Li			Na			K		
	Bond length (Å)	AE kcal/mol	AE/atom Kcal/mol	Bond length (Å)	AE kcal/mol	AE/atom kcal/mol	Bond length (Å)	AE kcal/mol	AE/atom kcal/mol
$BM_3$	2.133	94.7	31.6	2.511	63.1	21.0	2.932	48.8	16.3
$CM_4$	1.865	191.1	47.8	2.284	112.7	28.2	2.659	91.2	22.8
$NM_3$	1.722	157.8	52.6	2.159	81.1	27.0	2.414	69.6	23.2
$OM_2$	1.627	170.7	85.4	1.994	108.6	54.3	2.231	111.5	55.8
$PM_3$	2.218	141.4	47.1	2.593	97.4	32.5	2.924	85.1	28.4
$SiM_4$	2.342	148.5	37.1	2.703	105.8	26.5	3.092	90.7	22.7

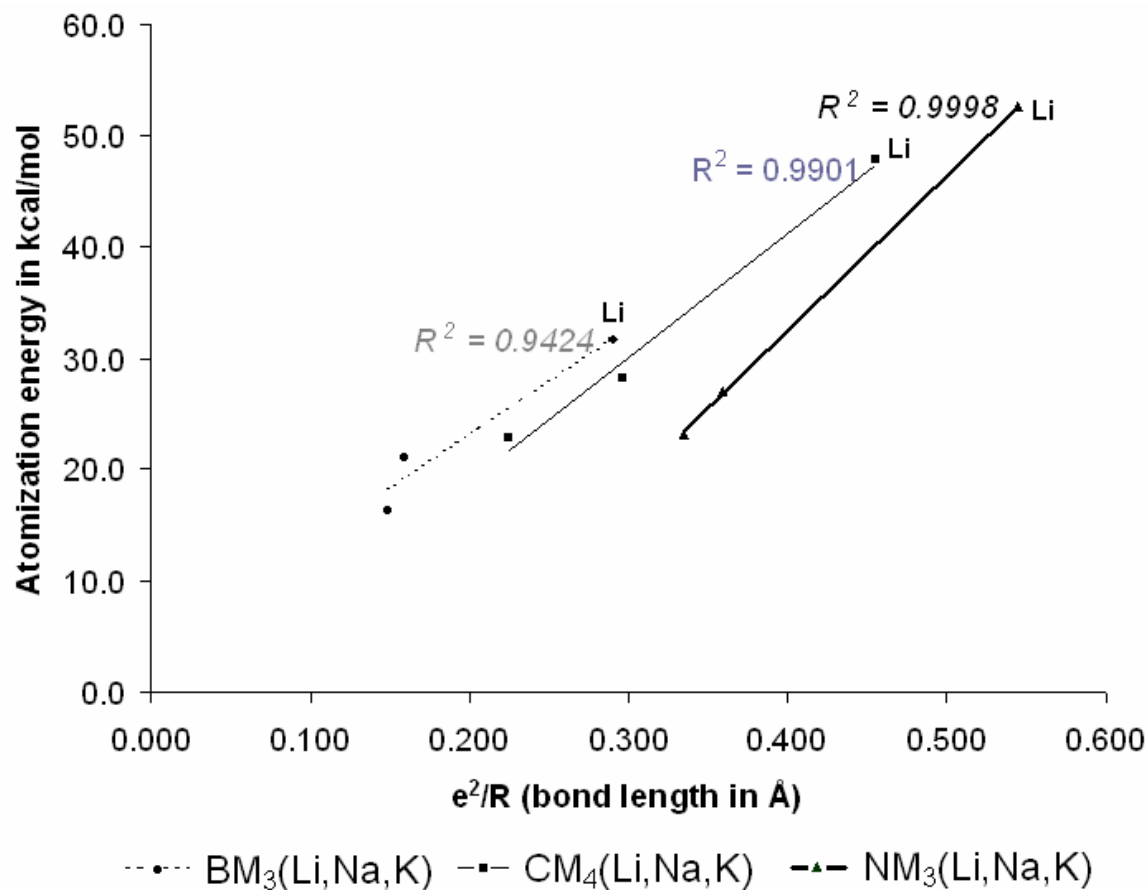
Why does Li (but not Na and K) react with  $N_2$  even at room temperature? The computed atomization energies (AE) of all the electrostatically bound species:  $BM_3$  ( $D_{3h}$ ),  $BM_2(2)(D_{\infty h})$ ,

BM<sub>4</sub> (C<sub>1</sub>), CM<sub>2</sub>(2) (D<sub>∞h</sub>), CM<sub>3</sub>(2) (D<sub>3h</sub>), CM<sub>4</sub> (T<sub>d</sub>), NM<sub>2</sub>(2) (D<sub>∞h</sub>), NM<sub>3</sub> (D<sub>3h</sub>), NM<sub>4</sub>(2) (T<sub>d</sub>) , OM<sub>2</sub> (D<sub>∞h</sub>), OM<sub>3</sub>(2) (D<sub>3h</sub>), OM<sub>4</sub>(2) (T<sub>d</sub>), SiM<sub>4</sub> (C<sub>2v</sub>), PM<sub>3</sub> (D<sub>3h</sub>) (M= Li, K, Na), reveal that the Li compounds have, by far, the highest AE's/atom for NM<sub>3</sub>, 52.6 (Li), 27.0 (Na), and 23.2 (K) kcal/mol. The bond length and AE data for all the above mentioned compounds are reported in Table 3-2.

Table 3-3. Bond length and Natural Charges for compounds of alkali metal- first row and second row elements (Charges computed with NBO 5.0 program@ B3LYP/6-311+G\* level).<sup>16</sup>

	Charge on first row elements	Charge on alkali metals
BLi <sub>3</sub> (D <sub>3h</sub> )	B -2.361	Li + 0.787
BNa <sub>3</sub> (D <sub>3h</sub> )	B -1.898	Na + 0.632
BK <sub>3</sub> (D <sub>3h</sub> )	B -1.982	K + 0.660
CLi <sub>4</sub> (T <sub>d</sub> )	C -3.685	Li + 0.921
CNa <sub>4</sub> (T <sub>d</sub> )	C -3.293	Na 0.823
CK <sub>4</sub> (T <sub>d</sub> )	C -3.098	K +0.774
NLi <sub>3</sub> (D <sub>3h</sub> )	N -2.816	Li +0.938
NNa <sub>3</sub> (C <sub>2v</sub> )	N -2.328	Na+0.776
NK <sub>3</sub> (D <sub>3h</sub> )	N -2.424	K +0.808
OLi <sub>2</sub> (D <sub>∞h</sub> )	O -1.900	Li 0.950
ONa <sub>2</sub> (D <sub>∞h</sub> )	O -1.858	Na 0.929
OK <sub>2</sub> (D <sub>∞h</sub> )	O -1.803	K 0.901
PLi <sub>3</sub> (C <sub>3v</sub> )	P -2.414	Li +0.804
PNa <sub>3</sub> (C <sub>3v</sub> )	P -2.098	Na +0.699
PK <sub>3</sub> (C <sub>3v</sub> )	P -2.321	K +0.773
SiLi <sub>4</sub> (C <sub>2v</sub> )	Si -2.622	Li +0.763/+0.547
SiNa <sub>4</sub> (C <sub>2v</sub> )	Si -2.198	Na+0.627/+0.472
SiK <sub>4</sub> (C <sub>2v</sub> )	Si -2.990	K +0.748

Moreover, the lithium compounds have the shortest Li-B/C/O/N/Si/P bond lengths and the largest charge separations (Table 3-3). For example, the natural charges for compounds of alkali metal- first row elements (charges computed with NBO 5.0 program <sup>[16]</sup> @ B3LYP/6-311+G\* level) on NM<sub>3</sub> (M=Li, Na, K) are: Li/N (+0.93/-2.81), Na/N (+0.77/-2.32), K/N (+0.80/-2.42). The atomization energy plotted against  $e^2/R$  for alkali metal containing B, C and N molecules



	$e^2/R$	AE/atom kcal/mol		$e^2/R$	AE/atom kcal/mol		$e^2/R$	AE/atom kcal/mol
BLi <sub>3</sub>	0.290	31.6	CLi <sub>4</sub>	0.455	47.8	NLi <sub>3</sub>	0.545	52.6
BNa <sub>3</sub>	0.159	21.0	CNa <sub>4</sub>	0.296	28.2	NNa <sub>3</sub>	0.359	27.0
BK <sub>3</sub>	0.149	16.3	CK <sub>4</sub>	0.225	22.8	NK <sub>3</sub>	0.335	23.2

Figure 3-9. Plot of atomization energy vs  $e^2/R$  for alkali metal containing B, C and N molecules ( $e$  = natural charge on M).

( $e$  = natural charge on M) gives a directly proportional relationship to  $e^2/R$  for a given series. The higher atomization energy for Li compounds can be attributed to the strong ionic nature of the Li-B/C/N bond (Figure 3-9).

### 3.5 Conclusion

To summarize, the reaction of the normally quite inert  $N_2$  with lithium is remarkably facile. As shown by our computed results,  $N_2$  readily complexes at various positions of  $Li_2$ ,  $Li_4$ ,  $Li_6$ , and  $Li_8$  model clusters. These isomeric complexes interconvert over generally low barriers, but their NN elongations with small cluster size ( $Li_4$ ) are only to double bond lengths (ca. 1.25 Å). Further reduction to oxidation state -2 and -3 only occurred with  $N_2Li_6$  and  $N_2Li_8$ . The key step in both  $N_2Li_6$  and  $N_2Li_8$  involved the sudden, exothermic (ca. 22.9 kcal mol<sup>-1</sup> and 19.0 kcal/mol, respectively, at B3LYP) double to single (~1.3 to 1.48 Å) NN bond length elongation. The final reduction stage separates the N atoms by over 3 Å and embeds them centrally in  $(NLi_3)_2$  and  $(NLi_4)_2$  dimer clusters. Although  $(NLi_3)_2$  is not the global  $N_2Li_6$  minimum, it is 37.9 kcal/mol (36.6 kcal/mol with MP2/6-311+G\*) more stable than separated  $N_2 + Li_6$ . The  $(NLi_4)_2$  dimer end product is the  $N_2Li_8$  global minimum and the exothermicity of the  $N_2 + Li_8$  reaction is enormous, 84.8 kcal/mol (76.4 kcal/mol with MP2/6-311+G\*). Moreover, we provide an explanation for the exceptional reactivity of  $N_2$  with Li, compared to the other alkali metals, e.g., Na and K. Li is a very strong reducing agent as its nitrides have the highest atomization energy, the shortest M-N bond distance, and the largest M-N charge separation as well as interaction energy. Our detailed mechanism of the insertion of  $N_2$  into model lithium clusters delineates the general manner in which molecular nitrogen can be activated sequentially by electron transfer and bond elongation, to give a series of increasingly reduced complexes. Lithium by itself is not a catalyst but lithium incorporation into complexes might facilitate the “development of nitrogen fixation catalyst”.

### 3.6 Acknowledgement

We thank Research Computing Center of University of Georgia for providing computational resources and Dr. Yamaguchi (UGA CCC) for numerous scientific discussions. This work was supported by National Science Foundation Grants CHE-0716718.

### 3.7 References

- 1) S. A. Johnson, M. D. Fryzuk, *Coord. Chem. Rev.*, 2000, **200**, 379-409.
- 2) M. P. Shaver, M. D. Fryzuk, *Adv. Synth. Catal.* 2003, **345**, 1061-1076.
- 3) N.N. Greenwood, A. Earnshaw, *Chemistry of the Elements*, School of Chemistry, University of Leeds, U.K., 1997.
- 4) V. Smil, *Enriching the Earth* (The MIT Press, Cambridge, MA, 2001).
- 5) a) M. Hidai, *Coord. Chem. Rev.* **1999**, **85**, 99-108. b) G. J. Leigh, *Acc. Chem. Res.* **1992**, **25**, 177-181. c) R. R. Eady, *Chem. Rev.* **1996**, **96**, 3013-3030. d) B. A. MacKey, M. D. Fryzuk, *Chem. Rev.* **2004**, **104**, 385-401 and references there in.
- 6) a) G. V. Chertihin, L. Andrews, C. W. Bauschlicher, *J. Am. Chem. Soc.* **1998**, **120**, 3205- 3212. b) G. V. Chertihin, W. D. Bare, L. Andrews, *J. Phys.Chem.A* **1998**, **102**, 3697-3704. c) A. Citra, L. Andrews, *J. Am.Chem. Soc.* **1999**, **121**, 11567-11568. d) H. J. Himmel, O. Hubner, W. Klopfer, L. Manceron, *Angew. Chem. Int. Ed.* **2000**, **45**, 2799-2802. e) E. E. Tamelen, G. Boche, S. W. El, R. B. Fechter, *J. Am. Chem. Soc.*, **1967**, **89**, 5707. f) N. Kuganathan, J. C. Green, H. J. Himmel, *New J. Chem.* **2006**, **30**, 1253-1261. g) M.F. Zhou, X. Jin, Y. Gong, J. Li, *Angew. Chem. Int. Ed.* **2007**, **46**, 2911 -2914. h) H. J. Himmel, M. Reiher, *Angew. Chem. Int. Ed.* **2006**, **45**, 6264-6288. i) V. Bonačić-Koutecký, P. Fantucci, J. Koutecký, *Chem. Rev.* **1991**, **91**, 1035. j) J. Li, and S. Li,

- Angew. Chem. Int. Ed.* **2008**, *47*, 8040- 8043. h) J. A. Pool, E.Lobkovsky, P. J. Chirik, *Nature* **2004**, *427*, 527–530. i) L. P. Spencer, B. A. MacKay, B. O. Patrick, M.D.Fryzuk, *Proc. Natl. Acad. Sci. U.S.A.* **2006**, *103*, 17094–17098. j) F. Akagi, T. Matsuo, H. Kawaguchi, *Angew. Chem., Int. Ed.* **2007**, *46*, 8778–8781.
- 7) a) S. Gambarotta, *J. Organomet. Chem.* **1995**, *500*, 117–126. b) S. Gambarotta, J. Scott, *Angew.Chem. Int. Ed.*, **2004**, *43*, 5298 –5308. c) R. R. Schrock, *Angew. Chem. Int. Ed.*,**2008**, *47*, 5512 – 5522 and references there in d) J. J. Curley, T. R. Cook, S. Y. Reece, P. Müller, C. C. Cummins, *J. Am. Chem. Soc.* **2008**, *130*, 9394 – 9405. e) H. Tanaka, H. Mori, H. Seino, M.Hidai, Y. Mizobe, K. Yoshizawa, *J. Am. Chem. Soc.* **2008**, *130*, 9037. d) M. D. Fryzuk, *Acc.Chem. Res.*, **2009**, *42* (1), 127-133. e) S. Schenk, M. Reiher, *Inorg. Chem.*, **2009**, *48* (4), 1638-1648. f)M.Mori, *Heterocycles*,**2009**,*78*(2),281-318. f) G. Christian, R. Stranger, B.F. Yates, *Chem Eur J*, **2009**, *15* (3), 646-655.
- 8) J, M. Mori, K. Hori, M. Akashi, M. Hori, Y. Sato, M. Nishida, *Angew. Chem. Int. Ed.*,**1998**, *37*, 636-637.
- 9) R. C. Spiker, L. Andrews, Jr., C. Trindle, *J. Am. Chem. Soc.* **1972**, *94*, 2401-2407.
- 10) a) P. Chen, Z. Xiong, J. Luo, J. Lin, K. L. Tan, *Nature* **2002**, *420*, 302-304. b)O. Palumbo, A. Paolone, R. Cantelli, D. Chandra, *Int J Hydrogen Energy* **2008**, *33*, 3107-3110.
- 11) a) A.D. Becke, *Phys. ReV. A*, **1988**, *38*, 3098-3100. b) C. Lee, W. Yang, R. G. Parr, *Phys. Rev. B*.**1988**, *37*, 785-789.
- 12) Gaussian 03, Revision C.02, M. J. Frisch, G. W. Trucks, H. B. Schlegel, G. E. Scuseria, M. A. Robb, J. R. Cheeseman, J. A. Montgomery, Jr., T. Vreven, K. N. Kudin, J. C. Burant, J. M. Millam, S. S. Iyengar, J. Tomasi, V. Barone, B. Mennucci, M. Cossi, G.

Scalmani, N. Rega, G.A. Petersson, H. Nakatsuji, M. Hada, M. Ehara, K. Toyota, R. Fukuda, J. Hasegawa, M. Ishida, T. Nakajima, Y. Honda, O. Kitao, H. Nakai, M. Klene, X. Li, J. E. Knox, H. P. Hratchian, J. B. Cross, C. Adamo, J. Jaramillo, R. Gomperts, R. E. Stratmann, O. Yazyev, A. J. Austin, R. Cammi, C. Pomelli, J. W. Ochterski, P. Y. Ayala, K. Morokuma, G. A. Voth, P. Salvador, J. J. Dannenberg, V. G. Zakrzewski, S. Dapprich, A. D. Daniels, M. C. Strain, O. Farkas, D. K. Malick, A. D. Rabuck, K. Raghavachari, J. B. Foresman, J. V. Ortiz, Q. Cui, A. G. Baboul, S. Clifford, J. Cioslowski, B. B. Stefanov, G. Liu, A. Liashenko, P. Piskorz, I. Komaromi, R. L. Martin, D. J. Fox, T. Keith, M. A. Al-Laham, C. Y. Peng, A. Nanayakkara, M. Challacombe, P. M. W. Gill, B. Johnson, W. Chen, M. W. Wong, C. Gonzalez, and J. A. Pople, Gaussian, Inc., Wallingford CT, 2004.

- 13) X. Xu, W. A. Goddard, *Proc. Natl. Acad. Sci. U S A.* **2004**, *101* (9), 2673-2677.
- 14) M. Saunders, *J. Comput. Chem.* **2004**, *25*, 621-626.
- 15) a) D. Roy, C. Corminboeuf, C. S. Wannere, R. B. King, P. v. R. Schleyer, *Inorg. Chem.* **2006**, *45*, 8902-8906. b) P. P. Bera, K. W. Sattelmeyer, M. Saunders, H. F. Schaefer, P. v. R. Schleyer, *J. Phys. Chem. A.* **2006**, *110*, 4287-4290.
- 16) A. E. Reed, L. A. Curtiss, F. J. Weinhold, *Chem. Rev.* **1988**, *88*, 899-926.
- 17) A. P. Scott, L. Radom, *J. Phys. Chem.* **1996**, *100*, 16502-16513.
- 18) J. Ho, R. J. Drake, D. W. Stephan, *J. Am. Chem. Soc.* **1993**, *115*, 3792-3793.
- 19) S. Hao, P. Berno, R. K. Minhas, S. Gambarotta, *Inorg. Chim. Acta*, **1996**, *244*, 37-49.
- 20) a) J. D. Dill, P. v. R. Schleyer, J. S. Binkley, J. A. Pople, *J. Am. Chem. Soc.* **1977**, *99*, 6159- 6173. b) P. v. R. Schleyer, *Pure Appl. Chem.* **1984**, *56*, 151-162. c) K. Gregory, P. v. R. Schleyer, R. Snaith. *Advances in Inorganic Chemistry*, **1991**, *37*, 47-142. d) M. N.



Glukhovtsev, P. v. R. Schleyer, *Isr. J. Chem.***1993**, 33, 455-466. e) A.M. Sapse, P. v. R. Schleyer, *Lithium Chemistry: A Theoretical and Experimental Overview*, (Wiley, New York, **1995**). f) S. E. Wheeler, K. W. Sattelmeyer, P. v. R. Schleyer, H. F. Schaefer, *J. Chem. Phys.***2004**, 120, 4683-4689.

21) The relative energy with CCSD(T)/aug-ccpVDZ single point calculation (with MP2/6-311+G\* geometry) was found to be 5.2 kcal mol<sup>-1</sup>.

22) G. Gardet, F. Rogemond, H. Chermette, *J. Chem. Phys.***1996**, 105, 9933-9947.

23) J. Jubb, S. Gambarotta, *J. Am. Chem. Soc.* **1994**, 116, 4477-4478.

CHAPTER 4

AROMATICS WITH ONE DELOCALIZED ELECTRON<sup>‡</sup>

---

<sup>‡</sup> Roy, D. Schleyer, P. v. R. To be submitted to *Chemistry – A European Journal*

## 4.1 Abstract

The criteria for aromaticity in case of neutral even-electron singlet species are cyclic conjugation of  $(4n+2)$   $\pi$ -electron, stabilization by enhanced delocalization, bond lengths equalization, diatropic  $^1\text{H}$  NMR shift and large negative NICS. However, the concept was extended in Post-Huckel period. From initial confinement to systems with  $\pi$  delocalized electrons, the concept of  $\sigma$ -aromaticity has been invoked to rationalize properties of saturated cyclic hydrocarbons. Moreover, aromaticity concept was extended from two to three dimensions. The extension of the concept of aromaticity to the odd-electron  $\pi$  systems may be considered questionable, as the first criterion for aromaticity is the presence of  $(4n + 2)$   $\pi$ -electron cyclic conjugation, thus not including odd electron systems. However, the second criterion refers to whether cyclic conjugation stabilizes or destabilizes a system, and this criterion is independent of whether there are odd number of electrons. Similarly, geometric criteria and others may be applied to odd-electron systems. We have theoretically designed a myriad of two and three dimensional “one electron aromatic” systems, and have evaluated the degree of electron delocalization by energetic, geometric, and magnetic criteria. While the realization of one  $\pi$ -electron electronic structures is not straightforward, the investigation of boron and aluminium rings appears as an obvious strategy. Unlike hydrocarbons, which favour 2c-2e bonds, the chemistry of boron is determined by Lipscomb’s electron-deficient 3c-2e bonding pattern, that beneficiaries from electron delocalization. Similarly, aluminium forms a large variety of compounds whose chemistry differs from that of carbon. We also predict that some of our theoretically designed “one electron aromatics”, e.g. doublet  $\text{C}_6\text{H}_{12}\text{B}_4^-$  are viable for experimental detection.

## 4.2 Introduction

The theoretical concept of aromaticity initially recognized the unique electronic structures of various cyclic (Hückel) hydrocarbons in which the  $\pi$ -delocalization of  $4n+2$  electrons results in unusual stabilities, bond length equalizations, specific magnetic properties, and/or definitive chemical reactivity patterns[1]. Further conceptual developments address  $\sigma$ -aromaticity[2], double aromaticity[3] and three dimensional aromaticity [4]. Here we extend the concept of aromaticity from even electron singlet species to open-shell systems with odd numbers of electrons. In practice, the question of whether odd-electron systems have an aromatic or antiaromatic character has only been raised by few authors [5-7]. The resonance energy (RE) of the neutral free radical  $C_7H_7$  was for instance evaluated empirically by Vincow *et al.* in 1969[7]. It was concluded that  $C_7H_7$  is an extensively stabilized molecule with a resonance energy (RE) almost equal to that of benzene [5a]. However, this interpretation has been questioned and the presence of antiaromaticity effects in  $C_7H_7$  has also been invoked [6]. The related question regarding the aromaticity of triplet ( $4n\pi$ )-electron annulenes was first raised by Baird in 1972 [7a], and further evidenced by Schleyer *et al.* [7b]. While the latter study was extended to the odd-electron cyclopentadienyl radical [7b], the aromatic nature of  $C_5H_5$  was, however, not discussed explicitly. In their review, Allen and Tidwell summarized the major studies on the aromaticity/antiaromaticity of odd-electron cyclopropenyl to cycloheptatrienyl cations, anions, neutral free radicals, and radical ions (with 3, 5 or 7 electrons) [6]. Amongst the series, only the Jahn-Teller distorted  $4c/3e$  cyclobutadienyl radical cation ( $C_4H_4^+$ ,  $C_{2v}$ ) is claimed to be stabilized by electron delocalization. Based on resonance energy estimates, the other odd-electron annulenes are described as less stabilized than their cyclic or linear analogs (e.g.  $C_3H_3$ ,  $C_s$ ,  $C_4H_4^-$ ,  $D_{2h}$ ,  $C_5H_5$ ,  $D_{5h}/C_{2v}$ ) or even as antiaromatic (e.g.  $C_6H_6^{+/-}$ ,  $D_{2h}$ ,  $C_7H_7$ ,  $C_{2v}$ ). Similarly, Fowler and

Gray computed the current-density maps of heptagonal boron wheels and predicted the doublet  $4\sigma/3\pi B_8^- C_{2v}$  to be  $\sigma$ -aromatic but  $\pi$ -non-aromatic [8].

More recently, Wang *et al.* detected early transition metal oxide clusters ( $M_3O_9^-$ ,  $M=W$ ,  $Mo$ ), which may exhibit one d-electron aromatic character[9] but no further analysis was provided. More of late, a 13-vertex carborane radical anion with  $2n + 3$  framework electrons has been isolated and structurally characterized [10]. Another recent example of this kind is an odd  $\pi$  electron ( $7\pi$ ) doublet boron oxide cluster,  $B_3O_4^-$  ( $D_{3h}$ ), with extremely high electron binding energy detected by Wang and his workers using Photo Electron Spectroscopy[11]. According to their computation the delocalized nature of the SOMO in  $B(BO)_3^-$  is responsible for its extremely high electron binding energy.

Despite these sparse and debatable examples of odd-electron (anti)aromatic compounds, one-electron aromatics have not yet been directly considered and many unanswered questions remain. Can one electron aromatics exist? Are they half as aromatic as their two electron singlet analogs? Can hydrocarbons form one  $\pi$ -electron rings? Here we extend the concept of aromaticity from 2 electron singlet species to open-shell doublet systems with one delocalized electron. In this paper we evaluate the degree of one electron delocalization using energetic, geometric and magnetic criteria for a multitude of theoretically designed two and three dimensional cationic, anionic and neutral monoradical systems.

### 4.3 Computational methods

Not only the geometric and energetic, but also the magnetic properties of open-shell species, which are generally not accessible experimentally by NMR measurements owing to line broadening, [12] but can be computed [13]. These open-shell calculations of magnetic properties may be “unphysical”, but they are instructive and useful in our case. Open-shell species are

strongly paramagnetic owing to the interaction between the spin of the unpaired electron with the magnetic field. In experimental measurements, this paramagnetic effect overwhelms the “normal” diamagnetic contribution due to the paired electrons. The chemical shift computations of open-shell systems, using Gaussian 03, do not include the effects due to the spin of unpaired electron. We thus have only computed the diamagnetic contributions. We use them here as an “index” to indicate the presence of induced diatropic ring currents in a basic set of the doublet 1e-electron systems.

The geometric and magnetic properties of both closed-shell and open-shell doublet species have been computed [13] to identify the presence of one electron induced diatropic ring currents. The spin-unrestricted Kohn-Sham formalism was used to describe the open-shell species. Nucleus-independent chemical shift[14] (NICS) were performed at the PW91/TZVPP level. In particular, the NICS<sub>zz</sub> [14c,15] index, provides a more detailed understanding of the extent of cyclic electron delocalization induced toward a magnetic field applied perpendicularly to the molecular plane (the z direction by the usual convention).

## 4.4 Result and discussion

### 4.4.1 Design principle: One electron analog of $2\pi$ aromatic hydrocarbon and Boron/Aluminium hydrides

The simplest and most common example of  $2\pi$  electron aromatic hydrocarbon is  $D_{3h}$   $C_3H_3^+$ . In reality, the cyclopropenyl cation is a contentious  $\pi$  aromatic system: the ring current arising from the totally symmetric  $\pi$  orbital (with no node except that in the xy plane [16] is weak and largely overwhelmed by the circulation of the  $\sigma$  charge. As expected, the radical dication undergoes a first-order Jahn-Teller distortion to the  $C_{2v}$  geometry. The  $\pi$  orbital of  $C_3H_3^{2+}$  is not the highest occupied molecular orbital (HOMO) as the electron is removed from one of the  $\sigma$

orbital with the Moebius topology. At the DFT level (B3LYP, PW91) the HOMO-1 of  $C_3H_3^+$  is the  $\pi$  orbital. In contrast, it is the HOMO at the HF and MP2 levels. However, all the unrestricted levels (UB3LYP,UPW91,UHF and UMP2) give a  $\sigma$  SOMO for  $C_3H_3^{2+}$  and  $\pi$  HOMO-2.

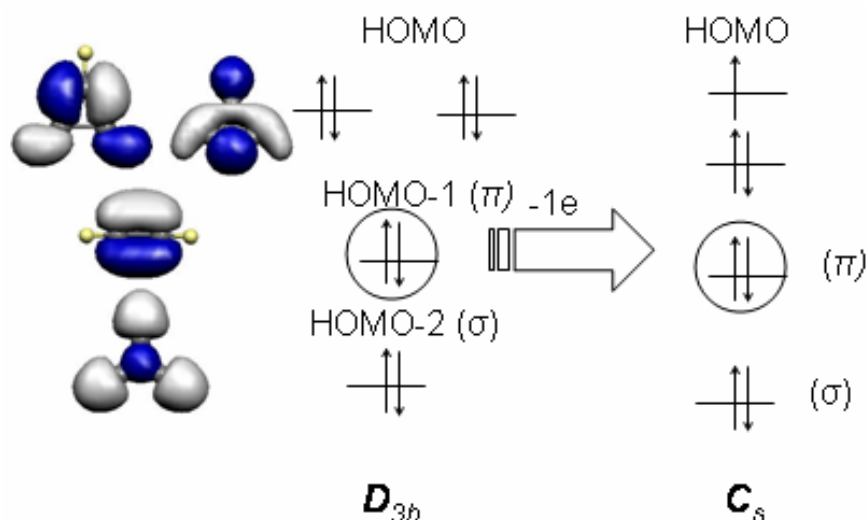


Figure 4-1. The frontier molecular orbital occupancy of  $C_3H_3^+$  and  $C_3H_3^{2+}$  (B3LYP and PW91/6-311+G\*\*).

The open shell doublet still has  $2\pi$  electrons (Figure 4-1). Iso-electronic analogs of  $C_3H_3^{2+}$  e.g.,  $C_3H_2^+$  ( $C_{2v}$ ),  $C_2BH_3^+$  ( $C_{2v}$ ),  $C_2BH_2$  ( $C_{2v}$ ),  $CB_2H_3^+$  ( $C_{2v}$ ),  $CB_2H_2^{1-}$  ( $C_s$ ),  $B_3H_3^-$  ( $C_s$ ),  $C_2NH_2^{2+}$  ( $C_{2v}$ ),  $CN_2H^{2+}$  ( $C_{2v}$ ),  $N_3^{2+}$  ( $C_{2v}$ ),  $CBNH_2^+$  ( $C_s$ ),  $BN_2H^+$  ( $C_{2v}$ ),  $B_2NH_3^{2+}$  ( $C_l$ ) also do not have a totally symmetric  $\pi$  HOMO. The  $\pi$  orbital is lower in energy (HOMO-1) and filled with two electrons. In contrast, closed-shell  $D_{3h}$   $Si_3H_3^{1+}$  has a totally symmetric  $\pi$  as a HOMO. Although it has been considered as  $2\pi$  aromatic [17a], its resonance and aromatic stabilization energies are only half that of  $C_3H_3^+$  [17b]. Similarly  $1\pi$  (quasi- $C_s$ )  $Si_3H_3^{2+}$  has negligible diatropic NICS<sub>zz</sub> value.

The primary goal of this report is to identify main group compounds with a singly occupied totally symmetric HOMO that sustains significant ring current. The demonstration of such examples is not straightforward. While the realization of one  $\pi$ -electron electronic structures is not straightforward, the investigation of boron and aluminium rings appears as an obvious strategy. Unlike hydrocarbons which favour 2c-2e bonds, the chemistry of boron is determined by Lipscomb's electron-deficient 3c-2e bonding pattern that beneficiaries from electron delocalization. Similarly, aluminium possesses a large variety of chemistry that differs from that of carbon.

The electron deficient  $D_{3h}$   $B_3H_3^{2+}$ , which has 4 less electrons than  $D_{3h}$   $C_3H_3^+$  *does* have a  $\pi$  HOMO. However, the removal of one electron results in a highly charged  $B_3H_3^{3+}$  species that readily decomposed at the B3LYP/6-311+G\*\* level. Interestingly, the lowest energy isomers of the  $B_3H_3/B_3H_3^+$  pair (both have a  $C_s$  symmetry with a bridging hydrogen) have a  $\pi$ -HOMO as well [18]. The diatropic nature of both the closed and open shell compound results in a substantial negative  $NICS_{zz}$  values at ring center (-49.1 and -48.2). Moreover the negative HOMO- $NICS_{zz}$  of the closed shell analog (-11.4) is indicative of the delocalized character of the HOMO/SOMO  $\pi$ . Alternative example of hydrocarbon boron analogs exist.  $C_{2v}$   $B_3H_6^+$ , which was for instance reported to be the first non-planar two  $\pi$  aromatic system [19] and has a  $\pi$  HOMO.  $NICS_{zz}$  is largely negative (-27.7) with most of the contribution coming from the  $\pi$  HOMO ( $NICS_{\pi zz}$  -16). Despite significantly longer B-B bond lengths, the  $1\pi$  electron analog ( $C_{2v}$ ,  $B_3H_6^{2+}$ , Figure 4-2) sustains a large diatropic  $NICS_{zz}$  both at ring center and 1 Å above (-31.9, -20.2).  $B_3H_6^{2+}$  can therefore be considered as a  $1\pi$  electron aromatic. However, high IP



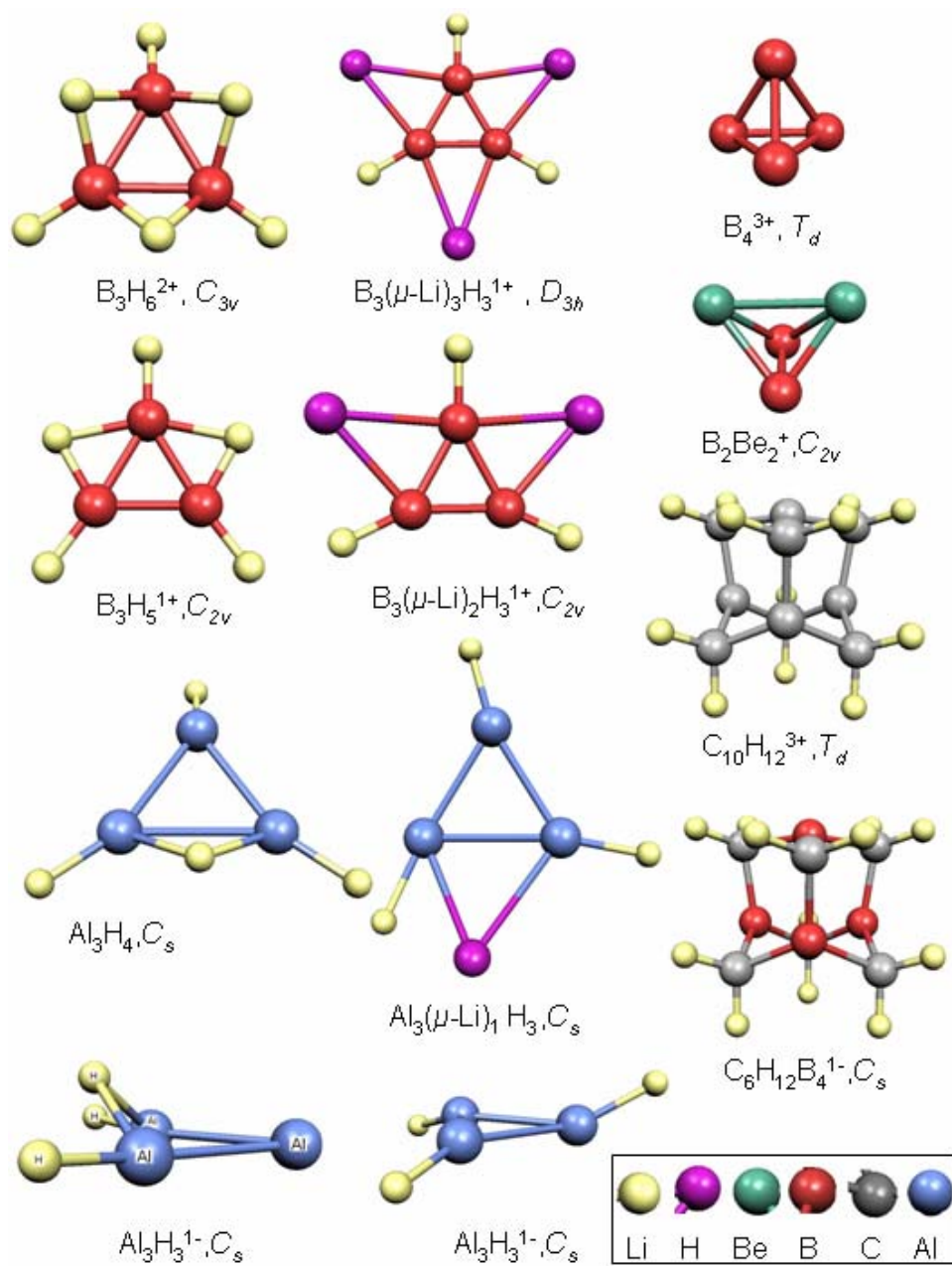

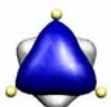
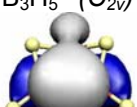
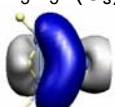
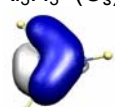
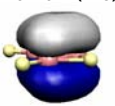
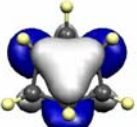


Figure 4-2. The two and three dimensional one  $\pi$  electron species.

Table 4-1. GIAO-NICS index for both the  $2\pi$  and  $1\pi$  electron aromatics in ppm at PW91/6-311+G\*\*. Negative NICS value at the ring center indicates the circulation of induced diatropic ring current. The totally delocalized SOMO<sup>a</sup> for the open shell compounds are depicted in column 1.

	NICS(0) $2\pi$ <b><math>1\pi</math></b>	NICSzz(0) $2\pi$ <b><math>1\pi</math></b>	NICSzz(1) $2\pi$ <b><math>1\pi</math></b>	HOMO- NICSzz (singlet)
$B_3^{1+}$ $B_3^{2+}(D_{3h})$ 	-65.3 <b>-8.8</b>	-65.9 <b>-61.2</b>	-31.4 <b>-25.4</b>	-12.2
$B_3H_6^{1+}$ $B_3H_6^{2+}(C_{3v})$ 	-24.6 <b>-19.3</b>	-27.6 <b>-31.9</b>	-3.4 <b>-20.2</b>	-16.0
$B_3H_5^{1+}$ $B_3H_5^{1+}(C_{2v})$ 	-40.1 <b>-21.3</b>	-48.1 <b>-31.5</b>	-32.0 <b>-20.5</b>	-11.7
$Al_3H_3^{2-}$ $Al_3H_3^{1-}(C_s)$ 	-22.5 <b>-12.3</b>	-14.8 <b>-9.6</b>	-17.3 <b>-3.2</b>	-6.3
$Al_3H_3^{2-}$ $Al_3H_3^{1-}(C_s)$ 	-12.6 <b>-3.7</b>	12.0 <b>-7.2</b>	1.4 <b>-10.2</b>	-6.5
$B_3H_3$ $B_3H_3^{1+}(C_s)$ 	-45.1 <b>24.2</b>	-49.1 <b>-48.2</b>	-12.3 <b>-6.8</b>	-11.4
$C_6H_9^{1+}$ $C_6H_9^{2+}(C_{3v})$ 	-46.3 <b>-21.9</b>	-45.7 <b>-22.0</b>	-22.8 <b>-24.6</b>	-10.5

[a] The isosurface value is 0.05 au.

(17.5 eV) for the  $2\pi$   $B_3H_6^{1+}$  system makes it unfavorable towards oxidation into the  $1\pi$   $B_3H_6^{2+}$ . Like  $B_3H_6^+$ , non planar  $2\pi$   $C_{3v}$   $Al_3H_6^+$  also has a totally symmetric pi HOMO. However the  $1\pi$   $C_{3v}$  is a second order saddle point and following imaginary modes finally leads to an acyclic structure. The removal of one of the three bridging proton leads to the non-planar hydrogen bridged doublet  $B_3H_5^{1+}$  (Figure 4-2). Both  $B_3H_5^{1+}$  and the closed-shell  $2\pi$  electron analog also have large diatropic NICS(0)<sub>zz</sub> (-31.5 and -48.5 respectively) (Table 4-1) but once again, the oxidation of the closed-shell species is not favored (IP=9.4 eV). Though the  $C_s$ , 2 and 1  $\pi$  Al analogues ( $Al_3H_5^-$  /  $Al_3H_5^+$ ) has lower IP (7.2 eV) towards oxidation compared to the B compounds, the diatropic character is negligible [NICS(0)<sub>zz</sub> = -7.0 and -4.1 respectively].

Unlike  $C_{2v}$ ,  $B_3H_4^{1-}$  (isoelectronic to both  $B_3H_6^+$  and  $B_3H_5^-$ )  $Al_3H_4^{1-}$ ,  $C_s$  has a  $\pi$  HOMO. The  $2\pi$  analogue has little diatropic character [NICS(0)<sub>zz</sub> = -3.0, NICS (1)<sub>zz</sub> -13.8]. Though the  $\pi$  HOMO contributes towards the diatropicity [HOMO-NICS(0)<sub>zz</sub> = -4.9, HOMO-NICS(1)<sub>zz</sub> = -7.3], the overall diatropic character is reduced by the huge paratropic contribution from the  $\sigma$  type HOMO-1 and HOMO-2 orbital. Moreover, the  $2\pi$  anionic compound has more tendencies to get oxidized, among all the hydro B/Al series discussed so far, due to very low IP (1.9 eV). However the resulting neutral  $Al_3H_4$ ,  $1\pi$  analogue, is very weakly diatropic [NICS(1)<sub>zz</sub> = -3.6].

Can this trend be changed by the introduction of substituents such as lithium or fluorine atoms? In their theoretical study of the  $B_3(\mu-H)_3X_3^+$  series (X=H, F, Li) and  $B_3(\mu-Li)_3H_3^+$ , Jemmis and Subramanian concluded that fluorination destabilizes the  $\pi$  electron cloud, while  $\mu$ -lithiation stabilizes the planar structure[19]. Our computations show that the lower ionization potential of lithium (5.4eV) in comparison to that of hydrogen (13.6 eV) results in a lower ionization potential of both  $D_{3h}$   $B_3(\mu-Li)_3H_3^+$  (11.6 eV) and  $C_{2v}$   $B_3(\mu-Li)_2H_3$  (IP=6.1 eV) compared to the hydrogenated analogs. The lithoborane species have a  $\pi$  HOMO and a large

diatropic character. In contrast, the lithiated  $\text{Al}_3\text{H}_5$  analogue cannot be considered as  $\text{C}_1$   $\text{Al}_3(\mu\text{-Li})_2\text{H}_3$  does not have a conventional  $\pi$  HOMO and the  $\text{C}_1$   $\text{Al}_3(\mu\text{-H})_3\text{Li}_2$  isomer is 14.7 kcal/mol higher in energy than the Li bridged compound.

However,  $\text{Al}_3(\mu\text{-Li})_1\text{H}_3^-$  has  $\pi$  HOMO and is weakly diatropic in nature [(NICS(1)= -11.9 NICS(1)<sub>zz</sub>= -2.9, HOMO-NICS<sub>zz</sub>= -5.7]. Like  $\text{Al}_3\text{H}_4^-$ , in these Li bridged species, the lower lying  $\sigma$  type orbitals have huge paratropic contribution. Fluorinated compounds were not considered as they are not  $2\pi$  systems.

$\text{Al}_3\text{H}_3^{2-}$  isomers represent another alternative for 1 and 2  $\pi$ -electron rings. Their electronic structures and geometries of the latter differ significantly from those of boron congeners. In contrast to  $\text{B}_3\text{H}_3^{2-}$ , which has two minima ( $\text{D}_{3h}$  and  $\text{C}_s$ ) and a low-lying  $\pi$  MO (HOMO-1, HOMO is degenerate),  $\text{Al}_3\text{H}_3^{2-}$  has a total seven minima [18] and higher energy  $\pi$  molecular orbitals.

As discussed by Jemmis *et al.* the singlet  $\text{D}_{3h}$   $\text{Al}_3\text{H}_3^{2-}$  is a minimum but is slightly higher in energy (1.8 kcal/mol at the B3LYP/6-311G\* level) than the H-bridged  $\text{C}_{2v}$  structure with the planar tetracoordinated aluminium atom. The lowest energy structure for the doublet is a H-bridged  $\text{C}_1$  structure with a  $\sigma$  SOMO. Although there are two  $\text{Al}_3\text{H}_3^-$  isomers (**4a** and **4b**) with a  $\pi$  HOMO (Figure 4-2), those are higher in energy than the former one (3.2 and 7.8 kcal/mol respectively). NICS for both the  $\text{C}_s$   $\text{Al}_3\text{H}_3^-$  (**4a** and **4b**) are reported in Table 4-1 **4a** ( $\text{C}_s$  with bridging hydrogen) and **4b** ( $\text{C}_s$  with out-of-plane hydrogen)  $\text{Al}_3\text{H}_3^{1-}$  (highlighted in Figure 4-2) can be considered as a weak one  $\pi$  electron aromatic but are not the lowest energy isomers. Additional one  $\pi$  electron aromatic candidates can be found amongst the pure boron ring series. The  $2\pi$ -HOMO of the smallest  $\text{D}_{3h}$   $\text{B}_3^+$  [20], is aromatic according to both NICS<sub>zz</sub> (-65.9 ppm) and the  $4n+2$  Hückel rule. The doublet  $\text{D}_{3h}$   $\text{B}_3^{2+}$  is a minimum that retains most of the diatropic

character of the parent singlet (NICS<sub>zz</sub>(0) -61.9 ppm) (Table 4-1). The large negative NICS<sub>zz</sub> values are compatible with the absence of filled  $\pi$ -orbitals with a high number of nodes.

$\text{Al}_3\text{H}_3^{2-}$ (closed shell singlet)							
Symmetry	$D_{3h}$	$C_{2v}$	$C_{3v}$	$C_{2v}$	$C_s$	$C_1$	$C_{2v}$
NIMAG	0	0	0	0	0	0	0
HOMO (totally delocalized pi)	✓	✓	✗	✓	✗	✗	✓
$\text{Al}_3\text{H}_3^{1-}$ (open shell doublet)							
Symmetry	$D_{3h}$	$C_{2v}$	$C_{2v}$			$C_{2v}$	
NIMAG	2	2	1			2	
Minima following imaginary frequencies							
	$C_s$	$C_1$	$C_s$			$C_s$	
HOMO (totally delocalized pi)	✓	✗	✓			✗	
Relative energies (kcal/mol)	0	-7.8	0.4	-4.6	-8.4	-4.4	-6.0
	<b>4b</b>		<b>4a</b>				

Figure 4-3. Isomers (minima on potential energy surface) of closed shell  $\text{Al}_3\text{H}_3^{2-}$  and open shell  $\text{Al}_3\text{H}_3^{1-}$ . Two potential one electron aromatic candidates are highlighted. However, other open shell species (devoid of totally symmetric HOMO) are lower in energy.

In annulenes, for instance, the later orbitals typically give large positive CMO-NICS values that compensate for the negative NICS contributions of others low-lying orbitals [21]. The filling

of one more orbital leads to  $B_3^-$ , which is a doubly ( $\pi$  and  $\sigma$ ) aromatic ring so as  $B_4$  [20]. The properties of the doublet analogs of these doubly aromatic compounds are discussed later in more detail. Unlike  $B_3^+$ , the triplet of  $D_{3h}$   $Al_3^+$  is more stable than the closed-shell singlet by 8.6 kcal/mol. In addition, the doublet analogue ( $Al_3^{2+}$ ) is unbound.

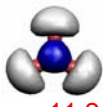


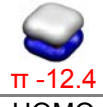
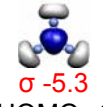

#### 4.4.2 One electron analogs of nonclassical cations

Possible 1  $\pi$  electron nonclassical cationic systems have also been investigated.  $C_6H_9^+$ , has a doubly occupied  $\pi$  HOMO (3c-2e bonding) and is diatropic according to  $NICS_{zz}$  and  $NICS_{\pi zz}$  (-45.7 and -10.5).  $C_6H_9^{2+}$ , obtained from removal of 1  $\pi$  electron from  $C_6H_9^+$  is almost half as aromatic ( $NICS_{zz}$  -22.0) as the  $2\pi$  aromatic compound.  $C_6H_9^{2+}$  can thus be categorized as 3c-1e  $\pi$  aromatics (Table 4-1). Similarly, the isoelectronic doublet borocarbon analogs  $C_5BH_9^{1+}$  and  $C_4B_2H_9$  belong to the 3c-1e  $\pi$  aromatic class of compounds: Their  $NICS_{zz}$  is substantial (-18.5, -12.1 respectively) as well.

#### 4.4.3 Open shell analogs of double aromatic systems

$2\pi/1\pi$  aromatic rings, that are doublet species with both  $\pi$  and  $\sigma$ -aromatic framework were also identified. As pointed out above  $B_3^{1-}$ ,  $B_4$ ,  $Al_3^{1-}$  (Table 4-2) all belong to this class of ( $\pi + \sigma$ )-double aromatics with both an in-plane radial  $\sigma$  HOMO and a  $\pi$  HOMO-1. Akin to the cyclic circulation of  $\pi$ -electrons, the in-plane delocalization of the  $\sigma$  electrons is associated with a strong diamagnetic current. The CMO- $NICS_{zz}$  analysis depicts significant contribution from both the totally symmetric  $\sigma$  in-plane HOMO and the  $\pi$  molecular orbital to  $NICS_{zz}$ . Similarly, the open shell doublets (Table 4-2) exhibit a significant residual diatropic character. Although these

Table 4-2. GIAO-NICS index in ppm for 4c-2e and 4c-1e aromatics (two dimensional double aromatics) at PW91/6-311+G\*\*.

	NICS(0)	NICS <sub>zz</sub> (1)	NICS <sub>zz</sub> (0)	CMO-NICS <sub>zz</sub> <sup>a</sup>
B <sub>3</sub> <sup>1-</sup> B <sub>3</sub> D <sub>3h</sub>	-71.1 -66.5	-38.2 -33.8	-74.5 -68.2	HOMO  σ -11.2 HOMO-1  π -11.5
B <sub>4</sub> <sup>+</sup> B <sub>4</sub> <sup>+</sup> D <sub>4h</sub>	-29.4 -28.9	9.0 5.0	-27.3 -28.2	HOMO  σ -14.4 HOMO -2  π -12.4
Al <sub>3</sub> <sup>1-</sup> Al <sub>3</sub> D <sub>3h</sub>	-36.6 -33.8	-32.0 -31.0	-36.4 -34.3	HOMO  σ -5.3 HOMO- 1  π -7.2

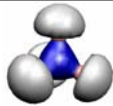
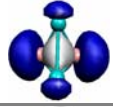
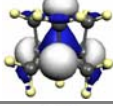
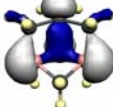
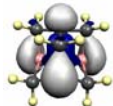
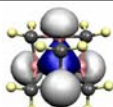
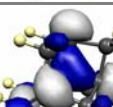
[a] The illustrative HOMO and HOMO-1 orbitals are shown with isosurface value 0.05 au.

compounds cannot be strictly categorized as one electron aromatics, they are examples of “odd electron aromatics” (1σ and 2π).

#### 4.4.4 Three dimensional delocalized systems

Three dimensional delocalized systems represent another class of one electron aromatics. Obvious examples include tetrahedral or adamantane frameworks following the  $2(N_{\pi}+1)^2$  electron counting rule [23]. For instance, the 3D aromatic prototype, 1,3-dehydro-5,7-

Table 4-3. GIAO-NICS index in ppm 4c-2e and 4c-1e three dimensional aromatics at PW91/6-311+G\*\*

Molecule 4c-2e/ 4c-1e	NICS 4c-2e/4c-1e	CMO NICS	SOMO <sup>b</sup> 4c-1e
$B_4^{2+}/B_4^{3+}$ $T_d$	-67.0/-59.6	a	
$B_2Be_2/B_2Be_2^+$ $C_{2v}$	-65.7/-53.4	-10.7	
$C_{10}H_{12}^{2+}/C_{10}H_{12}^{3+}$ $T_d$	-46.3/-22.6	-6.8	
$C_8B_2H_{12}/C_8B_2H_{12}^{1+}$ $C_{2v}$	-38.4/-24.0	-6.2	
$C_7B_3H_{12}^{1+}/C_7B_3H_{12}$ $C_{3v}$	-35.9/-22.4	-8.3	
$C_6H_{12}B_4^{2+}/C_6H_{12}B_4^{1-}$ $C_s$	-33.4/-21.7	-11.9	
$C_{11}H_{14}^{2+}/C_{11}H_{14}^{3+}$ $C_s$	-36.2/-25.7	-6.2	

[a] The strongly delocalized structures with three- or four-center bonds are not well described by the NBO procedure. [see ref 22][b] The isosurface value is 0.05 au.

adamantanediyl dication ( $C_{10}H_{12}^{2+}$ ) has two mobile electrons in its 4c-2e totally symmetric  $\pi$  HOMO. The removal of one electron leads to the doublet trication  $C_{10}H_{12}^{3+}$  with 1 electron delocalized over the four saturated carbon atoms. The large negative nucleus-independent chemical shift (NICS) values at both cage centers (-46.3, -22.6) (Table 4-3) clearly indicate the diatropic nature of these species. Atomic substitution with boron leads to doublet cationic, neutral and anionic boroadamantane analogs, which have similar magnetic properties (i.e.  $C_8B_2H_{12}^{1+}$ ,  $C_7B_3H_{12}$ ,  $C_6H_{12}B_4^{1-}$ ). While the latter have not yet been detected, the negative electron affinity value of one the doublet  $C_6H_{12}B_4^-$  (-3.38 eV|-3.24 eV), indicates its stability with



respect to the closed shell 4c-2e aromatic dianion. NICS values for the heteroatomic open shell doublet boroadamantanes cages are roughly two third of those of the closed-shell cages (NICS= -24.0, -22.4, -21.7 respectively) (Table 4-3). Similarly polyhomoadamantene  $C_{11}H_{14}^{2+}$ , one of the higher homologues of  $C_{10}H_{12}^{2+}$ , is stabilized by 4c-2e three dimensional delocalization [24]. The doublet  $C_{11}H_{14}^{3+}$  has a large negative nucleus-independent chemical shift (NICS) values at cage centers.

Experimentally known tetrahedral clusters such as  $E_4$  ( $T_d$ ) ( $E=N, P, As, Sb, Bi$ ), Zintl ion ( $E_4^{2-}$ ) also follow the  $2(N+1)^2$  electron-counting rule. However, the frontier occupied orbitals of these double spherical aromatic cages ( $2(N_{\sigma/\pi}+1)^2$   $N_{\sigma}=2$  and  $N_{\pi}=0$ ) [23] are the degenerate  $\sigma$  MOs. The alternative  $B_4^{2+} T_d$  cage has 8 less electrons and a totally symmetric 4c-2e  $\pi$  HOMO. However, neither  $B_4^{2+} T_d$  nor the doublet  $B_4^{3+} T_d$  are viable according to both the large electron affinity and low ionization potential. Similarly, the doublet  $B_2Be_2^+$ , that is isoelectronic to  $B_4^{3+}$ , is largely diatropic (NICS -53.4) however is prone to get reduced to the closed shell neutral compound due to high electron affinity (7.5 eV).

#### 4.5 Concluding remarks

The present study provides theoretical examples of main group mono  $\pi$ , 3c-1e and 4c-1e open-shell aromatic species. In some cases ( $D_{3h} B_3^{2+}$  and  $C_s B_3H_3^+$ ), there exists a general qualitative relationship between the aromaticity of the singlet and that of the doublet species:  $(HOMO-NICS(1)_{zz})/(2+n) \sim |NICS(1)_{zz,closed} - NICS(1)_{zz,open}|$  with  $n < 1$ ). Since CMO-NICS analysis cannot be done with open shell system this is an indirect way of probing the contribution of the SOMO towards the aromaticity. For  $B_3^{1+}$  (2e arom) the  $HOMO-NICS_{zz} = -12.2$  ppm,  $NICS(1)_{zz} = -31.4$

and for  $B_3^{2+}$  NICS(1)<sub>zz</sub> = -25.6. This trend confirms that the ring current originates mostly from the highest-occupied molecular orbital.

While theoretical design often offers prediction for plausible novel viable compounds, not all the above species are good candidates for experimental detection due the huge positive ionization potential for closed shell analogs. Nonetheless, the doublet  $Al_3H_3^{1-}$  isomers (**4a** and **4b**, Figure 4-2) have negative electron affinity (-2.86 and -2.79 eV at the B3LYP/TZVPP level respectively) indicating that those minima's are resistant toward reduction to the closed shell  $Al_3H_3^{2-}$  analog. Moreover, the negative electron affinity value of one of the cages, namely the doublet  $C_6H_{12}B_4^-$  (Table 4-3) (-3.38 eV | -3.24 eV), indicates its stability with respect to the closed shell 4c-2e aromatic dianion. We thus anticipate the detection of  $C_6H_{12}B_4^-$  by, for instance, photoelectron spectroscopy.

#### 4.6 References

- 1) a) P. von R. Schleyer, Guest Ed. Special issue on Delocalization Pi and Sigma ,*Chem. Rev.*2005, 105 (10) and references there in. b) P. von. R., Schleyer, Guest Ed. Special issue on aromaticity. *Chem. Rev.* 2001, 101 (5).
- 2) a) M. J. S. Dewar, *Bul. Soc. Chim. Belg.* 1979, 88, 957. b) M. J. S. Dewar; M. L. McKee,*Pure Appl. Chem.* 1980, 52, 1431. (c) M. J. S. Dewar, *J. Am. Chem. Soc.* 1984, 106, 669.
- 3) J. Chandrasekhar, E. D. Jemmis, P. von R. Schleyer, *Tetrahedron Lett.*1979,3707. This paper coined the terms “double aromaticity” and “in-plane aromaticity”.
- 4) a) J. Aihara, *J. Am. Chem. Soc.* 1976, 98, 2750. This paper coined the term three-dimensional aromaticity. b) J. Aihara, *Inorg. Chem.* 2001, 40, 5042. c) E. D. Jemmis,;

- P. von R. Schleyer, *J. Am. Chem. Soc.* 1982, **104**, 4781. (d) R. B. King, *Chem. Rev.* 2001, **101**, 1119 and references therein.
- 5) a) G. Vincow, H. J. Dauben, F. R. Hunter, W. V. Volland, *J. Am. Chem. Soc.* **1969**, **91**, 2823. b) G. Vincow, In *Aromaticity, Pseudo-aromaticity, and Anti-aromaticity*; Bergmann, E. D., Pullman, B., Eds.; Academic Press: New York, 1971; pp 336-347.
  - 6) A. D. Allen, T. T. Tidwell, *Chem. Rev.* 2001, **101**, 1333 and references there in.
  - 7) a) N. C. Baird, *J. Am. Chem. Soc.* **1972**, **94**, 4941-4948. b) V. Gogonea, P. von R. Schleyer, P. R. Schreiner, *Angew Chem., Int. Ed. Engl.* **1998**, **37**, 1945-1948.
  - 8) P. W. Fowler and B. R. Gray, *Inorg. Chem.*, **2007**, **46**, 2892–2897.
  - 9) X. Huang, H.-J. Zhai, B. Kiran, L.-S. Wang, *Angew. Chem. Int. Ed.* **2005**, **44**, 7251.
  - 10) X. Fu, H.-S. Chan, Z. Xie, *J. Am. Chem. Soc.* **2007**, **129**, 8964.
  - 11) H. J. Zhai, S. D. Li, L. S. Wang, *J. Am. Chem. Soc.* **2007**, **129**, 9254.
  - 12) E. D. Becker, C. L. Fisk, C. L. Khetrpal in *Encyclopedia of Nuclear Magnetic Resonance*, Vol. 1 (Eds.: D. M. Grant, R. H. Harris), Wiley, Chichester, 1996, p. 41; b) E. Wasserman, R. S. Hutton, *Acc. Chem. Res.* 1977, **10**, 27. c) For line broadening in the NMR spectrum of paramagnetic molecules in solution (bis(cyclopentadienyl) nickel), see H. M. McConnell, C. H. Holm, *J. Chem. Phys.* 1957, **27**, 314.
  - 13) M. J. Frisch, G. W. Trucks, H. B. Schlegel, G. E. Scuseria, M. A. Robb, J. R. Cheeseman, V.G. Zakrzewski, J. A. Montgomery, Jr., R. E. Stratmann, J. C. Burant, S. Dapprich, J. M. Millam, A. D. Daniels, K. N. Kudin, M. C. Strain, O. Farkas, J. Tomasi, V. Barone, M. Cossi, R. Cammi, B. Mennucci, C. Pomelli, C. Adamo, S. Clifford, J. Ochterski, G. A. Petersson, P. Y. Ayala, Q. Cui, K. Morokuma, P. Salvador, J. J. Dannenberg, D. K. Malick, A. D. Rabuck, K. Raghavachari, J. B. Foresman, J.

- Cioslowski, J. V. Ortiz, A. G. Baboul, B. B. Stefanov, G. Liu, A. Liashenko, P. Piskorz, I. Komaromi, R. Gomperts, R. L. Martin, D. J. Fox, T. Keith, M. A. Al-Laham, C. Y. Peng, A. Nanayakkara, M. Challacombe, P. M. W. Gill, B. Johnson, W. Chen, M. W. Wong, J. L. Andres, C. Gonzalez, M. Head-Gordon, E. S. Replogle, and J. A. Pople, Gaussian 98 (Revision A.11.3) Gaussian, Inc., Pittsburgh PA, 2001. b) J. B. Foresman, á. Frisch, *Exploring Chemistry with Electronic Structure Methods*, 2nd ed., Gaussian Inc., Pittsburgh, PA, 1996.
- 14) P. von R. Schleyer, C. Maerker, A. Dransfeld, H. Jiao, N. J. R. van Eikema Hommes, *J. Am. Chem. Soc.* **1996**, 118, 6317; b) P. von R. Schleyer, H. Jiao, N. J. R. van Eikema Hommes, V. G. Malkin, O. L. Malkina, *J. Am. Chem. Soc.* **1997**, 119, 12669. c) Z. Chen, C. S. Wannere, C. Corminboeuf, R. Puchta, P. von R. Schleyer, *Chem. Rev.* **2005**, 105, 3842.
- 15) a) P. W. Fowler, E. Steiner, *Mol. Phys.* **2000**, 98, 945. b) E. Steiner, P. W. Fowler, L. W. Jennesskens, *Angew. Chem., Int. Ed.* **2001**, 40, 362. c) C. Corminboeuf, T. Heine, G. Seifert, P. v. R. Schleyer, *Phys. Chem. Chem. Phys.* **2004**, 6, 273. d) H. Fallah-Bagher-Shaidaei, C. S. Wannere, C. Corminboeuf, R. Puchta, P. v. R. Schleyer, *Org. Lett.* **2006**, 8, 863.
- 16) I. Cernusak, P. W. Fowler, E. Steiner, *Mol Phys* **1997**, 91, 401.
- 17) G. N. Srinivas, E. D. Jemmis, A. A. Korkin, P. von R. Schleyer, *J. Phys. Chem. A* **1999**, 103, 11034. b) E. D. Jemmis, G. N. Srinivas, J. Leszczynski, J. Kapp, A. A. Korkin, P. von R. Schleyer, *J. Am. Chem. Soc.* **1995**, 117, 11 361.
- 18) G. N. Srinivas, A. Anoop, E. D. Jemmis, T. P. Hamilton, , K. Lammertsma, J. Leszczynski, H. F. Schaefer, III, *J. Am. Chem. Soc.* **2003**, 125, 16397.

- 19) E. D. Jemmis, G. Subramanian, G. N. Srinivas, *J. Am. Chem. Soc.* 1992, *114*, 7939.
- 20) D. Y. Zubarev, A. I. Boldyrev, *J. Comput. Chem.* **2007**, *28*, 251.
- 21) T. Heine, P. von R. Schleyer, C. Corminboeuf, G. Seifert, R. Reviakine, J. Weber, *J. Phys. Chem. A* **2003**, *107*, 6470.
- 22) L. V. Slipchenko, A. I. Krylov, *J. Chem. Phys.* **2003**, *118*, 6874.
- 23) a) Z. Chen, H. Jiao, A. Hirsch, W. Thiel, *J. Mol. Model.* **2001**, *7*, 161-163. b) A. Hirsch, Z. Chen, H. Jiao, *Angew. Chem. Int. Ed.* **2001**, *40*, 2834-2838.
- 24) A. A. Fokin, B. Kiran, M. Bremer, X. Yang, H. Jiao, P. von R. Schleyer, P. R. Schreiner, *Chem. Eur. J.* **2000**, *6*, 1615.

CHAPTER 5

PLANAR TETRACOORDINATE CARBON ATOMS CENTERED IN BARE FOUR-  
MEMBERED RINGS OF LATE TRANSITION METAL<sup>§</sup>

---

<sup>§</sup> Roy, D.; Corminboeuf, C.; Wannere, C. S.; King, R. B.; Schleyer, P. v. R. *Inorganic Chemistry*. **2006**, *45*, 8902-8906 Reproduced in part by permission of American Chemical Society, Copyright 2006

## 5.1 Abstract

Planar tetracoordinate carbons (ptC's) can be stabilized by four-membered ring perimeters comprised of four bare transition metal atoms. DFT analyses of the molecular orbitals, electronic structures, energies, and magnetic properties of these CM<sub>4</sub> species (where M represents isoelectronic combinations of Cu, Ni, Ag, and Pd) reveal striking similarities with main group metal ptC analogs (e.g. CAI<sub>2</sub>Si<sub>2</sub>, CAI<sub>4</sub>Na<sup>-</sup> and C<sub>5</sub>Li<sub>2</sub>). While the CCu<sub>4</sub><sup>2+</sup>, CAg<sub>4</sub><sup>2+</sup> and CNiCu<sub>3</sub><sup>+</sup> ions have the largest HOMO-LUMO separations, CCu<sub>4</sub><sup>2+</sup> is the best candidate for detection by gas-phase photoelectron spectroscopy.

## 5.2 Introduction

Van't Hoff and LeBel's tetrahedral carbon [1,2] pervades chemistry. Planar tetracoordinate carbon (ptC) alternatives were long thought to be too high in energy to be viable [3] until in 1970 Hoffmann, Alder, and Wilcox formulated "electronic" strategies for reducing the relative energies of ptC structures [4]. The systematic and extensive computational investigation of Schleyer and Pople [5] designed the first example of a ptC molecule, 1,1-dilithiocyclopropane, by employing an additional "mechanical" strategy [5]. The smaller bond angles of 3- and 4-membered rings favor ptC's. In addition, the in-plane electron-deficiency can benefit from  $\sigma$  donation by electropositive groups. Many compounds with a ptC are now known based on these electronic and mechanical principles [6-8].

Hoffmann et al [4] pointed out that the HOMO of planar methane, a p-orbital lone pair on the ptC, could be stabilized by delocalization to  $\pi$  acceptors [9]. In contrast, Wang and Schleyer [10] stressed the conceptual advantages of basing ptC designs on the *inherently planar methane dication* and the stabilization of its vacant ptC p-orbital by  $\pi$  donor substituents. The methane

radical cation may be an even better model, since the ptC p-orbitals of almost all of the many known examples [11] are occupied by one  $\pi$  electron, more or less. Overall neutrality of the ptC molecules can be achieved by appropriate isoelectronic atom replacements [10, 12a].

Schleyer and Boldyrev (SB) were the first to design ptC's with the minimum number of atoms (five), e.g., the neutral pentatomic  $\text{CAI}_2\text{Si}_2$  isomers and their analogs [12a]. The 1991 SB computational predictions were verified experimentally in 1998 by the detection of the isoelectronic anions,  $\text{CAI}_3\text{Si}^-$  [12a, 12d] and the closely related  $\text{NaCAI}_4^-$  [13]. The planarity of such ptC molecules comprised of second or third row main group ligand atoms in four-membered ring perimeters is characterized by multicenter  $\pi$  bonding involving all of the atoms as well as peripheral ligand-ligand bonding [12]. Can transition metal rings function effectively as well? Is it possible to have only four transition metal atoms in addition to the ptC?

A square planar carbon inside a four-membered nickel ring moiety has been known for some time in the  $\text{Ca}_4\text{Ni}_3\text{C}_5$  aggregate synthesized by Musanke and Jeitschko [14]. The bonding of the underlying  $\text{CNi}_4$  unit of this unusual nickel carbide polymer network has been analyzed using qualitative, band-structure calculations employing extended Huckel tight-binding theory [15]. The unusual carbide polymer network features infinite, one-dimensional, vertex-sharing chains of Ni squares. Each nickel atom has linear C-Ni-C coordination to the central square planar and/or external  $\text{C}_2$  with weak  $\text{Ni}\cdots\text{Ni}$  bonding. Inspired by the theoretical study of Tsipis on the hydrocopper  $\text{Cu}_4\text{H}_4$  ring, [16] Li *et al.* computed a ptC-containing  $\text{D}_{4h}$  “hydronickel” compound [17]. We now describe the smallest “naked” transition metal clusters that can host a ptC atom. These predictions developed from our theoretical investigation of bare transition metal rings (i.e. without hydrogen or other substituents) [18]. Such rings are inherently well suited to stabilize



central atom placements. While we focus on carbon as the central atom here, other elements can function equally well as the central tetracoordinate atom.

### 5.3 Computational Details

Our design strategy places the ptC inside suitable four-membered late transition metal element rings comprised of combinations of Ni and Cu or of their heavier congeners, Pd and Ag. The optimized geometries of these species are rather insensitive to the DFT level. The symmetry-constrained structures reported here are based on the B3LYP functional together with the standard Karlsruhe valence triple- $\xi$  valence basis sets augmented with double polarization functions (TZVPP for C, Ni and Cu)[19] or with the LANL2DZ combination of valence and ECP basis sets (Ag, Pd)[20]. The Gaussian03 program was employed [21]. The computed vibrational frequencies show the ptC structures in Figure 5-1 to be minima. The potential energy surfaces were explored using the Saunders' "kick" method [22] newly implemented as an automated procedure [23]. This stochastic method generates structures randomly and facilitates the thorough exploration of unknown isomers much more easily than manual methods. It does not involve any preconceived structures based on bonding principles. Instead, all the atoms are placed at the same point initially and then are "kicked" randomly within a box of chosen dimensions. The kick size was varied from 2.0 to 2.5 Å in the cubic boxes employed here. These initial geometries (in e.g., independent sets of 50 or 100 "kick" jobs) are then optimized automatically, typically at low levels of theory to begin with. HF/STO-3G was chosen in the present application. Redundancies in each set (energies within 0.00001 au) are eliminated. The sets of kick runs are continued until no new structures are generated. Since no symmetry constraints are imposed, the geometries obtained should correspond to minima. The lowest

energy structures at the preliminary level (and others, which seem attractive) are then reoptimized and refined at the higher B3LYP/TZVPP level, followed by vibrational frequency computations.

## 5.4 Structure and Energetics

The relatively short computed M-ptC bond lengths in the 1.871-2.040 Å and 1.680-1.700 Å ranges for the species in Figure 5-1), indicate significant stabilization as these lengths are shorter than the sum of van der Waals radii e.g., for Cu-C (2.190 Å) and Ni-C (2.150 Å) [24]. In addition, the rather short intramolecular metal-metal distances (<2.7 Å) favor cyclic electron delocalization and further stabilize the planar configurations relative to the corresponding tetrahedral forms.

Despite being a local minimum, **1** is not a good candidate for the experimental detection of a ptC singlet, as the butterfly ( $C_{2v}$ ) form is ~33.4 kcal/mol more stable. In addition, the  $CCu_4$  subunits aggregate in the bulk (described in detail later). The HOMO-LUMO energy separation of singlet **1** is small (0.27 eV) and the  $D_{2h}$  triplet electronic state is 22.9 kcal/mol lower in energy. Triplet **1** ( $D_{2h}$ ) is thus a better neutral candidate for the observation of a ptC! (Figure 1) Removal of two electrons from  $CCu_4$  (**1**) generates the  $D_{4h}$   $CCu_4^{2+}$  dication (**2**); its HOMO-LUMO energy separation is substantial, 2.72 eV (Figure 5-1). Moreover, pyramidal ( $C_{4v}$ ) and butterfly ( $D_{2d}$ )  $CCu_4^{2+}$  starting geometries give the  $D_{4h}$  minima (**2**) upon optimization.

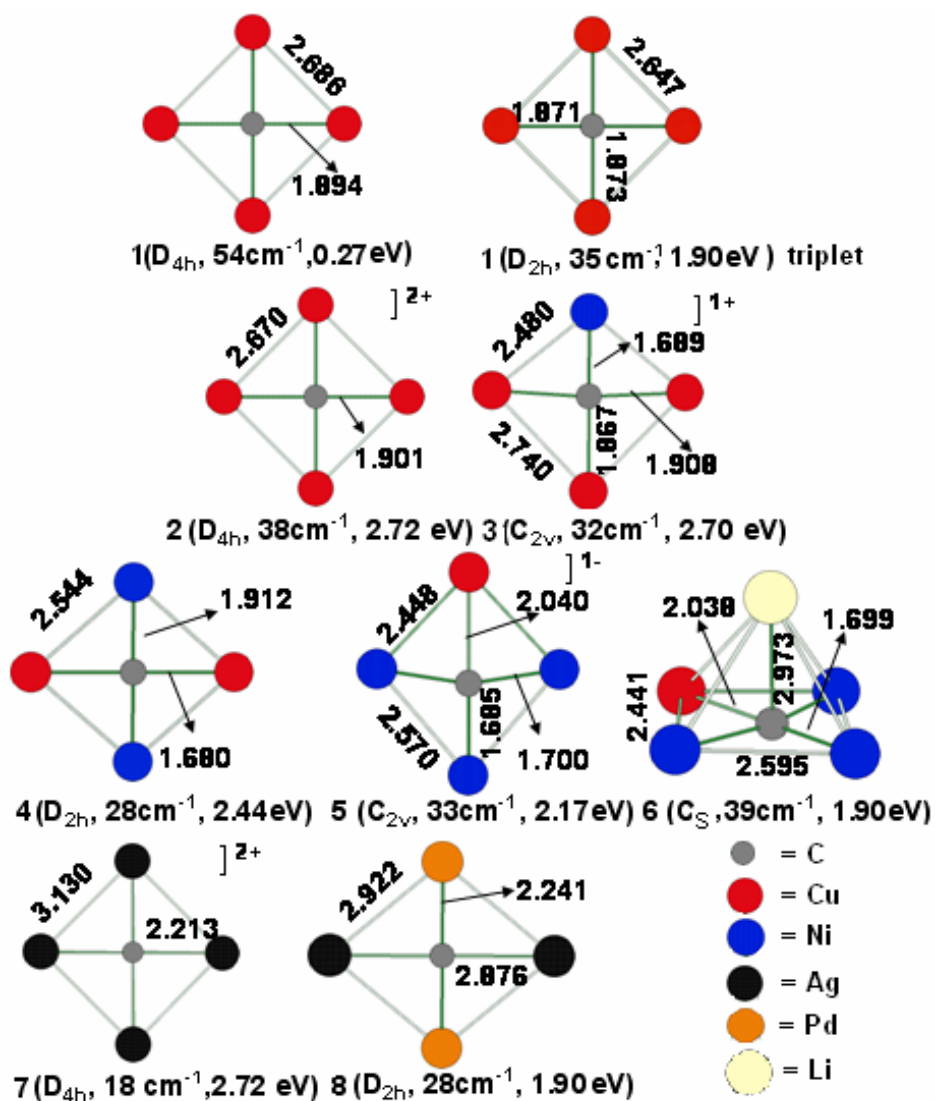


Figure 5-1. B3LYP/TZPP structures of the transition metal cages (for Ag, Pd B3LYP/LANL2DZ ECP and valence basis sets) containing planar tetracoordinate carbons. The selected bond lengths are in Å. The smallest vibrational frequency (mode corresponding to pyramidalization) and the HOMO-LUMO separations (in eV) are given for all the species.

The stability of **2** is further demonstrated by its large binding and atomization energy ( $24.5\text{ eV}$  and  $28.9\text{ eV}$ , respectively, at the B3LYP/TZVPP level). The viability of **2** is consistent with the

experimental characterization of the isoelectronic  $\text{Cu}_4\text{Na}^-$  cluster by Wang *et al.* [25] Although the neutral  $D_{4h}$   $\text{Cu}_4$  framework is electronically unstable by itself [26], it is stabilized by the presence of a central atom and two additional electrons. This is especially so in **2** since the vacant  $p_z$   $\text{C}^{2+}$  orbital interacts with the filled orbitals of the metal ring.

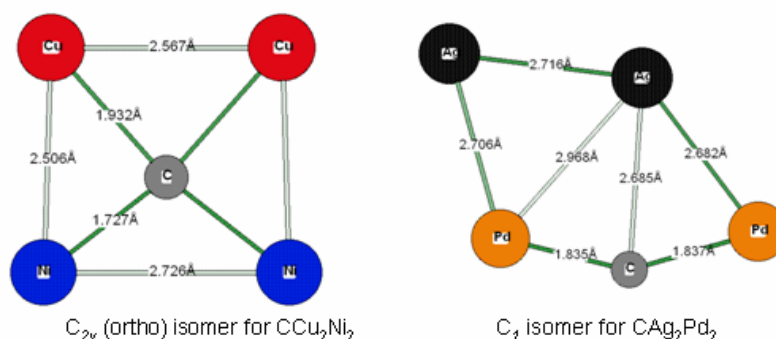


Figure 5-2 Alternative geometries for  $\text{CCu}_2\text{Ni}_2$  and  $\text{CAg}_2\text{Pd}_2$ .  $\text{C}_{2v}$   $\text{CCu}_2\text{Ni}_2$  is 6.0 kcal  $\text{mol}^{-1}$  less stable than the  $D_{2h}$  analog and  $\text{C}_1$   $\text{CAg}_2\text{Pd}_2$  is 7.0 kcal  $\text{mol}^{-1}$  more stable than the  $D_{2h}$  analog (reported in Figure 5-1).

Remarkably, the isoelectronic analogs of  $\text{Cu}_4\text{C}^{2+}$ ,  $\text{C}_{2v}$   $\text{CCu}_3\text{Ni}^+$  (**3**),  $D_{2h}$   $\text{CCu}_2\text{Ni}_2$  (**4**),  $\text{C}_{2v}$   $\text{CCuNi}_3^-$  (**5**), all are local minima and have ptC's. Like many anions, the  $\text{CCuNi}_3^-$  (**5**) HOMO has a positive eigenvalue (0.0007). However, the presence of the  $\text{Li}^+$  counter ion in the mono-capped  $\text{CCuNi}_3^-\text{Li}^+$  (**6**) precludes electron detachment; the HOMO energy is lowered to -0.1567. The  $\text{C}_s$  symmetry of **6** prevents perfect planarity of the  $\text{CCuNi}_3^-$  moiety, but the out-of-plane distortion is

small. While  $D_{4h}$   $CNi_4^{2-}$ , our final member of the isoelectronic Cu->Ni replacement series, also is

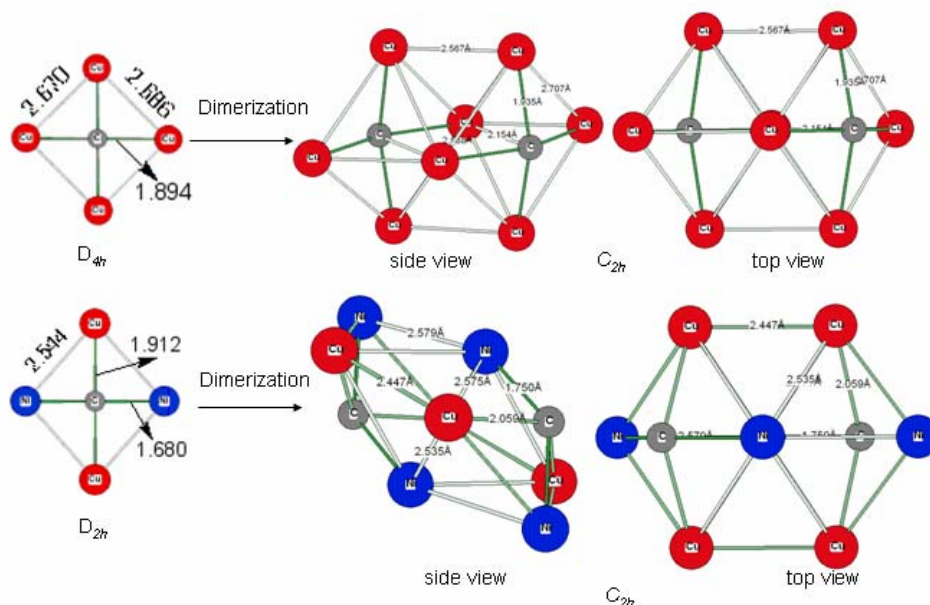


Figure 5-3 Dimerization of neutral  $CCu_4$  or  $CCu_2Ni_2$  subunits into their respective  $C_{2h}$  dimers is favored by more than 120 and 75 kcal mol<sup>-1</sup>.

a minimum, its HOMO-LUMO separation is large (1.9eV). Interaction with the two  $Li^+$  counterions destroys the planarity of the  $CNi_4$  unit. Thus  $D_{4h}$   $CNi_4Li_2$  has one imaginary vibrational frequency associated with the out-of-plane motion of Ni leading to  $C_{4v}$  symmetry.

$CCu_4^{2+}$  (**2**) and  $CCu_3Ni^+$  (**3**) have the largest HOMO-LUMO separations and may be the best candidates for gas-phase experimental detection among the isoelectronic **2-6** set. Neutral  $D_{2h}$   $CCu_2Ni_2$  (**4**) is about 6 kcal mol<sup>-1</sup> more stable than its  $C_{2v}$  counterpart (Figure 5-2) but is prone to aggregate. The aggregation of two neutral  $CCu_4$  or  $CCu_2Ni_2$  subunits into their respective  $C_{2h}$  dimers is favored by more than 120 and 75 kcal mol<sup>-1</sup>, respectively (Figure 5-3). Although  $D_{2h}$   $C_{Ag_2Pd_2}$  (**8**) is 7 kcal mol<sup>-1</sup> higher in energy than a  $C_1$  symmetry isomer (Figure 5-2), the

isoelectronic  $D_{4h}$   $CAg_4^{2+}$  (**7**) may be viable. Attention also is called to the planar triplet state of neutral  $CCu_4$  (**1**).

### 5.5 Molecular Orbital and NBO analysis

Molecular orbital (MO) analyses of **1-8** reveal features that stabilize the ptCs by interaction of the carbon  $p_z$  orbital with the transition metal ring skeleton. The full set of MO's is depicted in Figure 5-4. Note the important contribution of the perpendicular ptC p-orbital to the delocalized  $\pi$   $a_{2u}$  HOMO-14 of  $CCu_4^{2+}$  depicted in the left side of Figure 5-4. The peripheral metal-metal bonding interactions of the other MO's shown in Figure 5-4 also favor the planar structures strongly.

Natural bond orbital (NBO) analyses [27] of **1-8** indicate considerable electron transfer from the surrounding metal atoms to the more electronegative carbons in the centers. For example, the atomic charges of the  $CCu_4^{2+}$  dication (**2**) are +0.89 for Cu and -1.57  $e$  for the ptC, while those for the neutral (**4**) are +0.38 (Cu), +0.20 (Ni) and -1.16  $e$  (ptC). Such charge distributions show that the electron transfer is more effective from Cu than from Ni. NBO also reveals significant  $2p_z$  ptC orbital occupancies. Thus, the electronic population of the C atom valence shell is  $2s^{1.72}2p_x^{1.62}2p_y^{1.62}2p_z^{0.57}$  in (**2**),  $2s^{1.62}2p_x^{1.47}2p_y^{1.48}2p_z^{0.78}$  in (**3**),  $2s^{1.55}2p_x^{1.38}2p_y^{1.33}2p_z^{0.87}$  in (**4**), and  $2s^{1.51}2p_x^{1.32}2p_y^{1.35}2p_z^{1.05}$  in (**5**). The  $2p_z$  ptC orbital occupancies are in accord with the Wang-Schleyer ptC bonding model (see above) [10], which is based conceptually on stabilization of a vacant  $2p_z$  ptC orbital through electron transfer. In addition, the ptC benefits from  $\sigma$  donation<sup>4</sup> by the electropositive transition metals justifying the relatively high occupancy of both the  $2p_x$  and  $2p_y$  carbon orbitals. Finally, the delocalized character of the in-plane C-M bonding is well

illustrated by the atom-atom overlap weighted NAO bond orders, varying from 0.5 per C-Cu in  $\text{CCu}_4^{2+}$  to 0.7 for C-Ni in  $\text{CCu}_3\text{Ni}^+$ .

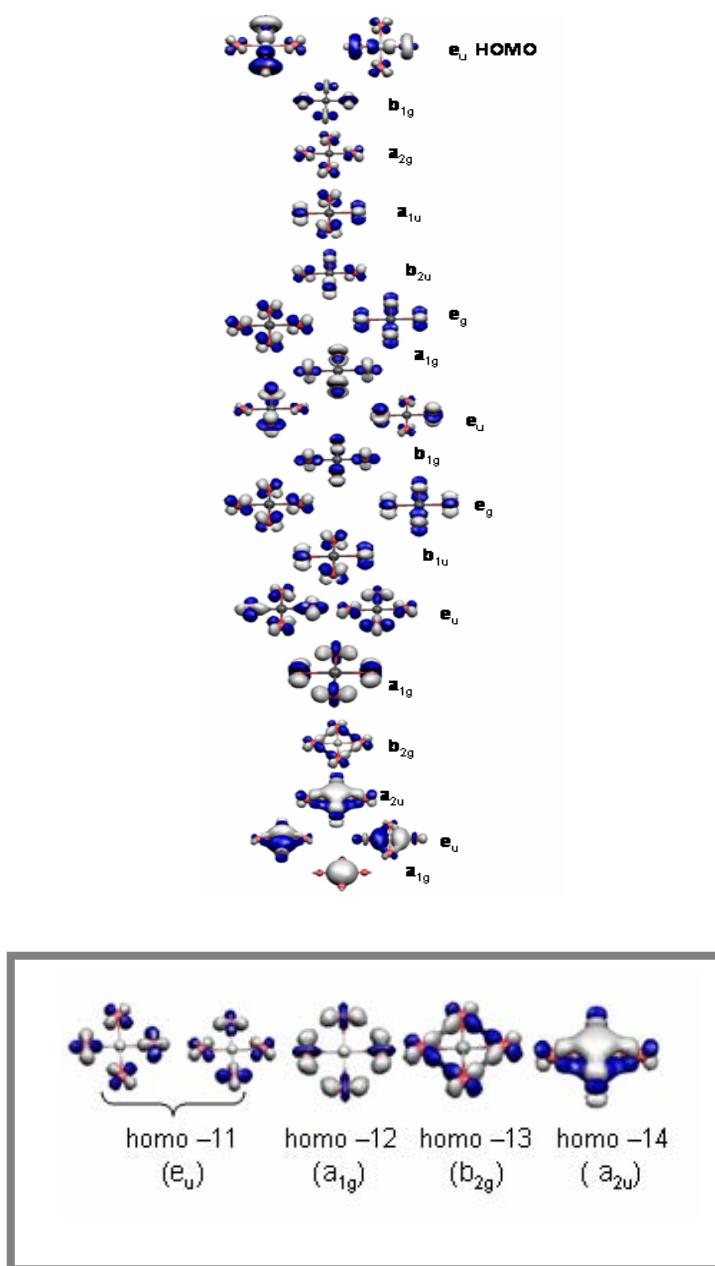


Figure 5-4 The full set of molecular orbitals of  $\text{CCu}_4^{2+}$  ( $D_{4h}$ ) (B3LYP/TZVPP). Illustrative molecular orbitals are enclosed in a square. The isosurface value is 0.05 au.

## 5.6 Magnetic Properties

$\delta^{13}\text{C}$  and nucleus-independent chemical shift [28] (NICS) PW91/TZVPP all-electron DFT computations provide more detailed understanding of the extent of cyclic electron delocalization in these systems. In particular, the NICS<sub>zz</sub> [28b, 29] index, which is closely related to the current density, reflects the magnetic response of a molecule toward a magnetic field applied perpendicularly to the plane (the z direction by the usual convention). Figure 5-5 displays grids of NICS<sub>zz</sub> points and  $^{13}\text{C}$  chemical shifts for **2-5**,  $\text{CAI}_4\text{Na}^+$  and for the previously-studied  $\text{C}_5\text{Li}_2$  [30] for comparison. The peculiar properties of the ptCs in **2-5** are best illustrated by their  $^{13}\text{C}$  NMR chemical shifts (Figure 5-5), which differ dramatically from the usual  $\text{sp}^2$  carbon shielding range (120-220 ppm). The out-of-plane component of the carbon shielding tensor

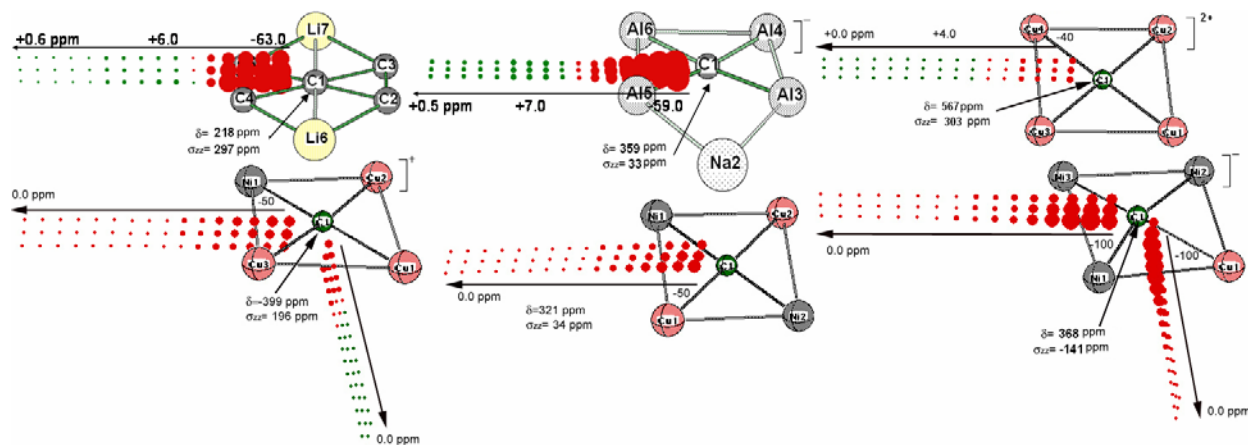


Figure 5-5. Two-dimensional grids (0.6 X 5.0 Å) of NICS<sub>zz</sub> points and  $^{13}\text{C}$  chemical shifts ( $\delta^{13}\text{C}$ ) for **2-5** (PW91/TZVPP)  $\text{CAI}_4\text{Na}^+$  (PW91/IGLOIII) and for the previously studied  $\text{C}_5\text{Li}_2$ .

( $\sigma_{zz}$ ) is more informative than the  $^{13}\text{C}$  chemical shift itself. Thus  $\text{C}_5\text{Li}_2$  and  $\text{CCu}_4^{2+}$  (**2**) have a fairly large  $^{13}\text{C}$ - $\sigma_{zz}$  value (>300 ppm) as compared to **3-5** (<200 ppm). This greater magnitude is



consistent both with a larger decrease of electron density at the planar tetracoordinated carbon and with a stronger electronic delocalization in the bare copper and carbon rings.

The magnetic behavior of  $C_5Li_2$  is known [30] to be similar to benzene: both have large diatropic (magnetic aromaticity) regions inside and deshielding regions outside the ring.  $CCu_4^{2+}$  (**2**) is confirmed to be a promising candidate for isolation as it exhibits the same  $NICS_{zz}$  pattern as  $C_5Li_2$  (Figure 5-5) and benzene, its deshielding outside is weaker (up to +3.5 ppm vs 5.6 ppm for  $C_5Li_2$ ). In sharp contrast, **4** and **5** do not exhibit a deshielding region but remain weakly diatropic outside the ring: vanishes at  $\sim 5\text{\AA}$ . Such unexpected magnetic behavior is inconsistent with Pople's ring current model [31] and hence with the existence of a diatropic ring current around the metal framework of **4** and **5**. Interestingly, the magnetic behavior of **3** is similar to that of **4** and **5** but with a fairly weak increase of the deshielding ( $>2.5$  ppm) along the direction perpendicular to a Cu-Cu bond.

## 5.7 Exploration of the potential energy surface

Finally, to explore the potential energy surface of our most promising candidate,  $CCu_4^{2+}$  (**2**), a total of 1000 “kick” jobs in independent sets of 50 were performed at the HF/STO-3G level of theory. The procedure is explained in the “Computational details” section, above. The best structures from the initial level were refined at B3LYP/TZVPP. Only two minima, the global minimum, **2** and the 92.1 kcal/mol less stable local minimum, **2A** (Figure 5-6) were located on

the PES of  $\text{CCu}_4^{2+}$ . Most of the “candidates” generated at the lower HF/STO-3G level did not

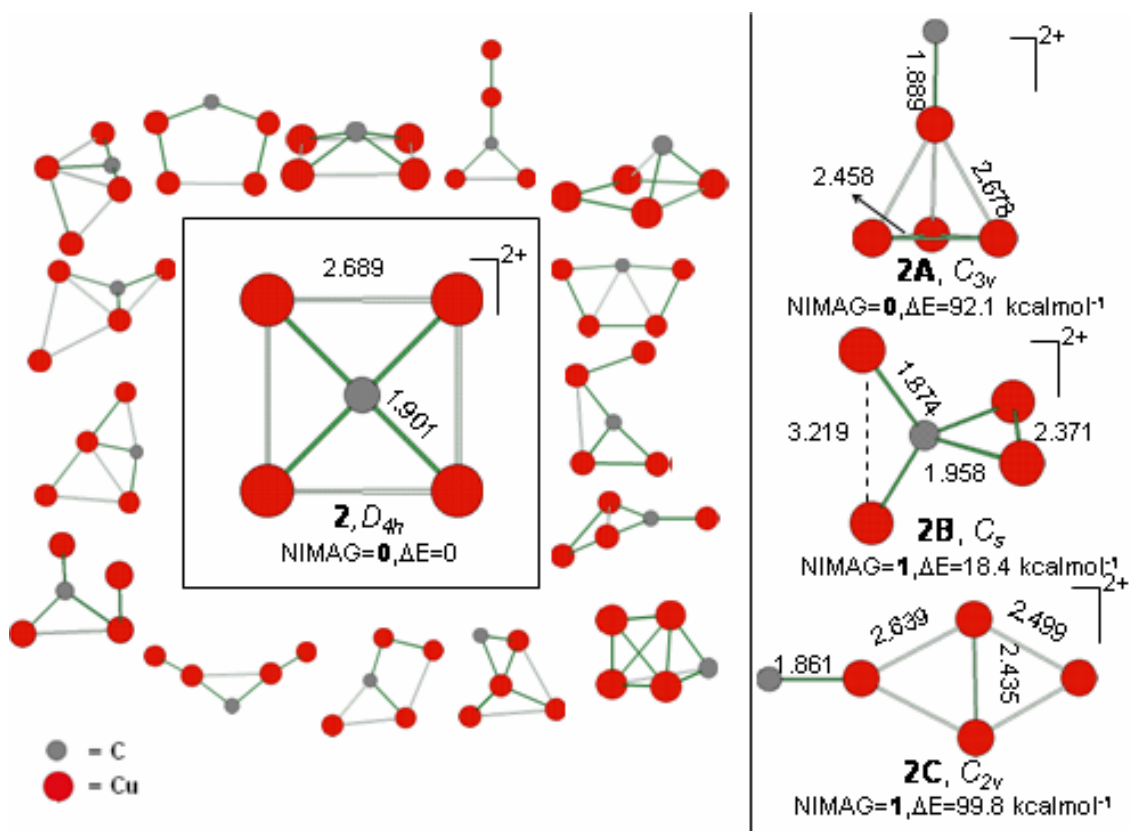


Figure 5-6. Three of the four stationary points of  $\text{CCu}_4^{2+}$  obtained at the B3LYP/TZVPP level are displayed on the right side. NIMAG is the number of imaginary harmonic frequencies.  $\Delta E$  is the energy relative to **2**. All distances are in Å. Illustrative preliminary structures, generated by the “kick” method at HF/STO-3G (see text) are shown on the left side. These all led to the ptC global minimum (**2**) upon further refinement at the higher theoretical level.

survive and optimized to **2** at B3LYP/TZVPP. We have also located two transition structures, both of which are involved (as shown by their IRC's) in different degenerate permutations of Cu

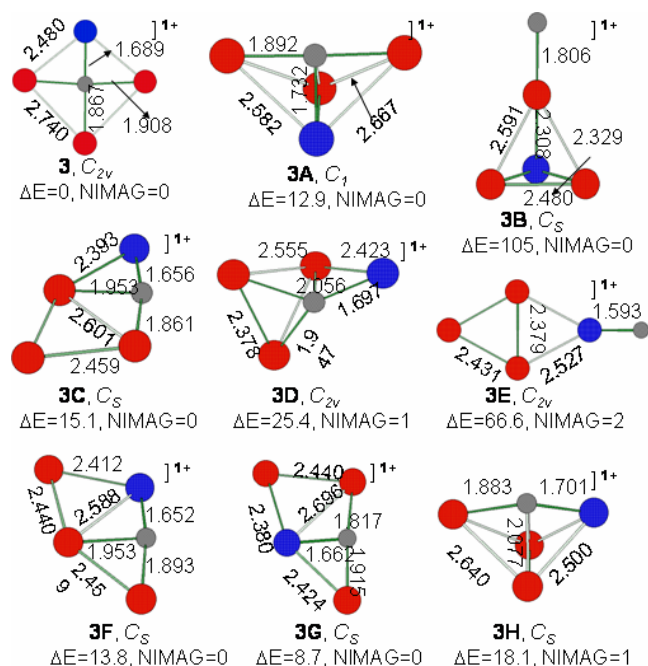


Figure 5-7. Stationary points on the potential energy surface of  $\text{CCu}_3\text{Ni}^+$ .

atoms: **2C** is the transition state between two stereo mutated **2A**'s and **2B** is the transition state between to stereo mutated **2**'s (Figure 5-6).

All “kick” optimizations proceed in point group  $C_1$ , but often lead very nearly to higher symmetries, which may then be imposed prior to the further refinement. Additional MP2/TZVPP calculations confirm that the dication **2** is a minimum and much more stable than the alternative geometries.

We have also explored the potential energy surfaces for  $\text{CCu}_3\text{Ni}^+$  (Figure 5-7),  $\text{CCu}_2\text{Ni}_2$  (Figure 5-8) and  $\text{CCuNi}_3^-$  (Figure 5-9) extensively using the “kick” method.<sup>22,23</sup> The structures with ptC's also were found to be the global minima. Stationary points of the  $\text{CCu}_3\text{Ni}^+$  skeleton

were obtained at B3LYP/TZVPP level. NIMAG is the number of imaginary harmonic

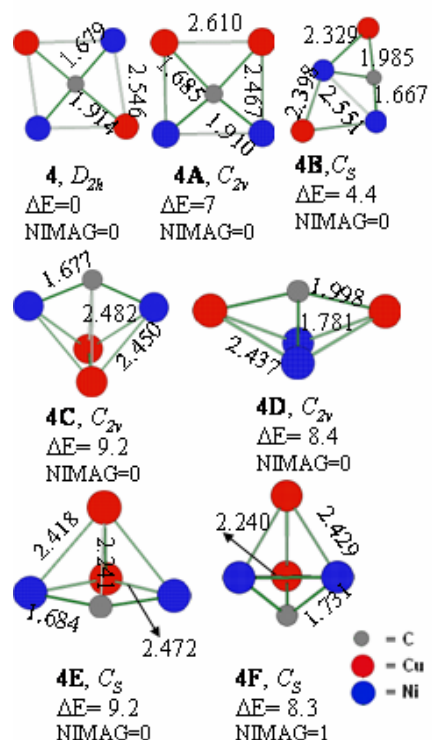


Figure 5-8. Stationary points on the potential energy surface of  $\text{CCu}_2\text{Ni}_2$ .

frequencies obtained for each structure using the same methodology, and  $\Delta E$  is the relative energy in  $\text{kcal mol}^{-1}$  with respect to **3** (Figure 5-7). All distances are in angstrom. Six structures are local minima on the PES including **3**. Structures **3A-3H** are higher in energy than the  $C_{2v}$  ptC containing compound **3**. Stationary points of the  $\text{CCu}_2\text{Ni}_2$  were skeleton obtained at B3LYP/TZVPP level. NIMAG is the number of imaginary harmonic frequencies obtained for each structure using the same methodology, and  $\Delta E$  is the relative energy in  $\text{kcal mol}^{-1}$  with respect to **4**. All distances are in angstrom. Six structures are local minima on the PES including **4** (Figure 5-8). It should be noted that structure **4C** is also planar and lies very close in energy to **4** ( $4.4 \text{ kcal mol}^{-1}$  higher without zero point corrections). Structures **4A-4F** are higher in energy

than the  $D_{2h}$  ptC containing compound **4**. Structure **4F** has one imaginary frequency and not connected to a ptC containing molecule.

Similarly Stationary points of the  $\text{CCuNi}_3^-$  skeleton obtained at B3LYP/TZVPP level. NIMAG is the number of imaginary harmonic frequencies obtained for each structure using the same methodology, and  $\Delta E$  is the relative energy in  $\text{kcal mol}^{-1}$  with respect to **5**. All distances are in angstrom. Seven structures correspond to local minima on the PES including **5** (Figure 5-9). Structures **5A-5G** are higher in energy than the  $C_{2v}$  ptC containing compound **5**. Structure **5B** has one imaginary frequency and it is not connected to the ptC containing molecule.

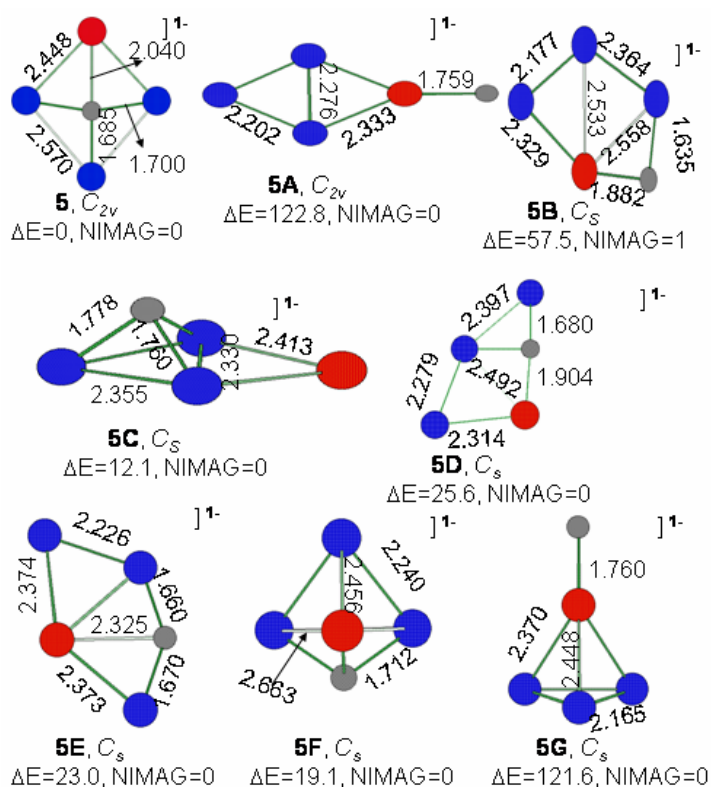


Figure 5-9. Isomers for  $\text{CCuNi}_3^-$  obtained by employing “kick” method.

## 5.8 Conclusion

We illustrate that a rational strategy can be employed to design four membered transition metal ring containing planar tetracoordinate carbon in their centers. The ring and carbon atomic radii must match. In addition, the  $\pi$  electron delocalization determines the stability of these molecules. As illustrated by the  $\text{CM}_4$  systems analyzed here, bare four-membered transition metal rings comprised of Cu, Ni, Ag, Pd are good candidates for stabilizing planar tetracoordinate carbons.  $\text{CCu}_4^{2+} \text{D}_{4h}$  is an ideal candidate which exemplifies the use of a bare four-membered ring of late transition metals for stabilizing a tetracoordinated planar carbon. A highly delocalized  $\pi \text{a}_{2u}$  MO with an important contribution from the vacant  $p_z$ -orbital of the central carbon atom stabilizes this species. In contrast to transition metal analogues, this copper compound is characterized by a large decrease of electron density at the ptC.  $\text{CCu}_4^{2+} \text{D}_{4h}$  is a promising candidate for isolation as it exhibits large diatropic (magnetic aromaticity) regions inside and deshielding regions outside the ring and exhibit the same  $\text{NICS}_{zz}$  pattern as  $\text{C}_5\text{Li}_2$  and benzene. While neutral examples are likely to aggregate, their isoelectronic cationic analogs and  $\text{CCu}_4^{2+}$  in particular are good prospects for detection by gas-phase photoelectron spectroscopy<sup>32</sup>,<sup>33</sup> when compared to highly accurate electron affinities.

## 5.9 Acknowledgement

This work was financially supported by NSF Grant No. CHE-0209857 and partly by the Petroleum Research Fund (grant#41888-AC4).

## 5.10 References

- 1) J. H. van't Hoff, *Arch. Neerl. Sci. Exactes Nat.* 1874, 445.
- 2) J. A. LeBel, *Bull. Soc. Chim. Fr.* 1874, 22.

- 3) H.J. Monkhorst, *J. Chem. Soc. Chem. Comm.* 1968, 1111.
- 4) R. Hoffmann, R. W. Alder, C. F. Wilcox *J. Am. Chem. Soc.* 1970, 92, 4992.
- 5) J. B. Collins, J. D. Dill, E. D. Jemmis, Y. Apeloig, P. v. R. Schleyer, R. Seeger, J. A. Pople, *J. Am. Chem. Soc.* 1976, 98, 5419.
- 6) See reviews: (a) K. Sorger, P. v. R. Schleyer *THEOCHEM* 1995, 338, 317. (b) D. Rottger, G. Erker *Angew. Chem., Int. Ed. Engl.* 1997, 36, 812 (c) L. Radom, D. R. Rasmussen, *Pure Appl. Chem.* 1998, 70, 1977. (d) W. Siebert, A. Gunale, *Chem. Soc. Rev.* 1999, 28, 367. (e) V. I. Minkin, R. M. Minyaev, R. Hoffmann, *Usp. Khim.* 2002, 71, 989.
- 7) M. P. McGrath, L. Radom. *J. Am. Chem. Soc.* 1993, 115, 332.
- 8) (a) D. R. Rasmussen, L. Radom *Angew. Chem., Int. Ed.* 1999, 38, 2876. (b) D. R. Rasmussen, L. Radom, *Chem. Eur. J.* 2000, 6, 2470.
- 9) P. M. Esteves, N. B. P. Ferreira, R. Correa *J. Am. Chem. Soc.* 2005, 127, 8680.
- 10) Z.-X. Wang, P. v. R. Schleyer *J. Am. Chem. Soc.* 2001, 123, 994.
- 11) (a) J. E. Lyons, D. R. Rasmussen, M. P. McGrath, R. H. Nobes, L. Radom *Angew. Chem., Int. Ed. Engl.* 1994, 33, 1667. (b) Z.-X. Wang; P. v. R. Schleyer *J. Am. Chem. Soc.* 2002, 124, 11979.
- 12) (a) P. v. R. Schleyer, A. I. Boldyrev *J. Chem. Soc. Chem. Commun.* 1991, 1536. (b) A. I. Boldyrev, J. Simons, *J. Am. Chem. Soc.* 1998, 120, 7967. (c) X. Li, L.-S. Wang, A. I. Boldyrev, J. Simons *J. Am. Chem. Soc.* 1999, 121, 6033. (d) L.-S. Wang, A. I. Boldyrev, X. Li, J. Simons *J. Am. Chem. Soc.* 2000, 122, 7681. (e) X. Li, H.-J. Zhai, L.-S. Wang *Chem. Phys. Lett.* 2002, 357, 415.
- 13) X. Li, H.-J. Zhai, L.-S. Wang, G. D. Geske, A. I. Boldyrev *Angew. Chem., Int. Ed.* 2000, 39, 3630.

- 14) U. E. Musanke, W. Jeitschko *Z. Naturforsch., B* 1991, 46, 1177.
- 15) E. F. Merschrod, S. H. Tang, R. Hoffmann *Z. Naturforsch., B* 1998, 53, 322.
- 16) C. A. Tsipis, E. E. Karagiannis, P. F. Kladou, A. C. Tsipis *J. Am. Chem. Soc.* 2004, 126, 12916.
- 17) S.-D. Li, G.-M. Ren, C.-Q. Miao, Z.-H. Jin *Angew. Chem., Int. Ed.* 2004, 43, 1371. They reported ptC containing D<sub>4h</sub> hydronickel compound. However, the planar D<sub>4h</sub> hydrocopper analogue (Cu<sub>4</sub>H<sub>4</sub>C) was found to be a first order saddle point and pyramidal C<sub>4v</sub> (in which C atom lies about 0.5 Å above the Cu<sub>4</sub> plane) to be the global minimum.
- 18) C. S. Wannere, C. Corminboeuf, Z.-X. Wang, M. D. Wodrich, R. B. King, P. v. R. Schleyer *J. Am. Chem. Soc.* 2005, 127, 5701.
- 19) F. Weigend, R. Ahlrichs, *Phys. Chem. Chem. Phys.* 2005, 18, 3297.
- 20) P. J. Hay, W. R. Wadt *J. Chem. Phys.* 1985, 82, 299.
- 21) M. J. Frisch, G. W. Trucks, H. B. Schlegel, G. E. Scuseria, M. A. Robb, J. R. Cheeseman, V. G. Zakrzewski, J. A. Montgomery, Jr., R. E. Stratmann, J. C. Burant, S. Dapprich, J. M. Millam, A. D. Daniels, K. N. Kudin, M. C. Strain, O. Farkas, J. Tomasi, V. Barone, M. Cossi, R. Cammi, B. Mennucci, C. Pomelli, C. Adamo, S. Clifford, J. Ochterski, G. A. Petersson, P. Y. Ayala, Q. Cui, K. Morokuma, P. Salvador, J. J. Dannenberg, D. K. Malick, A. D. Rabuck, K. Raghavachari, J. B. Foresman, J. Cioslowski, J. V. Ortiz, A. G. Baboul, B. B. Stefanov, G. Liu, A. Liashenko, P. Piskorz, I. Komaromi, R. Gomperts, R. L. Martin, D. J. Fox, T. Keith, M. A. Al-Laham, C. Y. Peng, A. Nanayakkara, M. Challacombe, P. M. W. Gill, B. Johnson, W. Chen, M. W. Wong, J. L. Andres, C. Gonzalez, M. Head-Gordon, E. S. Replogle, and J. A. Pople, *Gaussian 03*, revision C.02; Gaussian, Inc.: Wallingford, CT, 2004.



- 22) M. Saunders *J. Comput. Chem.* 2004, 25, 621.
- 23) P. P. Bera, K. W. Sattelmeyer, M. Saunders, H. F. Schaefer, P. v. R. Schleyer. *J. Phys. Chem. A* 2006, 110, 4287.
- 24) D. R. Lide, H. P. R. Frederikse CRC Handbook of Chemistry and Physics; CRC Press: New York, 1998, 9-51.
- 25) Y. C. Lin, D. Sundholm, J. Juselius, L.F. Cui, X. Li, H. J. Zhai, L. S. Wang *J Phys. Chem. A* **2006**, 110, 4244.
- 26) Neutral D<sub>4h</sub> Cu<sub>4</sub> suffers from wave function instability problems at the DFT level (PW91PW91/LANL2DZ).
- 27) A. E. Reed, L. A. Curtiss, F. J. Weinhold, *Chem. Rev.* **1988**, 88, 899.
- 28) (a) P. v. R. Schleyer, C. Maerker, A. Dransfeld, H. Jiao, N. J. R. v. E. Hommes *J. Am. Chem. Soc.* **1996**, 118, 6317. (b) Z. Chen, C. S. Wannere, C. Corminboeuf, R. Puchta, P. v. R. Schleyer *Chem. Rev.* **2005**, 105, 3842.
- 29) (a) P. W. Fowler, E. Steiner, *Mol. Phys.*, **2000**, 98, 945. (b) E. Steiner, P. W. Fowler, L. Jennesskens, W. *Angew. Chem. Int. Ed.*, **2001**, 40, 362. (c) C. Corminboeuf, T. Heine, G. Seifert, P. v. R. Schleyer *Phys. Chem. Chem. Phys.* **2004**, 6, 273. (d) H. Fallah-Bagher-Shaidaei, C.S. Wannere, C. Corminboeuf, R. Puchta, P.v.R. Schleyer *Org. Lett.* **2006**, 8, 863.
- 30) G. Merino, M. A. Mendez-Rojas; I. H. Beltran, C. Corminboeuf, T. Heine, A. Vela *J. Am. Chem. Soc.* **2004**, 126, 16160.
- 31) J. A. Pople *J. Chem. Phys.* **1956**, 24, 1111.
- 32) L.S. Wang, H.S. Cheng, J. Fan *J. Chem. Phys.* **1995**, 102, 9480.
- 33) L.S. Wang, H. Wu in *Advances in Metal and Semiconductor Clusters IV. Cluster Materials* (Ed.: M. A. Duncan), JAI, Greenwich, **1998**, pp. 299-343.

## CHAPTER 6

### CONCLUSION

The major conclusions from the dissertation chapters are summarized below:

- **Abiotic origin of adenine**

The thermodynamically viable step-by-step reaction mechanism for the formation of adenine, described in this dissertation, is based on extensive computations of sequences of reaction steps along several possible mechanistic routes. A plausible mechanism for formation of abiotic adenine is deduced starting from AICN (a tetramer of HCN). To explain the existence of a relatively higher barrier for the key step, one has to keep in mind that, although adenine formation from five HCN is highly exothermic, it does require some activation. Rather drastic reaction conditions (e.g, heating up at 70 °C, or keeping solution mixture for 25 years) were applied in abiotic synthesis of adenine. The reaction conditions provide us a clue that there must be some steps associated with considerable amount of reaction barrier. H<sub>2</sub>O or NH<sub>3</sub> can act as a catalyst (as shown in our study) to lower the barriers considerably. Moreover, prebiotic conditions (bulk solvation, for instance) is implicitly considered in calculations using the quantum chemical techniques which lowers the barrier of the rate determining step further. The neutral water or ammonia catalyzed mechanism proposed in this study may well have been a major route for the formation of adenine on primitive earth. However, detailed calculations on reactions of this kind are needed before a full picture emerges. Mechanisms modeling the formation of other remaining nucleic acid bases and biologically relevant molecules extra-terrestrially, under more restricted conditions, are further challenges.

#### ▪ Reaction mechanism for dinitrogen activation with model lithium clusters

The reaction of the normally quite inert  $\text{N}_2$  with lithium is remarkably facile. As shown by the computed results reported in this dissertation,  $\text{N}_2$  readily complexes at various positions of  $\text{Li}_4$ ,  $\text{Li}_6$ , and  $\text{Li}_8$  model clusters. These isomeric complexes interconvert over generally low barriers, but their NN elongations with small cluster size ( $\text{Li}_4$ ) are only to double bond lengths (ca. 1.25 Å). Further reduction to oxidation state -2 and -3 only occurred with  $\text{N}_2\text{Li}_6$  and  $\text{N}_2\text{Li}_8$ . The key step in both  $\text{N}_2\text{Li}_6$  and  $\text{N}_2\text{Li}_8$  involved the sudden, exothermic (ca. 22.9 kcal mol<sup>-1</sup> and 19.0 kcal/mol, respectively, at B3LYP) double to single (~1.3 to 1.48 Å) NN bond length elongation. The final reduction stage separates the N atoms by over 3 Å and embeds them centrally in  $(\text{NLi}_3)_2$  and  $(\text{NLi}_4)_2$  dimer clusters. Although  $(\text{NLi}_3)_2$  is not the global  $\text{N}_2\text{Li}_6$  minimum, it is 37.9 kcal/mol (36.6 kcal/mol with MP2/6-311+G\*) more stable than separated  $\text{N}_2 + \text{Li}_6$ . The  $(\text{NLi}_4)_2$  dimer end product is the  $\text{N}_2\text{Li}_8$  global minimum and the exothermicity of the  $\text{N}_2 + \text{Li}_8$  reaction is enormous, 84.8 kcal/mol (76.4 kcal/mol with MP2/6-311+G\*). We conclude that eight lithium atoms are needed to cleave the triple bonded nitrogen completely.

#### ▪ One electron aromatics

The present study provides theoretical examples of main group mono  $\pi$ , 3c-1e and 4c-1e open-shell aromatic species. In some cases ( $\text{D}_{3h} \text{B}_3^{2+}$  and  $\text{C}_s \text{B}_3\text{H}_3^+$ ), there exists a general qualitative relationship between the aromaticity of the singlet and that of the doublet species. This trend confirms that the ring current originates mostly from the highest-occupied molecular orbital. While theoretical design often offers prediction for plausible novel viable compounds, not all the species reported in the dissertation are good candidates for experimental detection due the huge

positive ionization potential for the two electron analogs. Nonetheless, the negative electron affinity value of one the cage, namely the doublet  $C_6H_{12}B_4^-$  (-3.38 eV | -3.24 eV), indicates its stability with respect to the closed shell 4c-2e aromatic dianion. Similarly, the  $Al_3H_3^{1-}$  isomers also are resistant toward reduction (-2.86 and -2.79 eV at the B3LYP/TZVPP level respectively). We thus anticipate the detection of “one electron aromatics”  $C_6H_{12}B_4^-$  and  $Al_3H_3^{1-}$  by, for instance, photoelectron spectroscopy.

#### ▪ Transition metal cages containing planar tetracoordinate carbon

Our efforts to design new planar tetracoordinate Carbon (ptC) containing molecules have concentrated on small five atom species, the smallest molecules that can contain ptC molecules, in which the bonding of central carbon atoms to its four ligands can be easily traced. Furthermore, planarity in these species is not enforced by their molecular architecture, but rather by their intrinsic and unique electron structure. We have extended the range of ligands from p-block elements to d-block transition metals. On the basis of DFT optimization results, we present the first theoretical evidence that, in the form of the  $CM_4^{n+}$ , C is tetracoordinated by four transition-metal ligands M (M=Cu, Ni) in perfect squares. From DFT analyses of the molecular orbitals, electronic structures, energies, and magnetic properties of these  $CM_4$  systems (M are the combinations of Cu, Ni, Ag, Pd), we found that bare four-membered transition metal rings are good candidates for stabilizing planar tetracoordinate carbons. While neutral examples are likely to aggregate, their isoelectronic cationic analogs and  $CCu_4^{2+}$  in particular are good prospects for detection by gas-phase photoelectron spectroscopy when compared to highly accurate electron affinities.